

2

AFOSR-TR- 89 - 0475

AD-A207 055

A FINAL TECHNICAL REPORT  
ON  
THE INTERACTION OF SOLID PARTICLES WITH LASER BEAMS  
Contract # F49620-85-C-0117

Approved for public release;  
distribution unlimited.

AIR FORCE OFFICE OF SCIENTIFIC RESEARCH (AFSC)  
REPORT # AFOSR-TR-89-0475  
This report is the property of the AFSC and is  
loaned to you for your use only. It and its  
contents are not to be distributed outside your  
organization without the express written  
approval of the AFSC.

DTIC  
ELECTE  
APR 24 1989  
S E D

089 4 24 17C

## REPORT DOCUMENTATION PAGE

1a. REPORT SECURITY CLASSIFICATION <b>Unclassified</b>			1d. RESTRICTIVE MARKINGS		
2a. SECURITY CLASSIFICATION AUTHORITY			3. DISTRIBUTION/AVAILABILITY OF REPORT <b>unlimited</b>		
b. DECLASSIFICATION/DOWNGRADING SCHEDULE			4. PERFORMING ORGANIZATION REPORT NUMBER(S)		
5a. NAME OF PERFORMING ORGANIZATION University of Florida			5b. OFFICE SYMBOL (If applicable)		
6a. ADDRESS (City, State, and ZIP Code) Space Astronomy Laboratory 1810 NW 6th Street Gainesville, FL 32609			7a. NAME OF MONITORING ORGANIZATION Air Force Office of Scientific Research <b>NE</b>		
8a. NAME OF FUNDING/SPONSORING ORGANIZATION Air Force Office of Scientific Research			8b. OFFICE SYMBOL (If applicable) AFOSR <b>NE</b>		
9a. ADDRESS (City, State, and ZIP Code) Building 410 Bolling Air Force Base, DC 20332			9. PROCUREMENT INSTRUMENT IDENTIFICATION NUMBER <b>AFOSR # F 49620-85-C-0117</b>		
10. SOURCE OF FUNDING NUMBERS			11. TITLE (Include Security Classification) The Interaction of Small Particles With Laser Beams		
PROGRAM ELEMENT NO. <b>61102F</b>			PROJECT NO. <b>2306</b>		
TASK NO. <b>A2</b>			WORK UNIT ACCESSION NO.		
12. PERSONAL AUTHOR(S) Misconi, Nebil Y., Ratcliff, Keith F., Rusk, Edwin T., and Oliver, John P.					
13a. TYPE OF REPORT <b>FINAL</b>		13b. TIME COVERED FROM 85/07/15 TO 89/02/08		14. DATE OF REPORT (Year, Month, Day) 890408	
15. PAGE COUNT 890408					
16. SUPPLEMENTARY NOTATION					
17. COSATI CODES			18. SUBJECT TERMS (Continue on reverse if necessary and identify by block number)		
FIELD	GROUP	SUB-GROUP	Laser Beam; Particle Interaction; light scattering; laser+particle levitation		
19. ABSTRACT (Continue on reverse if necessary and identify by block number)					
<p>Light scattering curves of intensity vs. scattering angle were made of 1) layers of transparent silica particles, 2) single silica particles isolated by optical levitation; using an Argon ion laser light source and a goniometer mounted silicon photodiode detector. Scattering measurements of spherical particles demonstrated an excellent agreement with Mie theory. Spheroids and irregular particles were also measured.</p> <p>Dynamics of particles in a space environment were studied both theoretically, and experimentally inside a <math>10^{-7}</math> Torr vacuum chamber. Research in this area will be continued to determine the effective moment arm of optically induced particle rotation. <i>Keywords:</i></p>					
20. DISTRIBUTION/AVAILABILITY OF ABSTRACT			21. ABSTRACT SECURITY CLASSIFICATION		
<input type="checkbox"/> UNCLASSIFIED/UNLIMITED <input checked="" type="checkbox"/> SAME AS RPT. <input type="checkbox"/> OTIC USERS			Unclassified		
22a. NAME OF RESPONSIBLE INDIVIDUAL Misconi, Nebil Y. <b>SCHOLER</b>			22b. TELEPHONE (Include Area Code) <b>(202) 767-4933</b>		
			22c. OFFICE SYMBOL <b>NE</b>		



April 8, 1989

A FINAL TECHNICAL REPORT  
ON  
THE INTERACTION OF SOLID PARTICLES WITH LASER BEAMS  
Contract # F49620-85-C-0117

Dr. N.Y. MISCONI: Principal Investigator<sup>1</sup>

Dr. E.T. RUSK: Co-Investigator<sup>1</sup>

Space Astronomy Laboratory  
University of Florida

Dr. K.F. RATCLIFF: Co-Investigator

Department of Physics  
State University of New York at Albany

Dr. J.P. OLIVER: Co-Investigator

Department of Astronomy  
University of Florida  
Gainesville, Florida

---

(1) Now At:

Space Research Institute (SRI)  
Center for Space Science Research  
Florida Institute of Technology (FIT)  
Melbourne, Florida



## OVERVIEW AND BACKGROUND

This project entitled "The Interaction of Solid Particles with Laser Beams" was initiated in July 1985 by AFOSR Contract # F49620-85-C-0117 that ended on February 8, 1989. This contract had three phases where the emphasis was different in each phase.

### PHASE ONE

The first year was devoted to the study of laser light scattering by thin layers\* of highly transparent (0.22-2.2  $\mu\text{m}$ ) and pure silicate particles. Measurements of the forward transmission and backward reflection were made for different types of silicate particles, highly irregular in shape, different in sizes, and different thicknesses of the layers. The light source throughout this investigation is an Argon laser with maximum intensity of 18 watts (CW all lines). Scattering angles from  $\theta = 0$  to  $165^\circ$  were scanned in clockwise and counterclockwise directions, and the intensity was measured by a photodiode detector.

We found that as the particles were smaller in size the backward reflected light became more intense. This was maximized for a mixture of particles of 68  $\mu\text{m}$  (the size of a sieve) and less. We achieved a ratio of the reflected light in the backward hemisphere to the transmitted light in the forward hemisphere of approximately 100. This ratio can be enhanced by making the layers thicker than 1mm for natural sand and suprasil particles. We also found that the former type of particles did not melt when exposed to 1.5 MW/cm<sup>2</sup> by focusing the 18 watt laser beam. Symmetry was found when scanning in clockwise and counterclockwise scattering angles. Also the scattering pattern did not change as long as the laser beam is perpendicular to the layer's surface. Details of these measurements were included in our annual report to AFOSR.

There are many questions that remains to be answered, the following is a list of these questions that we hope to find the necessary funds to investigate them using our existing Laser-particle Dynamics Facility at the

---

\* In the context of this report, the word "layer" is used to describe a sample of particles, tightly packed, many particles thick, and flattened on top and bottom surfaces.

Space Research Institute (SRI), of the Florida Institute of Technology (FIT):

1- Measurements of the polarization of the laser light from these layers of particles need to be made.

2- Other materials (other than silicates) have to be investigated for light scattering characteristics i.e. intensity, and polarization. These measurements should be carried out in the same fashion as we did with silicates i.e. different sizes, shapes, thicknesses, ...etc.

3- Different materials including silicates should be tested for their light absorption characteristics, and therefore their temperatures after being exposed to laser light, including the possibility of melting.

4- A theoretical model should be constructed that can predict the behavior of these materials given inputs such as type, size, absorption coefficient, thermal conductivity and capacity, etc.

5- A theoretical investigation that will explain the nature of the light propagation, inside as well as surface waves, using techniques such as random walk calculations in three dimensions, Monte Carlo type calculations, and better understanding of the process of multiple scattering of light by slabs of particles or the more easier case of clouds of particles.

Accession For	
NTIS GRA&I	<input checked="" type="checkbox"/>
DTIC TAB	<input type="checkbox"/>
Unannounced	<input type="checkbox"/>
Justification	
By	
Distribution/	
Availability Codes	
Dist	Avail and/or Special
A-1	

TIC

## PHASE TWO

The second year of this investigation was devoted to studying the light scattering nature of single particles (spherical and irregularly shaped), using the technique of laser-particle levitation. This technique allows the particle to be suspended in air inside a scattering chamber where photon pressure balances gravity. Details of this technique, instrumental and theoretical, is given in our annual report of the second year, and in a series of papers submitted to Applied Optics Journal for publication.

Many spherical and some irregular particles were levitated in the Argon laser beam, using the 5145A line a goniometer was built inside the scattering chamber with a photodiode and a light baffle mounted at opposite ends of the goniometer, that allows to make intensity measurements for scattering angles  $\theta$  from  $16^\circ$  to  $167^\circ$ . The remaining angles to  $180^\circ$  could not be measured for mechanical obstruction of the goniometer. The observed intensity at these angles were then compared to a Mie theory curve. Figure 1, is an example of these results.

It was found that these measurements agreed very well with the theoretical Mie curves in the case of using a perfect sphere. This indicated to us that the instrument and the technique worked extremely well. We did however, encounter some difficulties in matching the observed data with the Mie curves, since this comparison is extremely sensitive to the exact size of the particles and to the exact refractive index of the particles (see paper I for details). For spheroids and irregular particles, the results were interesting and sometimes baffling since this area in light scattering research is in its infancy. Theoretical scattering curves for spheroids have been developed recently, and the latest improvements that were made for these curves were used. We like here to acknowledge the help we received from Prof. H. Van de Hulst a world renknown authority in the field of light scattering along with Prof. J. Mayo Greenberg both of Lieden, and last but not least Dr. Wan Xian Wang's latest theory on the light scattering by spheroids. These results will be included in Paper IV and V of the series that we have started in Applied Optics Journal (Paper I and II already submitted).

As always, more is needed to be done in this important area of research. The following are some that we feel is urgently needed:

- 1- To construct a more sophisticated system that can enable us to measure backscattering down to  $180^\circ$ .

2- Create a library of Mie theory curves that will make it easy to match the observations to the respective curve, since determining the size and the refractive index of the particles to an accuracy of 0.01% is extremely difficult if not impossible

3- We are only in the beginning phases of a system that can measure the scattering from irregular particles. We also have the capability to characterize the scattering pattern with the surface irregularity responsible for it. This can be done using our existing, state of the art frame grabber and camera that has the capability to analyze frame by frame digital data

4- Our particle-levitation technique allows the particle to spin freely while scattering light. This ability can be utilized to perform studies on the scattering of light by spinning particles, which are more realistic, since particles normally spin in the atmosphere or in space.

### PHASE THREE

#### EXPERIMENTS WITH LASER-PARTICLE LEVITATION IN A VACUUM

##### INTRODUCTION

The main purpose of this phase is to study rotation of particles in a simulated space condition. The combination of both levitation vs. gravity and high vacuum simulate the space environment. The rotation will be caused by the interaction of photons with surface irregularities and thus causes the particles to spin like a "windmill". This mechanism is known as the "Windmill Effect".

The purpose of studying the rotation is two fold: one is to study the behavior of particles in orbits around the Earth, both natural and man-made. Second, and equally important is the rotation of cosmic dust particles in the universe as a whole. The latter is important because if this rotation is a steady phenomenon, then these particles will accelerate (in the absence of damping forces) continuously until the stress from rotation will overcome the internal cohesion of the particles thus bringing on bursting or breakup. If this phenomenon occurs in space, then it can explain the abundance of cosmic dust particles in the universe. The way this comes about is that if particle bursting takes place, then the size of the particles will decrease until the radiation pressure from the stars (including the sun) will overcome the gravitational attraction and these particles will be injected into interstellar space.

Such particles leaving the solar system have been observed by numerous Earth satellites and spaceprobes. These particles were called  $\beta$  meteoroids, where  $\beta$  stands for the ratio of the solar radiation to the gravitational attraction. Other dynamical forces under study include the optical forces that do confine the particle in the beam, the force needed for bringing the particle to its point of equilibrium in the absence of air, and other dynamical behavior that the particles may exhibit in vacuum.

To meet these objectives, we have constructed an apparatus designed to allow optical levitation in a vacuum. The vacuum levitation chamber can be interchanged with the scattering chamber used in the Phase two experiments. The experimental design was based partially upon papers by Ashkin and Dziedzic (1977).

#### VACUUM CHAMBER DESIGN:

The vacuum chamber has dimensions (cylindrical, 5 inches in diameter, 4.5 inches high) comparable to the scattering chamber used in earlier experiments. This allows the easy interchange of the vacuum chamber with the scattering chamber, and the utilization of the same illumination and viewing systems, as well as the same data acquisition apparatus.

The "O"-ring sealed chamber allows the removal of the top plate for cleaning and replacement of particle charge. Optically flat windows are provided on the top and bottom surfaces for the passage of the laser illumination beam, and on the side walls of the chamber for the viewing optics. Vacuums below  $10^{-7}$  Torr could be achieved.

A translation/rotation vacuum mechanical feedthru in the top plate supports the particle launching plate. This was necessary to allow the movement of the launching plate out of the optical path, thus avoiding the possibility that particles remaining on the plate might distort the illumination of the levitated particle. In practice, it was found that it was relatively easy to lower the launching plate to the bottom of the chamber, and then rotate it out of the beam quickly without interrupting the illumination long enough to cause the particle to drop. A pair of electrical feedthrus in the top plate carry the voltage to the piezo-electric launching mechanism.

In order to select a particle for levitation, it is necessary to translate the launching plate in the x-y plane perpendicular to the laser illumination beam. Rather than place an x-y translation system within the vacuum, we translate the entire vacuum chamber on a large load supporting precision x-y translation stage.

#### VACUUM SYSTEM:

In order to achieve vacuums below  $10^{-7}$  Torr, the vacuum system consists of a mechanical forepump and a turbo-molecular high vacuum pump. Thermocouple and Ion vacuum gauges are installed in the vacuum lines coupling the turbo-molecular pump to the chamber. A flexible coupling allows the x-y translation of the vacuum chamber for particle selection. A right-angle cross-section allows control of the pumping rate, while (when full open) avoiding restriction in the maximum vacuum achievable. Figure 1 and 2 show the components of the vacuum system as well as the vacuum chamber.

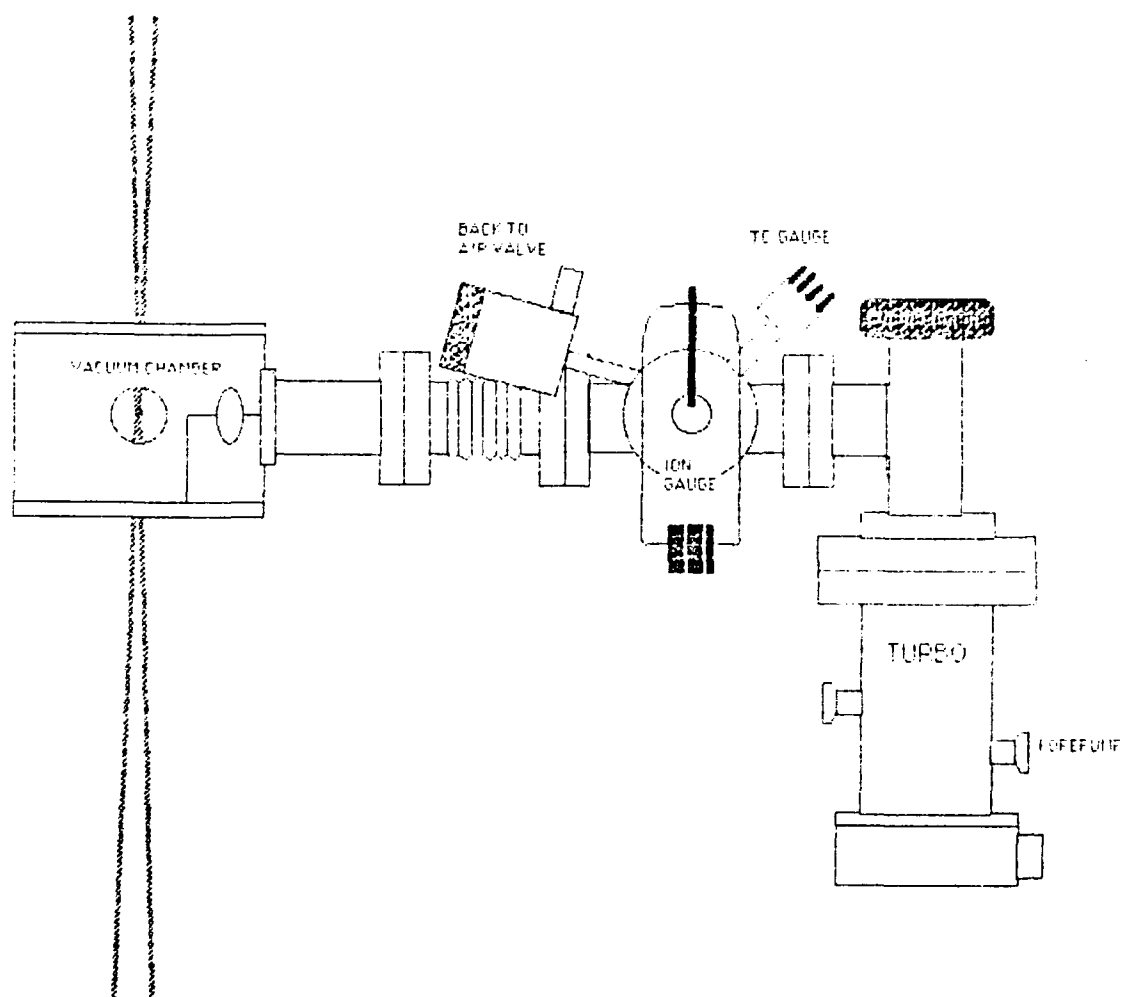


Figure 1. A skematic diagram of the vacuum system, consisting of a Turbo-molecular pump, forepump, and associated mechanical parts.

When a vacuum is pulled, the flexible coupling contracts. This puts a strain on the mounting of the vacuum chamber. The viewing system (especially the height servo system) is very sensitive to small angle tilts. In order to avoid displacing the vacuum chamber, the turbo-molecular pump is mounted on a precision translation slide which allows it to move closer to the chamber.

A small back-to-air valve vents the chamber between vacuum runs. Early in the experiment, we observed that a fog appeared within the vacuum chamber when a vacuum run was initiated. This fog was clearly visible in the laser illumination beam, and a considerable reduction in transmitted light resulted from scattering in the fog. Consequently, a dry Nitrogen supply was used to fill the chamber between vacuum runs.

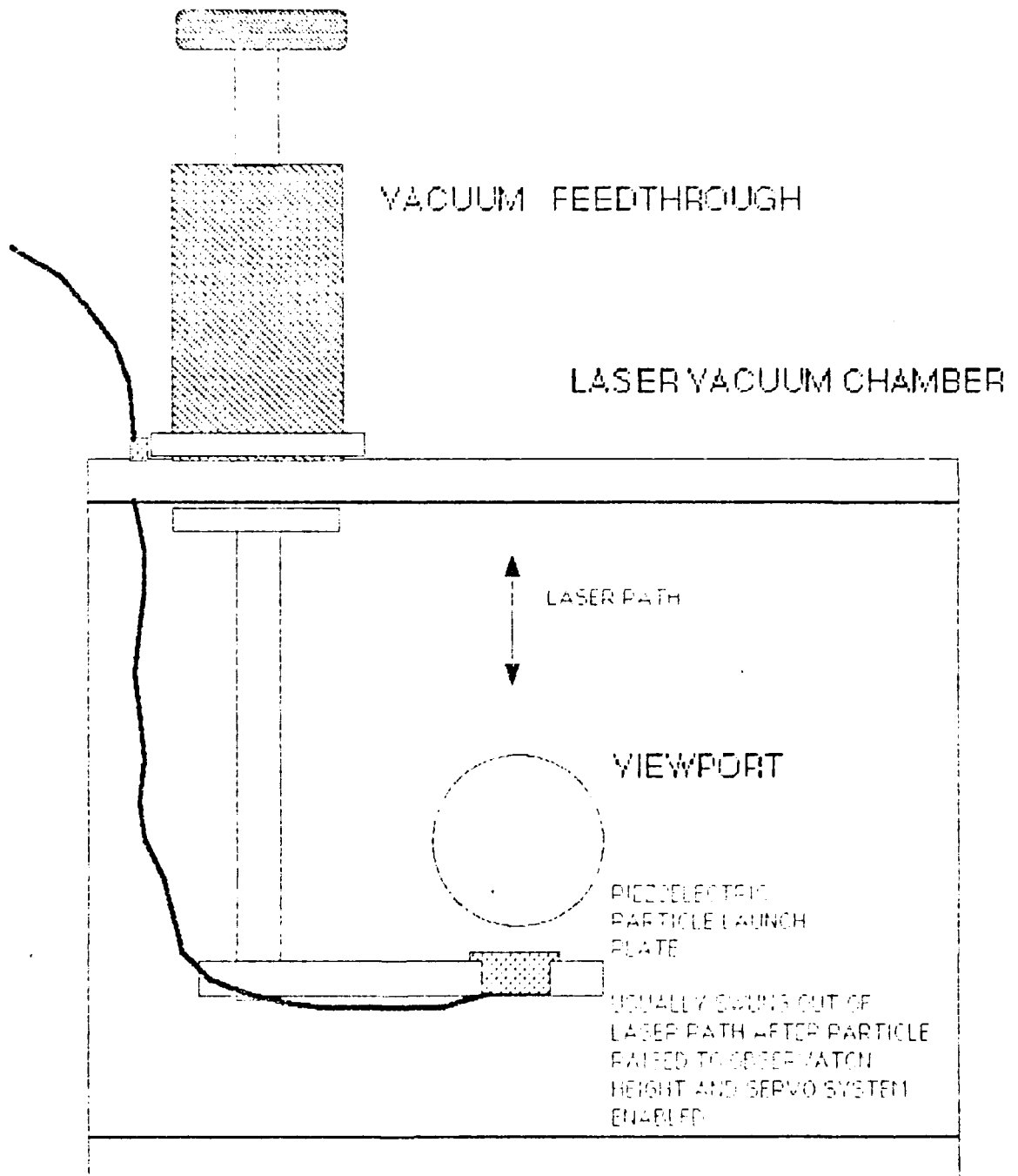


Figure 2. A skematic diagram of the vacuum chamber and and the launching plate.

#### PARTICLE IMAGING SYSTEM:

In order to investigate the dynamics of a vacuum-levitated particle, we devised a video imaging system which would provide relatively high time-resolution images of the levitated particle. This is an extension of the television imaging system used in earlier experiments. A high-resolution CCD camera was interfaced to the data acquisition computer. This camera was placed so as to image the vertical (0 degree) and side views of the particle. A high speed frame grabber allowed digital storage of 8 sequential video frames at intervals of 1/60th of a second. The camera allowed re-scanning of 1/4 of the frame 4 times per "frame" to allow a time resolution (for 1/4 frame images) of 1/240th of a second.

For viewing of the side image (90 degrees) a small red laser was mounted as an illumination source. Thus the green 90 degree image from the levitation laser could be directed to the height servo detector while the red image was directed to the video system.

#### HEIGHT SERVO SYSTEM:

When a small particle is levitated in air, stability is provided by the damping effect of the air. This facilitates "trapping" of the particle in the laser illumination beam, and damps out perturbation caused by radiometric forces (due to particle surface heating) on the particle. In a vacuum this damping is lacking, and some sort of external stabilization becomes necessary. We imaged the 90 degree image of the particle on a split photodiode to provide feedback on the height of the particle. The computer system processed the height data and provided an error rate damped feedback signal to modulate the laser power.

The natural frequency of a levitated particle in the size range used in our research is a few tens of hertz. Since the power supply for the laser has provision for external modulation at frequencies of more than 100 hertz, we modulate the laser power supply to provide feedback. The alternative of using an electro-optical modulator in the laser beam was not feasible since (at the time that the equipment was purchased for the experiment) no reasonably priced electro-optical modulator was available which could handle the laser beam power (up to 18 watts).

## EXPERIMENTAL RESULTS:

The height servo sensor worked well at atmospheric pressure. An oscillating particle "freezes" when the servo system is activated, and remains at essentially a constant height, even as the position of the focus of the laser beam is moved up and down. However, as the pressure in the chamber was reduced, several problems developed.

First, the particle was observed to "drift" downward steadily as the vacuum was pulled. Initially this was ascribed to the development of the "fog" mentioned above. However, even after dry Nitrogen was used as the working gas, eliminating the fog, the downward drift continued to be observed. Eventually the particle was pulled below the range of the height servo detector and it immediately dropped. After considerable experimentation with changes in the vacuum pumping rate, location of the vacuum port on the chamber, etc., it was concluded that the flow of gas from the chamber was the source of the problem. The servo system equations were modified to include an integral term which reflected continuous displacement of the particle from the desired height. This was successful, allowing rapid pumping without any significant downward displacement of the particle. The servo system increased the laser power by as much as a factor of 3 over the power necessary to levitate at 1 atmosphere while in the process of holding the height constant during pumping.

In spite of maintenance of constant height during pumping, after the pressure in the chamber dropped below approximately 50 Torr, the particle always became increasingly unstable, oscillating in the vertical direction with increasing amplitude and frequency. It was clear that the height servo system was unable to stabilize the particle as the pressure became low. The oscillations were observed at frequencies of several kilohertz - clearly much faster than the response of the laser power supply.

We were able to locate another means of modulating the laser beam at a high enough frequency to damp out these oscillations. An electro-optical modulator was obtained on loan which was rated at 10 watts maximum power (barely enough as we had observed power excursions exceeding 4 watts when stabilizing the downward drift of the particle during pumping). This modulator allowed a beam up to 2.5 mm to pass safely and unobstructed. Unfortunately, although the laser beam in use was specified as 1.6 mm diameter, it was - in fact - somewhat more than 3 mm in diameter. Careful realignment of the laser was unsuccessful in reducing the beam diameter.

Numerous attempts were made to levitate the particle initially in vacuum. Unfortunately, the particle generally

leaves the launching plate with some sideward motion which takes it through the optical trap above the laser focus. In the absence of damping, the particle does not remain in the trap. Although we managed to keep particles in the trap for short periods in vacuum (less than 2 seconds), we did not manage to hold a particle stable for a period long enough to investigate its dynamic properties.

## CONCLUSIONS

Even though our prime objective was not met, we brought the experiment to a level where the utilization of minor equipment and electronics can take us in a very short time to get the answers that we were unable to obtain. The Principal Investigator (Misconi) and one Co-I (Rusk), have recently joined The Space Research Institute (SRI), at The Florida Institute of Technology (FIT). The Facility was moved to FIT under a Collaborative Agreement with The University of Florida (the sole owner of all inventions made so far). We intend to continue the research under this collaborative agreement between UF and FIT at the FIT Campus.

The following is a list of suggested follow up research (for Phase Three as was done in the last two phases) that we intend to conduct with the help of FIT resources and other funds that we are in the process of seeking:

- 1- Stabilize the particle levitation in vacuum for periods sufficient enough (order of a day or two) so we can establish a) the spin axis orientation with respect to the laser beam direction, b) the rate of rotation and the rotational acceleration. This will lead to determining the effective moment arm of the rotation (a physical parameter indicating the degree of the irregularities on the surface of the particle).
- 2- Repeat the experiment for different particles until a canonical value of the effective moment arm is established.
- 3- To accomplish 1) and 2), one must develop an adequate imaging system using the TV cameras that we have to get a high quality good image of the particle in order to determine it's shape and the orientation of the spin axis.
- 4- We want also to study most of the strong and weak optical forces that play a role in levitation and rotation of the particle. This will lead to a thorough understanding of the physics and the dynamics of laser-particle interaction.

## REFERENCES

Ashkin A. and Dziedzic, J.M., (1977), App. Phys. Letters,  
Vol. 30, No.4, 202-204.

DYNAMICAL FORCES ON SOLID PARTICLES NEAR EARTH  
AND INTERPLANETARY SPACE

BY

N.Y. MISCONI\* AND E.T. RUSK\*  
SPACE ASTRONOMY LABORATORY  
UNIVERSITY OF FLORIDA

---

\* PRESENTLY AT THE  
SPACE RESEARCH INSTITUTE  
CENTER FOR SPACE SCIENCE RESEARCH  
FLORIDA INSTITUTE OF TECHNOLOGY

# TABLE OF CONTENTS

	PAGE
INTRODUCTION.....	1
RADIATION PRESSURE.....	2
POYNTING-ROBERTSON DRAG.....	5
P-R DRAG AND ITS EFFECT ON THE SPATIAL DENSITY DISTRIBUTION OF INTERPLANETARY DUST.....	12
COULOMB DRAG.....	13
FORCES PERTURBING SOLID PARTICLES IN AN EARTH'S ORBIT.	18
ION PRESSURE AND RADIATION PRESSURE .....	24
ION PRESSURE AND RADIATION PRESSURE UNDER SHOCK CONDITIONS.....	26
ION DRAG AND P-R DRAG UNDER SHOCK CONDITIONS .....	27
PARTICLE SPIN DUE TO THE WINDMILL EFFECT.....	30
PARTICLE SPIN DUE TO THE ALBEDO/ RADZIEVSKII EFFECT...	31
PARTICLE SPIN DUE TO SOLAR WIND IONS.....	34
PARTICLE ELECTRIC CHARGE.....	41
PARTICLE INTERACTION WITH THE INTERPLANETARY MAGNETIC FIELD.....	43
PARTICLE-PARTICLE COLLISION.....	49
PARTICLE INTERACTION WITH SPACE-BASED LASER BEAMS.....	51
CONCLUSIONS.....	53
REFERENCES.....	56

## INTRODUCTION

This report deals with the many complex forces that act on solid particles near Earth and interplanetary space. The purpose is have a general understanding of how these forces act, their origin, and their magnitude relative to each other. This report can be used as a first step in trying to understand what happens to particles when they are released in a space environment. Examples of these situations are the chemical release experiments on board CERES that are being planned by NASA, waste materials ejected from the space shuttle, Earth orbiting debris, and in general solid particles in interplanetary space.

The report covers all the important dynamical forces that effect particles in space which are caused by solar radiation, solar wind, the interplanetary magnetic field, and the Earth's magnetic field. It also contains an in depth analysis of the spin of the particles due to several mechanisms. Conclusions are made as to which forces are dominant which eventually determines the fate of these particles. A brief description of the interaction of small particles with laser beams in a space environment is included.

## A. RADIATION PRESSURE

Solar photons are absorbed and reflected by interplanetary particles, also including large bodies such as the planets themselves. J. H. Poynting (1903) formulated an expression for the force on a particle due to solar radiation which was later rigorously re-derived by H.P. Robertson (1937) using special relativity. Re-written in vector notation, this expression is

$$m \frac{d\vec{v}}{dt} = \frac{\alpha Q_{pr} c}{r^2} \left[ \left(1 - \frac{\dot{r}}{c}\right) \vec{r} - \frac{\vec{v}}{c} \right], \quad (\text{A.1})$$

where  $\vec{v}$  is the velocity of the particle of mass  $m$ ,  $c$  is the speed of light,  $r$  is the distance to the source and  $\vec{r}$  is the unit vector directed from the source to the particle. Dots denote time derivatives and the total radiation momentum intercepted by a particle at unit distance per unit time is  $3 E_{\odot} / (16\pi \rho s) \equiv \alpha c$ . Here  $E_{\odot}$  is the solar luminosity and  $\rho$  and  $s$  are the density and radius, respectively, of the particle.

$Q_{pr}$  is called the radiation pressure efficiency factor and is defined from the corresponding efficiency factors of absorption and scattering ( $Q_{abs}$  and  $Q_{sca}$ ) which are the ratios of the absorption and scattering cross-section to the geometrical area of the particle. The definition is then:

$$Q_{pr} = Q_{abs} + (1 - \overline{\cos \theta}) Q_{sca} \quad (\text{A.2})$$

where  $\cos \theta$  is determined by the geometry of the scattered radiation.

### Scattering Geometry

### $\overline{\cos \theta}$

pure forward scattering  
isotropic scattering  
pure backscattering

+1  
0  
-1

For large particles,  $Q_{pr}$  can never be less than 0 (for perfectly transparent particles) or greater than 2 (for a perfect reflector). In general,  $Q_{pr}$  is a function of a particles' size and electrical properties, as well as the wavelength of the radiation. An iron sphere Van de Hulst (1957, p. 276) is plotted in Figure 1 as an example. It can be seen that when the size of a particle is comparable to the wavelength of the radiation,  $Q_{pr}$  can reach values greater than the limits imposed by geometrical optics.

Each term in equation 1 can be considered separately, since forces are additive. The radially directed term which is independent of the velocities of both the source and the particle is frequently called the radiation pressure force. Because the radiation pressure decreases as the inverse of the square of the distance from the source, as does the gravitational force, an object in orbit about the sun will move as if the sun were a dark body of lesser mass. The equations of motion of an object under the influence of radiation pressure and the solar gravitational force alone are

$$\ddot{r} - r \dot{\theta}^2 = \frac{\alpha Q_{pr} c - G M_{\odot}}{r^2}, \quad (\text{A.3})$$

where  $G$  is the gravitational constant and  $M_{\odot}$  is the mass of the Sun. If  $\alpha$  is constant in time, these equations reduce to the usual conic solution of a gravitational field by substituting

$$M'_{\odot} \equiv M_{\odot} - \frac{\alpha Q_{pr} c}{G} \equiv M_{\odot} (1 - \beta) \quad (A.4)$$

For  $M'_{\odot}$ , where the ratio of radiation pressure force to gravitational force,

$$\beta = (\alpha Q_{pr} c) / (GM_{\odot}) \quad (A.5)$$

$M'_{\odot}$  is then the "effective mass" of the central force field.

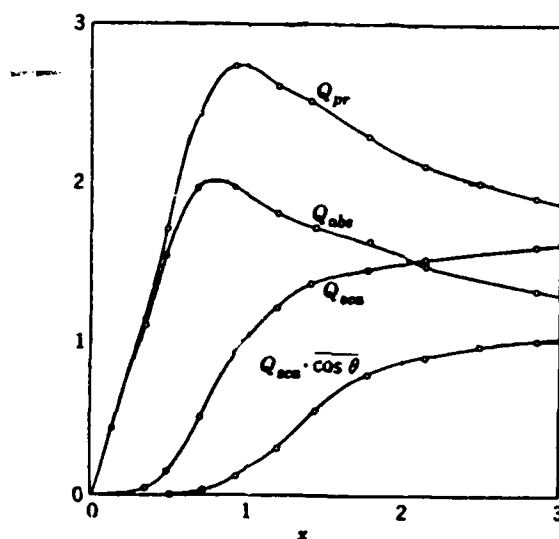


Figure 1. Radiation Efficiency factors plotted versus relative size,  $x = 2\pi r/\lambda$ , for an idealized iron sphere of complex refractive index  $m = 1.27 - 1.37i$  (van de Hulst, 1957, p. 276)

If the value of  $\alpha$  changes, then the change in the effective mass of the central field will send the particle into new orbit. This can occur when the particle size is reduced, as, for example, when a small particle breaks off from a larger "parent" body. In the usual case of a decrease in particle size, the new orbit of a particle will become more eccentric and the semi-major axis will increase. In particular if,

$$\beta > 1/2 (1 - e_0 \cos E_0) \quad (A.6)$$

where  $e_0$  is the eccentricity of the parent body and  $E_0$  is the eccentric anomaly of the parent body at release, the particle will be released into an hyperbolic orbit. Solar flares will also cause a change in the orbits of interplanetary dust, from the temporary increase in solar luminosity, but these changes are expected to be small because of the short duration of the flares. This can be observed from the expression for the net change in semi-major axis of a particle after a flare occurs.

The new semi-major axis ( $a$ ) relates to the original semi-major axis ( $a_0$ ) by the equation

$$a = a_0 \left[ 1 - \frac{2a_0(r-r_0)}{rr_0} \left( 1 - \frac{\mu_f}{\mu_0} \right) \right]^{-1}, \quad (\text{A.7})$$

where  $r_0$  and  $r$  are the radial distances from the sun at the beginning and the end of the flare respectively, and  $\mu_0$  and  $\mu_f$  are the respective "effective masses" of the sun before and during a flare, multiplied by the gravitational constant. Unless  $\Delta r (\equiv r - r_0)$  is large, the change in semi-major axis ( $\Delta a$ ) can be approximated by the expression

$$\Delta a \approx \frac{2\Delta\beta}{1-\beta_0} \left( \frac{a_0}{r_0} \right)^2 \Delta r, \quad (\text{A.8})$$

where  $\beta_0$  is the force ratio for a quiet sun and  $\Delta\beta$  is the change in due to the flare. Because of the short duration of solar flares,  $r$  will be quite small unless the particle is very close to the sun.

Sublimation and sputtering will also change the value of  $\alpha$ . Sublimation effects only become important near the sun, and here, Belton (1963) discovered that the orbit of a small particle will reach a stable semi-major axis due to this effect. More will be said about this after the section on Poynting-Robertson drag.

## B. POYNTING-ROBERTSON DRAG

In the early part of this century, J. H. Poynting (1903) considered the effects of the absorption and subsequent re-emission of sunlight by small isolated particles in the solar system. His findings were later modified by H. P. Robertson, who used a relativistic treatment of the problem to establish the equations of motion for interplanetary particles. The motion of each particle creates a force of order in  $v/c$  ( $v$ , particle velocity;  $c$ , velocity of light) from the solar radiation due to both the Doppler shift of the radiation and an aberration effect. These two second order effects combine to form the Poynting-Robertson (henceforth; P-R) drag. This drag force opposes the motion of the dust particle, reducing the particle's orbital velocity and hence, the kinetic energy of its orbit. The retarding force results in a slow secular decrease in semi-major axis and eccentricity of the orbit of any small body. Ultimately the body will fall into the sun.

The assumptions in deriving this force are as follows: (1) the particles are spherical and of uniform density, (2) their size is larger than the critical size where radiation pressure overcomes the sun's gravitational attraction (see section A), (3) the size should be larger than the wavelength of light so that diffraction effects are not appreciable, (4) the particles absorb all incident radiation from the sun and re-emit this radiation isotropically at the same rate over a cross-section of  $\pi s^2$ , where  $s$  is the radius of the particle. This assumption was modified by Burns, et al. (1979) and is discussed below.

From Robertson's (1937) expression, we can derive the equations of motion of a particle under the combination of gravitation, radiation pressure, and P-R drag. The force equation in vector form is

$$m \ddot{\vec{r}} = (m\mu\vec{r}/r^3) + (m\alpha c/r^3) \cdot (\vec{r} - 2\dot{\vec{r}}\vec{r}/c - r^2\dot{\hat{\theta}}\hat{\theta}/c). \quad (B.1)$$

The left hand side of this equation can be written in terms of the vector components on the right hand side of the equation by twice taking the time derivative of the position vector  $\vec{r}$ . The time derivative of any vector involves derivatives of both the magnitude of the vector and of the direction, or

$$\frac{d\vec{r}}{dt} = \frac{d(r\hat{r})}{dt} = \hat{r} \frac{dr}{dt} + r \frac{d\hat{r}}{dt} \quad (B.2)$$

The term involving the change in direction will be perpendicular to the position vector, so this expression can be re-written

$$\frac{d\vec{r}}{dt} = \hat{r} \frac{dr}{dt} + \vec{\omega} \times \vec{r} \quad (B.3)$$

where the vector  $\vec{\omega} \times \vec{r}$  has a direction normal to  $\hat{r}$  which is in fact  $\hat{\theta}$ , and the magnitude of  $\vec{\omega}$ ,  $|\vec{\omega}| = \dot{\theta}$ . This equation for the time derivative of a vector will hold for any vector, if  $\vec{\omega}$  is chosen appropriately.

Equation 1 can now be written as

$$m \frac{d}{dt} (\dot{\vec{r}} + \vec{\omega} \times \vec{r}) = -\frac{m\mu\hat{r}}{r^2} + \frac{m\alpha c}{r^2} \left( \hat{r} - \frac{2\dot{\vec{r}}\hat{r}}{c} - \frac{r\dot{\theta}\hat{\theta}}{c} \right) \quad (B.4)$$

or, once again using expression B.3, and dividing by  $m$ ,

$$\begin{aligned}
& \ddot{\hat{r}} + \vec{\omega} \times \dot{\hat{r}} + \dot{\omega} \hat{\omega} \times \hat{r} + \vec{\omega} \times \dot{\hat{r}} + \vec{\omega} \times (\vec{\omega} \times \hat{r}) \\
& = \frac{1}{r^2} (-\mu + \alpha c - 2\alpha \dot{r}) \hat{r} - \frac{\alpha \dot{\theta} \hat{\theta}}{r} .
\end{aligned} \tag{B.5}$$

Collecting terms and substituting for  $\vec{\omega} \times \hat{r} = \dot{\theta} \hat{\theta}$ , we get two equations in the  $\hat{r}$  and  $\hat{\theta}$  directions respectively:

$$\ddot{r} - r\dot{\theta}^2 = -\frac{(\mu - \alpha c)}{r^2} - \frac{2\alpha \dot{r}}{r^2} \tag{B.6}$$

$$2\dot{r}\dot{\theta} - r\ddot{\theta} = -\frac{\alpha \dot{\theta}}{r} \tag{B.7}$$

Equation B.7 can be written as

$$\frac{1}{r} \frac{d}{dt} (r^2 \dot{\theta}) = -\frac{\alpha \dot{\theta}}{r} \tag{B.8}$$

and integrated to give

$$r^2 \dot{\theta} = h - \alpha \theta \tag{B.9}$$

If the P-R drag terms

$$\vec{F}_{PR} = \frac{m\alpha c}{r^2} \left( \frac{2\dot{r}}{c} \hat{r} - \frac{r\dot{\theta}}{c} \hat{\theta} \right) \tag{B.10}$$

are considered as perturbations on an osculating orbit, inserted into the Gaussian perturbation equations and integrated over one orbit holding the orbital elements constant, then we can derive the time rate of change of semi-major axis (a) and eccentricity (e).

$$\frac{da}{dt} = \frac{2}{n\sqrt{1-e^2}} \left[ S e \sin f + \frac{a(1-e^2)}{r} T \right], \tag{B.11}$$

and

$$\frac{de}{dt} = \frac{\sqrt{1-e^2}}{na} \left[ S \sin f + T (\cos E + \cos f) \right], \tag{B.12}$$

where S and T are the radial and tangential components of the perturbing acceleration, n is the frequency of the orbit and f and E are the true anomaly and eccentric anomaly respectively. Now

$$\begin{aligned}
 \frac{da}{dt} &\approx \frac{1}{P} \oint_{\text{ONE ORBIT}} da \\
 &= \frac{1}{\pi \sqrt{1-e^2}} \int_0^P \left[ \frac{2\alpha \dot{r}}{r^2} e \sin f + (1+e \cos f) \frac{\alpha \dot{\theta}}{r} \right] dt \quad (\text{B.13})
 \end{aligned}$$

where  $P = 2\pi/n$  (= orbital period), and

$$\begin{aligned}
 \dot{r} &= e \sin f \left( \frac{na}{\sqrt{1-e^2}} \right) \\
 r\dot{\theta} &= (1+e \cos f) \left( \frac{na}{\sqrt{1-e^2}} \right)
 \end{aligned}$$

$$r = \frac{a(1-e^2)}{1+e \cos f}$$

so

$$\frac{da}{dt} = \frac{\alpha n}{\pi a (1-e^2)^{3/2}} \int_0^P \left[ 2e^2 \sin^2 f + (1+e \cos f)^2 \right] (1+e \cos f)^2 dt \quad (\text{B.14})$$

and

$$dt = \frac{(1-e^2)^{3/2}}{n(1+e \cos f)^2} df \quad (\text{B.15})$$

therefore

$$\begin{aligned}
 \frac{da}{dt} &= \frac{-\alpha}{\pi a (1-e^2)^{3/2}} \int_0^{2\pi} \left[ 2e^2 \sin^2 f + (1+e \cos f)^2 \right] df \\
 &= \frac{-\alpha}{\pi a (1-e^2)^{3/2}} \left[ 2e^2 \pi + 2\pi + e^2 \pi \right] \\
 &= \frac{\alpha (2+3e^2)}{a (1-e^2)^{3/2}} \quad (\text{B.16})
 \end{aligned}$$

likewise

$$\begin{aligned}
 \frac{de}{dt} &= \frac{\sqrt{1-e^2}}{2\pi a} \int_0^P \left[ \frac{2\alpha}{r^2} \frac{na}{\sqrt{1-e^2}} e \sin^2 f + (e + 2\cos f + e^2 \cos^2 f) \frac{na\alpha}{r^2 \sqrt{1-e^2}} \right] dt \\
 &= \frac{-\alpha}{2\pi a^2 \sqrt{1-e^2}} \int (2e + e \sin^2 f + 2\cos f) df \\
 &= \frac{-\alpha}{2\pi a^2 \sqrt{1-e^2}} [4\pi e + \pi e] \\
 &= \frac{-5\alpha e}{2a^2 (1-e^2)^{1/2}}
 \end{aligned} \tag{B.17}$$

If we deal with initially circular orbits, equation (B.16) is simplified and integrates to

$$t = \frac{a^2}{4\alpha} = 7.0 \times 10^6 s \rho a_0^2 \tag{B.18}$$

where  $t$  is the total time of fall for the particle in years, and  $s$  and  $\rho$  are the particle's radius (cm) and density (gm/cm<sup>3</sup>) respectively and  $a_0$  is the initial semi-major axis of the particle in A.U. (astronomical units). For a more general case, i.e. considering eccentric orbits, an integrable relation between  $a$  and  $e$  can be found from dividing equation (6) by equation (7) and after integration:

$$a = \frac{C e^{4/5}}{1-e^2} \tag{B.19}$$

The constant in equation (B.19) should hold at all times for any given particle orbiting the sun. If the initial semi-major axis and eccentricity of the particle is given at any time, then one can compute the constant  $C$ :

$$C = a_0 e_0^{-4/5} (1-e_0^2) \tag{B.20}$$

Now, in order to find a relation involving only the eccentricity and time, Wyatt and Whipple (1950) find:

$$\frac{de}{dt} = - \frac{5\beta GM (1-e^2)^{3/2}}{2C^2 e^{3/5}} \tag{B.21}$$

or

$$t - t_0 = \frac{-2C^2 c}{5\beta GM} \int_{e_0}^e \frac{e^{3/5} de}{(1-e^2)^{3/2}}$$

$$= 1.13 \times 10^7 \rho s C^2 \int_{e_0}^e \frac{e^{3/5} de}{(1-e^2)^{3/2}}, \quad e_0 > e \quad (\text{B.22})$$

where  $C$  is measured in A.U. and  $s$  and  $\rho$  are in cm and  $\text{gm/cm}^3$ , respectively.  $(t - t_0)$  is in years and can be obtained since  $C$  can be evaluated using eq. B.20.

Wyatt and Whipple (1950) performed numerical integration (since the integral cannot be solved directly) and found the values of

$$G(e_0) = \int_0^{e_0} \frac{e^{3/5} de}{(1-e^2)^{3/2}} \quad (\text{B.23})$$

which are shown in table (1). Thus, using these values one can easily obtain the spiraling time to the sun of a particle in an eccentric orbit.

TABLE 1  
THE TIME INTEGRALS

$e$	$G(e_0)$	$(t-t_0)/10^7 \text{ s } \rho q^2$ years	$e$	$G(e_0)$	$(t-t_0)/10^7 \text{ s } \rho q^2$ years
0.00		0.704	0.78	0.771	4.10
.05	0.0052	0.778	.80	0.846	4.42
.10	.0158	0.858	.81	0.889	4.60
.15	.0305	0.946	.82	0.934	4.79
.20	.0489	1.04	.83	0.983	5.00
.25	.0710	1.15	.84	1.04	5.23
.30	.0969	1.27	.85	1.10	5.49
.35	.127	1.40	.86	1.16	5.77
.40	.162	1.55	.87	1.23	6.08
.45	.202	1.72	.88	1.32	6.43
.50	.249	1.92	.89	1.41	6.83
.55	.305	2.15	.90	1.51	7.29
.60	.370	2.42	.91	1.63	7.82
.62	.400	2.54	.92	1.78	8.45
.64	.432	2.68	.93	1.96	9.22
.66	.468	2.82	.94	2.17	10.17
.68	.506	2.98	.95	2.45	11.39
.70	.548	3.16	.96	2.82	13.06
.72	.595	3.36	.97	3.37	15.50
.74	.647	3.57	.98	4.30	19.60
0.76	0.705	3.82	0.99	6.37	28.89

However, a simplification was made in order to find the total spiraling times to the sun from any initial  $e$  and the perihelion distance of  $q$  by reducing equation (B.22) using equation (B.19) and since

$$q = a(1-e)$$

then

$$C^2 = q^2 (1 + e)^2 e^{-3/5}$$

and equation (B.22) will be

$$t - t_0 = 10^7 \rho q^2 \left[ \frac{1.13 (1 + e_0)^2}{e_0^{3/5}} \int_0^{e_0} \frac{e^{3/5} de}{(1 - e^2)^{3/2}} \right] \quad (\text{B.24})$$

Wyatt and Whipple give in table 1 the bracketed quantity in equation (B.24), which then gives the total spiraling times into the sun for any given particle. The second and fifth columns of table 1 may be used for the times between arbitrary eccentricities.

The P-R drag is very effective as a sink of interplanetary dust particles into the sun in astronomically short times. To give a simple example: a particle of 10 $\mu$ m radius, of medium density of 1 gm/cm<sup>3</sup> (fluffy particles), and in a circular orbit at the Earth's orbital distance will sink into the sun in 7,000 years. A particle in an eccentric orbit will reach the sun even more rapidly.

Recently, Burns et al. (1979) pointed out the departure from reality of assumption (4) as was noted earlier by Mukai et al. (1974), namely that the particles absorb all the light from the sun and re-emit the energy isotropically. In general, small particles scatter or transmit most of the energy incident on them. Lamy (1976) also noted this error but incorrectly considered the drag to be caused by the absorbed energy only, whereas the scattered energy is just as important. Also, Lyttleton (1976) derived these forces for a specific, but artificial, scattering law, and Hameen-Anttila (1962) treated the problem erroneously by multiplying the radiation force by a constant.

A small spherical particle of geometrical section  $\pi s^2 = A$  will scatter the light incident on an area  $AQ_{\text{sca}}$  and also absorb an amount  $AQ_{\text{abs}}$  (where  $Q_{\text{sca}}$  and  $Q_{\text{abs}}$  are the scattering and absorption efficiency factors, respectively). Figure 1 (Burns et al. 1979) illustrates the interaction of light with the particle and the efficiency factors mentioned above. These efficiency factors are wavelength dependent and they can be computed for dust in the solar system by integrating over the solar spectrum.

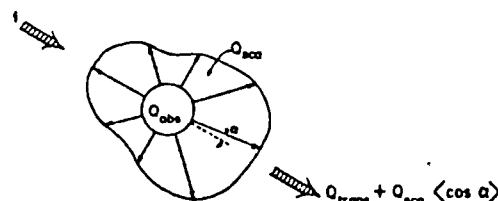


FIG. 1. An illustration of the efficiency factors of optics. One unit of energy is seen entering the upper left-hand edge:  $Q_{\text{abs}}$  is absorbed by the particle,  $Q_{\text{sca}}$  is scattered in a pattern that is symmetric about the radiation beam while  $Q_{\text{trans}}$  is transmitted. In the scattered beam a momentum of  $Q_{\text{sca}} \langle \cos \alpha \rangle$  is sent in the forward direction, where  $\langle \cos \alpha \rangle$  is the asymmetry factor, i.e., the weighted average of the angular dependence of the scattered radiation.  $Q_{\text{abs}} + Q_{\text{sca}} + Q_{\text{trans}} = 1$ , ignoring diffraction.

While Burns et al. (1979) go on and compute the radiation forces applied to particles which both scatter and absorb the radiation, we note here that the final outcome of the radiation force is given by:

$$F_{rad} = m\dot{v} = Q_{pr} M' (c-v) \quad (B.25)$$

and  $M' = M(1 - v \cos \xi / c)$ , where  $M$  is the "mass" of the photons striking the particle ( $h\nu/c^2$ ) and  $\xi$  is the angle between the radius vector from the source of radiation and the direction of motion of the particle. The radiation force here is really a drag force created by the relative velocity  $c - v$  of the particle subject to a beam of photons. The final form of this net force on the particle can be written to terms of order  $v/c$ :

$$m\dot{\vec{v}} \approx \frac{SAQ_{pr}}{c} \left[ \left(1 - \frac{\dot{r}}{c}\right) \hat{S} - \frac{\vec{v}}{c} \right] \quad (B.26)$$

where  $SA$  is the total energy intercepted per second from a radiation beam of integrated flux density  $S$  (ergs cm sec<sup>-2</sup>) by a stationary, perfectly absorbing particle of geometrical cross section  $A$ .  $S$  is a unit vector in the direction of the incident beam. For totally absorbing particles  $Q_{pr} = 1$ . This equation only differs from Robertson's (1937) expression by the addition of the concept of  $Q_{pr}$ .

For particles in heliocentric orbits  $\vec{v} = \dot{r}\hat{r} + r\dot{\theta}\hat{\theta}$ , where  $\hat{r} = \hat{S}$ , which is the orbital radius unit vector and  $\hat{\theta}$  is normal to  $\hat{r}$ . One can then write the radiation force equation as:

$$m\dot{\vec{v}} \approx \frac{SAQ_{pr}}{c} \left[ \left(1 - 2\dot{r}/c\right) \hat{r} - \frac{r\dot{\theta}}{c} \hat{\theta} \right] \quad (B.27)$$

the constant radial term is called the radiation pressure, and the velocity dependent portion the P-R drag. In order to understand the role  $Q_{pr}$  has in the radiation force equation one would consider the following: in complete absorption, which is the case considered by Robertson (1937),  $Q_{pr} = Q_{abs} = 1$ , in forward scattering of sunlight by these particles ( $\cos \theta = 1$ )  $Q_{pr} = 0$  which does not produce any radiation pressure or P-R drag since the radiation in this case does not see the particle, and isotropic scattering has  $Q_{pr} = Q_{sca}$ , or  $Q_{pr} = 1$ . In the case of perfect backscattering of light,  $Q_{pr} = 2$ , and the particles are subjected to twice the drag of a totally absorbing or an isotropically reflecting particle. This is so because in perfect backscattering twice the momentum of light is taken away from the particle.

C. P-R DRAG AND ITS EFFECT ON THE SPATIAL DENSITY  
DISTRIBUTION OF INTERPLANETARY DUST:

P-R drag, as we mentioned earlier, acts to reduce both eccentricities and semi-major axes of the particles. If one computes the dust concentration in the inner solar system (inside the Earth's orbit) and disregards eccentricity, the drift speed is

$$\frac{da}{dt} = -\frac{2\alpha}{a} \quad , \quad (C.1)$$

Where the negative sign implies the spiraling in of the dust towards the sun. The dust density in any incremental volume  $dV$  defined by the solid angle  $\Omega$  and thickness  $da$  at distance  $a$  from the sun is

$$\rho(a) = \frac{dn(a)}{dV} = \frac{1}{\pi a^2} \left| \frac{dn(a)}{da} \right| \quad , \quad (C.2)$$

where  $dn(a)$  is the number of dust particles in volume  $dV$ . Now the factor  $dn(a)/da$  can be re-written

$$\frac{dn(a)}{da} = \frac{\frac{dn(a)}{dt}}{\frac{da}{dt}} \quad (C.3)$$

If we assume a constant source of interplanetary dust outside the Earth's orbit, the creation rate  $dn(a)/dt$  should be a constant. Substituting equation C.1 into equation C.3 and then the result into equation C.2, we get

$$\rho(a) = \frac{1}{2\pi\alpha a} \frac{dn(a)}{dt} \quad , \quad (C.4)$$

or defining  $\rho_0 = \rho(a=1)$  ,

$$\rho(a) = \rho_0 \left( \frac{1}{a} \right) \quad (C.5)$$

This result shows that, (from the P-R drag alone), one can expect the spatial density distribution of interplanetary dust in the inner region of the solar system to follow a power law of  $n \propto r^{-1}$  , where  $r$  is the heliocentric distance.

### D. Coulomb Drag

In this section we will deal with the interaction of interplanetary particles with the steady flow of electrons in the solar wind. We first consider a particle of radius  $s$  moving through an electron gas with a speed  $W$  and in the direction  $z$  relative to the electrons which move in a monodirectional stream with velocity components  $v_x, v_y, v_z$ . Let us first consider the electrons that actually hit the particle and bounce back. The force ( $F_1$ ) from these impinging electrons can be formulated as:

$$F_1 = \{\text{momentum transfer/electron}\} \times \{\# \text{ of electrons/unit time}\} \quad (D.1)$$

All electrons with an impact parameter less than  $S_1$ , will hit the particle. Then the force can also be written as

$$F_1 = \{\text{momentum transfer/electron}\} \times \{\text{number density of electrons}\} \times \{(\text{volume}) \text{ per unit time}\} \quad (D.2)$$

where the volume is just  $\pi s_1^2 v dt$ ,  $v$  being the relative velocity of each electron with respect to the particle. Now since the momentum transfer depends on the velocity of each electron, we write the increment of force delivered from each increment of velocity space

$$\begin{aligned} dF_1 &= \{\text{momentum transfer/electron}\} \\ &\quad \times \{\# \text{ density of electrons/unit velocity space}\} \\ &\quad \times \{\text{volume per unit time}\} \times \{\text{increment of velocity space}\} \\ &= \{\Delta p\} \{N(v)\} \{V/dt\} \{d^3v\} \end{aligned} \quad (D.3)$$

The momentum transfer of each electron ( $p$ ) is

$$\Delta p = m_e v (1 - \cos \theta) \quad (D.4)$$

where  $m_e$  is the mass of the electron,  $v$  is its relative velocity with respect to the dust particle and  $\theta$  is the angular change in direction of the scattered electron (effectively  $90^\circ$  in the case of absorption). Although  $\theta$  varies from electron to electron, when we sum over all electrons striking the particle then the expression  $(1 - \cos \theta)$  becomes the average  $\langle 1 - \cos \theta \rangle$ . In this case,

$$p = m_e v \langle 1 - \cos \theta \rangle \quad (D.5)$$

To find an expression for the maximum impact parameter  $s_1$ , we use the laws of conservation of angular momentum ( $\mathcal{L}$ ) and energy ( $\mathcal{E}$ ) (Goldstein, Classical Mechanics, p. 82).

$$\mathcal{L} = m_e v s_1 = m_e v_2 s \quad (D.6)$$

or

$$s_1 = s^2 v_2^2 / v^2$$

where  $v_2$  is the electron velocity at distance  $s$  from the center of the particle, and

$$\mathcal{E} = \frac{1}{2} m_e v^2 = \frac{1}{2} m_e v_2^2 - e V_0 \quad (\text{D.7})$$

so

$$v_2^2 = v^2 + \frac{2eV_0}{m_e} \quad (\text{D.8})$$

or

$$s_1^2 = \frac{s^2}{v^2} \left( v^2 + \frac{2eV_0}{m_e} \right) = s^2 \left( 1 + \frac{2eV_0}{m_e v^2} \right) \quad (\text{D.9})$$

For convenience, we will substitute

$$\beta^2 \equiv \frac{2eV_0}{m_e} \quad (\text{D.10})$$

where  $\beta$  is the escape velocity of an electron from the surface of the particle. Then

$$s_1^2 = s^2 \left( 1 + \beta^2 / v^2 \right) \quad (\text{D.11})$$

Incidentally, we can determine the value of  $\beta$  by substituting numerical values for the constants in equation D.10. We then get

$$(\text{D.12})$$

or  $\beta = 1,886 \text{ km./sec.} \sim 5 v_{\text{sw}}$ . This result will be used later.

The volume per unit time is the area implied by the impact parameter times the velocity or

$$\pi s^2 (1 + \beta^2 / v^2) v \quad (\text{D.13})$$

We can use the Maxwellian displacement velocity distribution for the second term in equation D.3 to get

$$\begin{aligned} F_1 &= \int_{\text{velocity space}} \langle 1 - \cos \theta \rangle m_e v N(v) \pi s^2 \left( 1 + \frac{\beta^2}{v^2} \right) v dv \\ &= \pi s^2 m_e \langle 1 - \cos \theta \rangle \int_{\text{v.s.}} N(v) \left( 1 + \frac{\beta^2}{v^2} \right) v^2 dv \end{aligned} \quad (\text{D.14})$$

In the interplanetary environment, the solar wind velocity is much greater than the thermal velocity of the electrons, as well as the space velocity of the dust. Therefore we will assume that all electrons are travelling at their average velocity  $v_{\text{sw}}$ . Then the number density of electrons per unit velocity space is a delta function ( $v_{\text{sw}}$ ) times the number density  $N_e$ . The integral then becomes

$$F_1 = \langle 1 - \cos \theta \rangle m_e N_e \int_{v.s}^{\infty} \delta(V_{sw}) \pi s^2 (1 + \beta^2/v^2) v^2 dv \quad (D.15)$$

which gives

$$F_1 = \langle 1 - \cos \theta \rangle m_e N_e \pi s^2 (v_{sw}^2 + \beta^2) \quad (D.16)$$

We can judge the magnitude of  $F_1$  by comparing it with that from ion collisions ( $F_i$ ). Approximating, we get

$$F_1 \approx \pi s^2 m_e v_{sw}^2 N_e (1 + \beta^2/v_{sw}^2), \quad (D.17)$$

and

$$F_i \approx \pi s^2 \langle M_i \rangle v_{sw}^2 N_i. \quad (D.18)$$

Since, the solar wind is a neutral plasma,  $N_e = N_i$ , the ratio becomes

$$\frac{F_1}{F_i} = \frac{m_e}{\langle M_i \rangle} (1 + \frac{\beta^2}{v^2}) \sim 10^{-2} \quad (D.19)$$

The contribution from impacting electrons is negligible.

Now we consider the drag force due to Coulomb-deflected electrons ( $F_2$ ). These electrons do not strike the particle but nevertheless transfer momentum to the particle through the electromagnetic force. In this case, the angle of deflection ( $\theta$ ) depends on the velocity of each electron and its impact parameter. The volume is larger, and we must integrate over all possible impact parameters ( $s_2$ ). Each increment of volume is

$$dV = 2\pi s_2 ds_2 v dt \quad (D.20)$$

We can find  $\theta$  in terms of  $s_2$  and  $v$  from classical electrodynamics (cf. Goldstein, p.83). We get an expression for  $\theta$ ,

$$\tan \frac{\theta}{2} = \frac{e V_0 s}{m_e v^2 s_2} = \frac{1}{2} \cdot \frac{s}{s_2} \cdot \frac{\beta^2}{v^2} \quad (D.21)$$

where  $V_0$  is the electrostatic potential of the particle and  $s$  is its size (radius for spherical particles). Substituting into equation D.3, we get

$$dF_2 = \int_{s_2=s_1}^{s_{MAX}} \left\{ m_e v_z (1 - \cos \theta) \right\} \cdot \left\{ N_e(v) \right\} \left\{ \frac{2\pi v s_2 ds_2 dt}{dV} \right\} dV \quad (D.22)$$

We can separate terms in  $s_2$  and integrate

$$dF_2 = 2\pi N_e(v) v_3 m_e dv_x dv_y dv_z \int_{s_2=s_1}^{s_{max}} s_2 (1 - \cos \theta) ds_2 \quad (D.23)$$

now  $1 - \cos \theta = 2 \tan^2 \frac{\theta}{2} / (1 + \tan^2 \frac{\theta}{2})$ , so the integral term in equation D.23 is

$$I(s_2) = 2 \int_{s_2=s_1}^{s_{max}} s_2 \frac{\tan^2 \frac{\theta}{2}}{1 + \tan^2 \frac{\theta}{2}} ds_2 \quad (D.24)$$

or substituting for  $\tan^2 \frac{\theta}{2}$  and multiplying top and bottom by  $s_2$ ,

$$I(s_2) = 2 \int_{s_2=s_1}^{s_{max}} s_2 \frac{l^2 ds_2}{s_2^2 - l^2}, \quad \text{with } l^2 \equiv \frac{\beta^4 s^2}{v^4}, \quad (D.25)$$

where  $s_{max}$  is the "shielding radius" of the particle. This is the distance from the particle such that the total charge of the electrons inside  $s_{max}$  equals the charge of the particle plus the positive ions inside  $s_{max}$ . Electrons outside this region "see" it as a neutrally charged area and thus are not deflected.  $F_2$  is fairly insensitive to the value of  $s_{max}$ , and that is fortunate, since it is difficult to accurately determine the shielding radius. We shall take it to be of the order of the distance between electrons ( $s_{max} = N_e^{-1/3}$ ). Equation D.25 then integrates to

$$I(s_2) = \frac{\beta^4 s^2}{v^4} \left[ \ln(s_{max}^2 - \frac{\beta^4 s^2}{v^4}) - \ln(s_1^2 - \frac{\beta^4 s^2}{v^4}) \right] \quad (D.26)$$

The case of  $v_w/c \gg 1$  ( $c^2 \equiv \frac{2kT_e}{m} = \text{velocity of sound}$ )

Since  $v_w/c \gg 1$ , we can ignore the thermal velocity of the electrons. Then, as was the case for impacting electrons, we substitute  $N_e \delta(v_{sw})$  for  $N(v)$ , to get

$$F_2(v_w \gg c) = 2\pi m_e N_e \left( \frac{\beta^4 s^2}{4v_{sw}^2} \right) \left[ \ln \left( 1 + \frac{4v_{sw}^2 s_{max}^2}{\beta^2 s^2} \right) - \ln \left( 1 + \frac{4v_{sw}^2}{\beta^2} \right) \right] \quad (D.27)$$

if  $v_w/c \gg 1$  then the dust particle imparts momentum on the electrons, since the particle would be seen streaming into the electrons. Therefore, we use a Boltzmann distribution for  $N(v)$  to get

$$dF_2 = \int_{s_1}^{s_{max}} m_e v_3 (1 - \cos \theta) \left\{ N_e \left( \frac{m_e}{2\pi kT_e} \right)^{3/2} e^{-\frac{m_e v^2}{2kT_e}} \right\} \left\{ \frac{2\pi v s_2 ds_2 dt}{dt} \right\} d^3v \quad (D.28)$$

which, expanding the exponential and integrating, gives

$$F_2(c \gg v_w) = \frac{4\sqrt{\pi}}{3} s^2 m_e c^2 N_e \frac{\beta^4}{c^4} \ln \left( 1.12 \frac{s_{max}}{s} \cdot \frac{c^2}{\beta^2} \right) \quad (D.29)$$

putting equations D.27 and D.29 into similar form allows a comparison,

$$F_2 (V_{sw} \ll c) = \frac{4}{3} \pi s^2 m_e \beta^2 \left( \frac{\beta^2}{c^2} \right) \ln \left( 1.12 \frac{c^2}{\beta^2} \frac{s_{max}}{s} \right) \quad (D.30a)$$

$$F_2 (V_{sw} \gg c) = \pi s^2 m_e \beta^2 \left( \frac{\beta^2}{V_{sw}^2} \right) \ln \left( 2.00 \frac{V_{sw}^2}{\beta^2} \frac{s_{max}}{s} \right) \quad (D.30b)$$

The inverse square of the electron velocities in each equation dominates, giving a much higher value of the coulomb drag force for the slower non-thermal case. Inserting numbers values into equation D.30b, gives the ratio of coulomb drag to ion drag as

$$F_2(c \ll w) = 1.2 F_i \quad (D.31)$$

Coulomb drag is greater than ion drag! Note that for thermal electrons, coulomb drag is negligible.

## E. FORCES PERTURBING SOLID PARTICLES IN AN EARTH'S ORBIT

The predominant nongravitational force on particles in Earth orbit is that of solar radiation. The effects of these radiation forces depend on the shape, orientation, and chemical composition of the particle. Another force of significant effect is the Lorentz force resulting from the Earth's magnetic field interacting with the charge of the particle. Let us consider first the solar radiation effects.

### 1- SOLAR RADIATION PRESSURE

For particles orbiting the Earth in the 1-1000  $\mu\text{m}$  size range and 1  $\text{gm/cm}^3$  median density, the acceleration due to sunlight pressure (to zeroth order in  $v/c$ ) was found by Shapiro et al. (1966) to be:

$$a = \frac{A I_0}{m_p c} \underline{K} \cdot \hat{r} \quad (\text{E.1})$$

where  $A$  is the cross section of the particle,  $m_p$  is the particle's mass,  $v$  and  $c$  are the orbital velocity of the particle and the speed of light, respectively.  $I_0$  is the solar flux at 1 AU from the sun,  $\hat{r}$  is the unit vector that points toward the particle from sun.  $\underline{K}_{ij}$  is a second rank tensor with magnitude and components that depend on the reflection properties and orientation of the particle (the magnitude norm of  $\underline{K}$  must satisfy  $0 \leq |\underline{K}| \leq 2$ ).  $\underline{K}_{ij}$  is the unit tensor (to zeroth order in  $v/c$ ) provided that the particles scatter or absorb the light and reradiate it.

The direction of acceleration is along that of the impinging solar photons. The force on a particle due to solar radiation is given by Robertson (1937) as:

$$\vec{F} = -F_0 \left[ (1 + \dot{r}/c) \hat{r} + \vec{v}_t/c \right] \quad (\text{E.2})$$

where  $F_0$  is the force that the particle will experience if its were at rest with the incoming radiation from the sun,  $\vec{v}_t$  is the relative velocity of the particle to the sun,  $\dot{r}$  is the component of this velocity in the direction  $r$ ,  $\hat{r}$  is a unit vector in the direction outward from the sun and  $c$  is the speed of light. The velocity of the particle is  $\vec{v}_t = \vec{v}_e - \vec{v}$ , where  $\vec{v}_e$  is the orbital velocity of the Earth, and  $v$  is the velocity of the particle relative to Earth. By substituting this into equation E.2, Peale (1966) gets:

$$\vec{F} = +F_0 \left( \hat{r} - \frac{\vec{v}_e}{c} \right) + F_0 \frac{\vec{v} \cdot \hat{r}}{c} \hat{r} - F_0 \frac{\vec{v}}{c} \quad (\text{E.3})$$

The Earth's orbit is assumed to be circular here. The first term of the right-hand side of equation E.3,  $-F_0 \hat{r}$ , is the radiation pressure force and the remaining terms are due to the P-R drag.

The coordinate system being used is illustrated in Figure 3 (Peale, 1966). The unit vectors  $e_1, e_2, e_3$  define a coordinate system that is

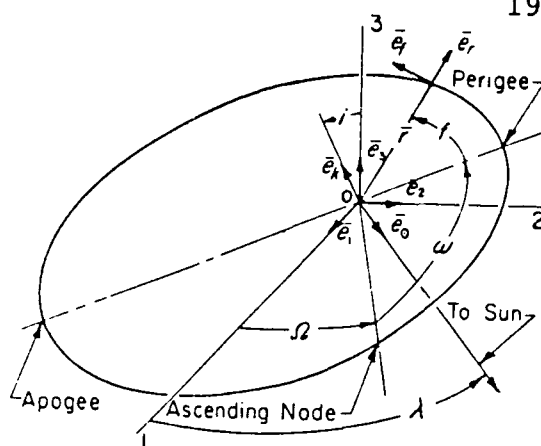


Fig. 3. Descriptive parameters of an elliptic orbit.

non-rotating with its origin at the center of the Earth. The 1-2 plane is the ecliptic plane.  $e_s$  is a unit vector in this plane toward the sun, so that  $e_s = r$ . The unit vectors  $e_r$ ,  $e_f$ ,  $e_k$  define an orthogonal system.  $e_k$  is perpendicular to the orbital plane in the direction of the angular momentum vector of the orbiting particle.  $e_r$  is along  $r$  which is the position vector of the particle.  $e_f$  is defined by  $e_k \times e_r$ . Also,  $a$  is the semi-major axis, and  $e$  is the eccentricity. The angles  $\Omega$ ,  $\omega$ ,  $f$ ,  $i$ , and  $\lambda$  are: the longitude of the ascending node, the argument of perigee, the true anomaly, the inclination of the orbit plane with respect to the ecliptic plane, and the mean longitude of the sun in the ecliptic plane. By definition  $\tilde{\omega} = \omega + \Omega$ ,  $\lambda = n_s t$  where  $n_s$  is the angular velocity of the sun in the ecliptic and  $t$  is the time.  $M = n(t - t_0)$  where  $M$  is the mean anomaly,  $n$  is the mean orbital angular velocity of the particle, and  $t_0$  is the time of perigee passage.

For high inclinations there are no simple analytic solutions to the perturbation equations. But since  $di/dt$  is proportional to  $\sin i$ , a particle which oscillates erratically will, on the average, spend more time in low inclination orbits. This suggests a statistical preference toward the ecliptic plane. This concentration is further enhanced if the moon is the major source of the particles or aided in their orbital capture.

Shapiro (1963) worked out the details of an approximate analytic solution of the radiation pressure perturbation equations for small inclinations. If the effects of the Earth's oblateness are removed from his solutions, Peale finds that:

$$e^2 = \frac{2K_1^2}{n_s^2} (1 - \cos n_s t) + \frac{2K_1}{n_s} [e_0 \sin \tilde{\omega}_0 \sin n_s t + e_0' \cos \tilde{\omega}_0 \times (\cos n_s t - 1)] + e_0'^2 \quad (E.4)$$

$$\tan \tilde{\omega} = \frac{\sin n_s t + (e_0 n_s / K_1) \sin \tilde{\omega}_0}{\cos n_s t - 1 + (e_0 n_s / K_1) \cos \tilde{\omega}_0} \quad (E.5)$$

$$\text{where } K = \frac{3}{2} \sqrt{a/\mu(1-e_0^2)} \left( \frac{F_0}{m\eta} \right)$$

Here  $\mu = GM_e$ ,  $G$  is the gravitational constant and  $M_e$  the mass of the Earth.  $K$  is considered to be constant here and the shadow of the Earth has been neglected. The semi-major axis is constant in this approximation.

Considerable error has been introduced by using several approximations to solve the perturbation equations. These include the Kryloff-Bogolinoff average over an orbit, the neglect of variation of terms of order  $e^2$  ( $1 - e^2$  is assumed  $1 - e_0$  in K) the assumption of constant radiation pressure force  $F_{rp}$ , the neglect of the Earth's shadow, and the replacement of the true solar motion by the mean solar motion. These assumptions; however, lead to small errors for particles orbiting below  $20 R_e$ . The error of the Earth's shadow is about 10% for orbits inside the magnetosphere. Variations in the value of  $1 - e^2$  causes error of a factor of 2 during a year for  $a = 8R_e$ .

Greater accuracy involving the estimate of the critical particle size below which the lifetime in orbit is less than 1 year cannot be expected. This is due to other uncertainties in the problem, including the shape and albedo of the particles as well as the value of  $F_{rp}$ .

Peale states that the effect of the radiation pressure perturbation on the orbiting particles is to create a diffuse concentration of particles near the ecliptic plane. The radiation pressure also determines the lifetimes of the orbiting particles such that secular drags become unimportant. Smaller particles have shorter lifetimes, and the slope of any exponential type size distribution of orbiting particles may be flatter than the size distribution of the set of particles being introduced into orbit.

Peale (1966) also maintains that this symmetry of concentration about the ecliptic plane is almost undisturbed by the gravitational perturbations beyond a geocentric distance of 7.7 Earth radii. The oblateness of the Earth destroys the ecliptic symmetry of orbiting dust particles larger than an approximately determined critical size that varies from 1 to 100 for ratios of  $a/R_e$  from 2 to 8 respectively. This decrease in the critical size as a function of geocentric distance ( $R_e$ ) is such that within 1 to 2 Earth radii from the Earth's surface essentially all ecliptic symmetry is destroyed.

Peale also contends that radiation pressure also causes large-amplitude oscillations in the eccentricity of the particle's orbit, which makes this perturbation the dominant factor in determining the lifetimes of the particles in orbit. Furthermore, when the area to mass ratio exceeds about  $1500 \text{ cm}^2/\text{gm}$  the lifetime of an orbiting particle is less than 1 year. The effects of Coulomb drag and P-R drag are negligible by comparison.

## 2- THE INTERACTION WITH ATMOSPHERIC DRAG

To find the importance of this effect on solid particles in an orbit say 500 km above the Earth's surface, let us start estimating the air density to be of the order of  $10^7 \text{ particles/cm}^3$ . The corresponding mean free path is  $> 50 \text{ cm}$ , for solid particles of this diameter or less. To find the rate of momentum transfer due to collisions with the air particles; there are two cases; a) the motion of the solid particles  $<$  the thermal motion of the air; b) the motion of the solid particles  $>$  the thermal motion of the air particles. The rate of momentum transfer in a) is (Jastrow and Pearse, 1957):

$$\frac{dP}{dt} = -\frac{4\pi R^2}{3} n m \bar{v} V \quad \text{for } V < v \quad (\text{E.6})$$

where  $R$  is the radius of the solid particle,  $n$  is air particles number density,  $m$  and  $V$  are the solid particle mass and orbital velocity, respectively.  $\bar{v}$  is the mean thermal velocity of the air particles. For case b):

$$\frac{dP}{dt} = -\bar{v} R^2 n m V^2 \left[ 1 + \frac{\pi \bar{v}^2}{4 V^2} + O\left(\frac{\bar{v}}{V}\right)^4 \right] \quad (E.7)$$

Since, the orbital velocity of particles in an Earth's orbit (of the order of  $8 \times 10^5$  cm/sec) is larger than the thermal velocity of the air particles (of the order of  $10^5$  cm/sec), equation (E.7) is the applicable one in this case. One should add to this the recoil of particles impinging on the solid particles. Measurements have revealed that the coefficient of reflection may be close to unity. Under these assumptions, the total momentum transfer is:

for specular elastic reflection

$$f_n = -\pi R^2 n m V^2 \quad (E.8)$$

for diffuse elastic reflection

$$f_n = -\frac{4}{3} \pi R^2 n m V^2 \quad (E.9)$$

These terms can be inserted as the perturbing force element in the Gaussian perturbation equations of the orbital elements of the orbiting particles and the change in the semi-major axis, eccentricity, inclination and ascending node can be calculated, for different altitudes above the Earth's surface.

There are also mechanisms for charging these particles, by the interaction with the plasma. The thermal velocity of the electrons is  $\sim 60$  times greater than that of the positive ions. Consequently, on the night side of the Earth, the particles will be negatively charged. On the day side, however, photo-emission due to the absorption of solar UV photons and thus electron ejection may diminish the negative charging during the night. A calculation of these competing mechanisms can be executed for different altitudes from the Earth's surface. This information is very important in the analysis of the interaction of these charged particles with the Earth's magnetic field, i.e. the Lorentz Force, and the electrical part of the Lorentz force (see section M).

The charge distribution can be calculated from the following relation (Jastrow and Pears, 1957):

$$\rho = e [ n_i e^{-e\psi/KT} - n_e e^{e\psi/KT} ] \quad (E.10)$$

Here,  $i$  stands for ions and  $e$  for electrons. From this relation one can calculate the potential by solving the Poisson equation

$\nabla^2 \psi = -4\pi \rho$ . It is noteworthy here to mention that the charged particles will polarize the nearby atmosphere, from which coulomb drag will take place. For a spherical particle, the potential solution of the Poisson equation is:

$$\psi = -\frac{2\pi}{3} n e r^2 + \frac{a}{r} + b \quad (E.11)$$

The constants  $a$  and  $b$  are determined by the conditions

$$\psi(R) = \psi_0 \quad (E.12)$$

$$\psi(R+1) = 0 \quad (E.13)$$

The shielding radius  $l$  can be calculated, if  $l \ll R$  from:

$$l = \sqrt{2 \frac{e\phi_0}{kT_e} \lambda_D} \quad (E.14)$$

Where  $\lambda_D$  is the Debye length. This length can be calculated, once one knows the charge of the particle, the thermal energy of the medium and the Debye length. For example: if the charged particles were 30 volts (for spherical particles, charge is expressed in volts),  $KT_e = 1.5$  ev, and the Debye length is 2 cm, then  $l$  will be 12.6 cm.

### 3- THE INTERACTION WITH THE EARTH'S MAGNETIC FIELD

The interaction of charged dust particles with the Earth's magnetic field will affect the orbital elements of dust surrounding the Earth. These particles are charged chiefly through two mechanisms: photoionization due to solar ultraviolet radiation, and capture of electrons in the Earth's exosphere. Singer (1961) calculated that particle charges will vary from a potential of -7.5 V near the Earth to +60 V at 10 Earth radii. Beard and Johnson (1960) calculated potentials of fractions of a volt. For numerical estimates, we will use 1 V as an example, although this could be off by an order of magnitude.

Because the semimajor-axis can be perturbed only by a force along the orbital path, and the magnetic lorentz force

$$\vec{F} = q/c (\vec{v} \times \vec{B}) \quad (E.15)$$

must be normal to the velocity vector, any change in semimajor-axis can only arise from the motion of the magnetic field relative to the orbital path (possible since the field is not coaxial with the Earth's rotation axis). This effect can be neglected because the Earth's magnetic field moves relatively slowly near the Earth, and the field is weak far from the Earth. Thus

$$\frac{da}{dt} = 0. \quad (E.16)$$

Shapiro and Jones (1961) calculated the perturbations on the other orbital elements. They found

$$\frac{de}{dt} = -K\phi(1+e-e^2) \sin i_m \sin i \sin \Omega^* \quad (E.17a)$$

$$\frac{di}{dt} = -K \sin i \sin \Omega^* \quad (E.17b)$$

$$\frac{d\omega}{dt} = K \{ 3 \cos i \cos i_m + (3 \sin i - \csc i) \sin i_m \cos \Omega^* \} \quad (E.17c)$$

$$\frac{d\Omega}{dt} = -K \{ \cos i - \cot i \sin i_m \cos \Omega^* \} \quad (E.17d)$$

where  $a$ ,  $e$ ,  $i$ ,  $\omega$ , and  $\Omega$ , are the usual orbital elements,  $\Omega^* = \Omega' - \Omega$ , where  $i'$  and  $\Omega'$  are the inclination and longitude of the ascending node of the Earth's magnetic field,  $K = 2\pi\lambda$ , where  $\lambda$  is the ratio of the average force due to the magnetic field to the gravitational force, and  $\phi$  is the ratio of the orbital period of the satellite to that of the Earth's rotation.

For a potential of +1 V, the change in the orbital elements due to the Earth's magnetic field over the course of a day for a particle of  $1\text{ }\mu\text{m}$  in a low inclination orbit will be:

$$\Delta e = .002 \quad (\text{E.18a})$$

$$\Delta \omega = 0.1^\circ / e \quad (\text{E.18b})$$

$$\Delta i = 0 \quad (\text{E.18c})$$

$$\Delta \Omega = 0.6^\circ \quad (\text{E.18d})$$

The lifetime of dust grains orbiting the Earth would be limited to less than a year due to the change in eccentricity, and the subsequent decrease in the perigee distance. In practice, these forces are much smaller than those due to radiation pressure, and the latter will limit dust lifetimes more so than the Lorentz force.

### F- ION PRESSURE AND RADIATION PRESSURE

The solar wind protons exert pressure through physical impacts upon the dust particle. The number of protons that hit the dust particle is given by

$$N = \pi s^2 F = \pi s^2 N_p v_p \quad (\text{F.1})$$

where  $s$  is the radius of the particle,  $F$  is the flux of the solar wind protons,  $N_p$  is the number of protons per unit volume, and  $v_p$  is the velocity of the proton. If all the incident protons stick or are isotropically reflected, the force resulting from the linear momentum carried by the protons will be

$$F_p = \pi s^2 M_p v_p^2 N_p \quad (\text{F.2})$$

where  $M_p$  is the proton mass. For the solar wind ions, equation (F.2) is given by

$$F_{\text{ion}} = \pi s^2 \bar{M}_i v F \quad (\text{F.3})$$

where  $\bar{M}_i$  is an average mass of the ions and can be taken to be  $2 \times 10^{-24}$  grams, and  $v$  is the solar wind ions velocity  $4 \times 10^7$  cm/sec. Another force comes from solar photons which exert pressure on the dust particles. Since the energy of a photon  $E_\nu = h\nu$ , its momentum  $p = h\nu/c$ , where  $c$  is the velocity of light,  $\nu$  is the frequency of the radiation, and  $h$  is Planck's constant. Since  $p = E_\nu/c$ , the rate at which momentum is intercepted from the radiation field and not re-radiated in the forward direction becomes

$$F_R = \pi s^2 (E_\nu/c) Q_{\text{PR}} F_{\text{ph}} \quad (\text{F.4})$$

where  $F_R$  is the force from radiation pressure,  $F_{\text{ph}}$  is the flux of photons  $\text{cm}^{-2} \text{sec}^{-1}$ ,  $Q_{\text{PR}}$  is a radiation pressure efficiency factor (Van de Hulst, 1957), which may be larger than unity. Rewriting equation (F.4) in terms of the solar constant

$$F_R = \frac{\pi s^2}{r^2 c} E_\odot Q_{\text{PR}} \quad (\text{F.5})$$

where  $E_\odot = E_\nu F_{\text{ph}}$  at 1 A.U. =  $1.36 \times 10^6$  ergs/cm<sup>2</sup> sec, and  $r$  is in A.U. Now we can compare the solar wind pressure with the solar radiation pressure. Rewriting equation (F.3) for an arbitrary heliocentric distance and making use of equation (F.5), we find

$$F_{\text{ion}} = s^2 \bar{M}_i v F \left( \frac{r_\odot}{r} \right)^2, \text{ and} \quad (\text{F.6})$$

$$\frac{F_{\text{ion}}}{F_{\text{PR}}} = \frac{M_i v F c}{E_0 Q_{\text{PR}}} \quad (\text{F.7})$$

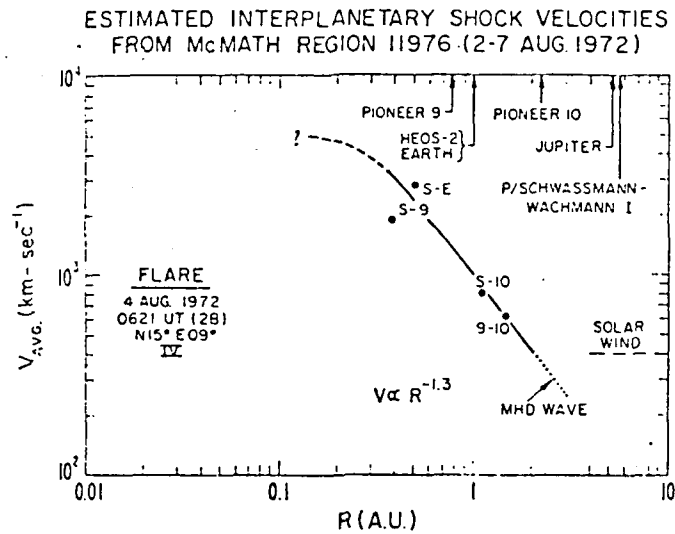


Figure 4 A strong-decelerated shock wave from the flare of 4, 1972 (Dryer et al., 1972).

August

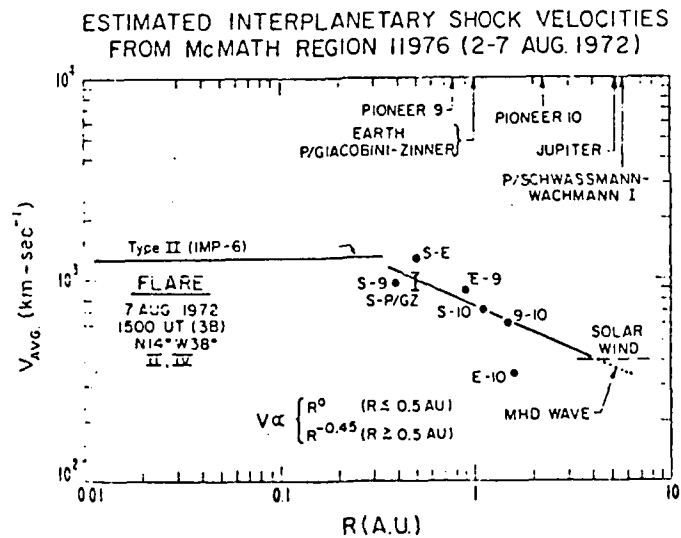


Figure 5 A decelerated shock wave form the flare of August 7, 1972 Dryer at al. (1972)

### G- ION PRESSURE AND RADIATION PRESSURE UNDER SHOCK CONDITIONS

Ion pressure creates a very weak force on particles in heliocentric orbits. If we let  $Q_{PR} = 1$ , the ratio of ion pressure to radiation pressure, which is independent of heliocentric distance, is of the order of  $4.4 \times 10^{-20} v F$ . For  $F = 2 \times 10^8 \text{ cm}^{-2} \text{ sec}^{-1}$  and  $v = 400 \text{ km/sec}$  (quiet conditions), the ratio is very small (0.0003).

During the interaction of a shock wave with the dust, this ratio will no longer be independent of heliocentric distance, because the velocity in the flux term is  $r$  dependent due to the deceleration of the shock wave from its initial velocity at the inner boundary. Gosling et al. (1968) noted that in situ shock velocities were lower than the average velocity, thereby suggesting deceleration. An example of a strongly-decelerated blast wave from the flare of 4 August 1972 is shown in Figure 4 (Dryer et al., 1972). An estimated power law relation suggests that  $v \propto r^{-1.3}$  for that shock wave. Another example of a less strong-decelerated shock wave is given in Figure 5 (Dryer et al., 1972), for the flare of 7 August 1972. This figure shows the resulting shock to have  $v \propto r^0$  for  $r < 0.5$  A.U. and  $v \propto r^{-0.45}$  for  $r > 0.5$  A.U. There are several dissipative mechanisms that explain this deceleration. For example, Wu and Fu (1970) have clearly shown that ionization becomes significant because a portion of the kinetic energy of the gas goes into excitation of the interim state, resulting in a lower shock velocity. Chow (1967) and Nakagawa et al. (1973) have demonstrated similar results with thermal radiation. Possible indirect experimental evidence for the suggestion that shock deceleration can be caused partly by local particle acceleration is given by Armstrong et al. (1970).

Following these results, we can rewrite equation (F.7) in order to evaluate this ratio under disturbed conditions:

$$F_{\text{ion}} = \frac{M_i v_s^2 r_0^\alpha N_i c}{E_0 Q_{PR} r^\alpha} \quad (\text{G.1})$$

where  $v_s$  is the shock wave velocity at 1 A.U., and  $\alpha$  is the exponent of an estimated power law for the deceleration of the shock wave. For values of  $v_s = 750 \text{ km/sec}$  at 1 A.U.,  $\alpha = 1.3$ , and  $r \approx 0.5$ , this ratio is still very small (0.003).

### H- ION DRAG AND POYNTING-ROBERTSON DRAG UNDER SHOCK CONDITIONS

To compare the drag caused by these two dynamical forces we will start with the Poynting-Robertson drag. In order to find the radiation drag caused by the particles' absorption of photons coming radially from the sun and re-emitted isotropically in the particles' own rest frame we consider that a re-emitted photon carries off angular momentum proportional to:

- (1) its equivalent mass  $h\nu/c^2$ ,
- (2) the velocity  $R\dot{\theta}$  of the dust particle in its orbit,
- (3) the dust particle's heliocentric distance from the sun,  $R$ .

Following this and considering only terms linear in  $v/c$ , the rate of angular momentum lost by the dust particle Harwit (1973) is

$$dL_{\text{photons}} = \frac{h\nu}{c^2} \dot{\theta} R^2 \quad (\text{H.1})$$

However, to compare radiation drag to ion drag, we must derive an expression for the rate of loss of angular momentum from the dust particle due to ion impacts:

$$dL_{\text{ion}} = \bar{M}_i \dot{\theta} R^2 \quad (\text{H.2})$$

where  $\bar{M}_i$  is an average mass of the ions. For a steady radial flow of both photons and ions, we re-write equation (H.1) and (H.2):

$$\frac{dL}{dt} \text{ photons} = \frac{\pi s^2 E_{\odot} \dot{\theta}}{c^2} \quad (\text{H.3})$$

and

$$\frac{dL}{dt} \text{ ions} = s^2 \bar{M}_i \dot{\theta} F.$$

Therefore, the ration of ion drag to radiation drag is

$$\frac{\text{ion drag}}{\text{radiation drag}} = \frac{\bar{M}_i c^2 F}{E_{\odot}} = 1.3 \times 10^{-9} F, \quad (\text{H.4})$$

where  $F$  is the solar wind ion flux. This ratio is also independent of heliocentric distance. For  $F = 2 \times 10^8 \text{ cm}^{-2} \text{ sec}^{-1}$ , we find that this ratio  $\approx 0.26$  which is much higher than the ratio of equation (G.1).

To evaluate this ratio under conditions of dust particles subjected to a passing shock wave, we have to re-write equation (H.5) so as to deal with the deceleration of the shock. Therefore, assuming a power law for the deceleration of the shock,  $1/r^\nu$ , equation (H.5) becomes

$$\frac{\text{ion drag}}{\text{P-R drag}} = 1.3 \times 10^{-9} N_i \frac{v_s}{r^\nu}, \quad (\text{H.5})$$

where  $r$  is heliocentric distance in A.U. and therefore, the ratio is higher than the ratio in equation (H.5). Does this increase in the ratio have any appreciable effect on the dust particles' lifetimes in their orbits? In order to answer this question, we must first calculate the change in the dust particle's heliocentric distance (assuming circular orbits) due to the P-R effect per unit time. To do that, we take the equation, calculated first by Robertson, for the secular perturbations of an osculating ellipse of semi-major axis  $a$  and eccentricity  $e$  Wyatt and Whipple (1950):

$$\frac{da}{dt} = \frac{-\alpha(2+3e^2)}{a(1-e^2)^{3/2}} \quad (\text{H.6})$$

where =

$$\alpha = \frac{3 E_\odot}{16 \pi c^2 s \rho} = \frac{3.55 \times 10^{-8}}{s \rho} \frac{\text{AU}^2}{\text{yr}} \quad (\text{H.7})$$

$E_\odot$  is the solar constant, and  $s$  and  $\rho$  are the radius and density of the particle, respectively. If we assume circular orbits and integrate equation (H.15) we obtain

$$\int_{a_0}^{a_1} \frac{da}{a^2} = -2\alpha \int_0^t dt \quad (\text{H.8})$$

and

$$a_1 = \left( a_0^2 - \frac{14.6 \times 10^{-11} t_s}{3.1536 s} \right)^{1/2} \quad (\text{H.9})$$

where  $t_s$  is the time in seconds, and  $a_0$  and  $a_1$  are the initial and final heliocentric distances of the particle, respectively. In Table 2 we show the result of using equation (H.17) to determine the effect of the increased ratio of ion drag to P-R drag, under the condition of a progressing shock wave. The ratios given for values  $R_0$  from 0.05 A.U. to 1 A.U. were calculated using values of  $N_i = 50 / \text{cm}^3$ ,  $v = 7.5 \times 10^7 \text{ cm/sec}$ , and  $\nu = 1.3$  (Figure 6).  $a_1$  was calculated for two particle sizes,  $1 \mu$  and  $0.1 \mu$ , in order to show the effect of the change in radius.  $t_s$ , which depends on the velocity and thickness of the shock front was averaged for 1 hour Hundhausen and Pizzo (unpublished), and  $d$  is the difference between the values of  $a$  for particles of  $1 \mu$  and  $0.1 \mu$  radius. From these results, we conclude that this effect, although very short in time, can be significant at heliocentric distance  $< 0.1 \text{ AU}$ ; at these distances, the size distribution of the dust particles may be

altered due to this effect. This is conceivable since smaller particles would spiral faster than bigger particles towards the sun, during this short period of time.

## I- PARTICLE SPIN DUE TO THE WINDMILL EFFECT

Paddack (1969) proposed that the rotational bursting of interplanetary dust particles can take place due to the interaction of Solar radiation with the irregular surface geometry of the particles. Solar Photons hitting the particles cause a so-called "windfall effect", which makes the particles spin with their long axis perpendicular to the solar radius vector. Paddack (1973) designed a laboratory experiment to investigate the possibility of rotational bursting due by this mechanism.

Paddack and Rhee (1975) found that such induced rotational bursting is possible (for specific surface geometry of the dust) in a relatively short lifetime; shorter by approximately one order of magnitude than the P-R lifetime for metallic particles, and shorter by about two orders of magnitude for nonmetallic particles. This difference between metallic and nonmetallic particles is due to the inclusion of magnetic damping. This magnetic damping is caused by the interaction of the magnetic field generated by the spinning charged dust particles with the interplanetary magnetic field. Sparrow (1975) suggested that these magnitudes have been overestimated, and that they do not work significantly faster than the P-R effect.

From this we can see that the spin problem is a complicated one, especially so when one considers the problem of alignment, where ion collisions may be more significant than photon collisions (Harwit, 1971). The dust particle's angular momentum axis takes on a direction perpendicular to the solar radius vector. Since it was shown by Greenberg (1968) that a dust particle tends to align its long axis perpendicular to its angular momentum axis, the result is a preferential alignment of the long axis of the particle along the solar radius vector.

# J- PARTICLE SPIN DUE TO THE ALBEDO/RADZIEVSKII EFFECT

Paddack (1969) proposed that the rotational bursting of interplanetary particles could be caused by the interaction of the Solar radiation force with irregular surface geometry. Radzievskii (1954) suggested a differential torque driven by irregular (or uneven) albedo over the entire surface, although he might have oversimplified the situation in his paper and roughly demonstrated the "bursting time" for cubic grains. Due to the radiative energy transfer and the effect of magnetic damping, some other terms should be taken into account. Here we re-derive an expression for combined net force imposed on the particle and spinning rate under some realistic considerations.

The normal momentum of the sunlight is

$$G_{fn} = \frac{1}{c} \vec{S} \cdot \hat{n} A \cos \theta_i dt \quad (I.1)$$

where  $\vec{S}$  is the Poynting vector of the radiation, and  $\hat{n}$  is a unit vector in the direction of motion. Subscripts f and i refer to the final and initial values, respectively.  $G_{fn}$  is a negative quantity, since the angle between  $\vec{S}$  and  $\hat{n}$  is greater than  $90^\circ$ . The change in the normal momentum of the sunlight then is  $dG = G_{fn} - G_{in} = (dt A \cos \theta_i / c) |\vec{S}_f \cdot \hat{n} - \vec{S}_i \cdot \hat{n}|$  which, if we explicitly take the signs into account, becomes

$$dG = -\frac{A}{c} \cos \theta_i [|\vec{S}_f \cdot \hat{n}| + |\vec{S}_i \cdot \hat{n}|] dt \quad (I.2)$$

Because the change in normal momentum during the time interval  $dt$  is  $dG = -F_n \cdot dt$ , the radiation force can be obtained as

$$F_n = \frac{A}{c} \cos \theta_i \{ |\vec{S}_f \cdot \hat{n}| + |\vec{S}_i \cdot \hat{n}| \} = A(1+R) \cos^2 \theta \frac{\langle S_i \rangle}{c} \quad (I.3)$$

The maximum value of  $F$  corresponds to  $\theta = 0$  and  $R = 1$ , that is, normal incidence on a perfect conductor, and we see that

$$F_{max} = \frac{2 A \langle S_i \rangle}{c} \quad (I.4)$$

On the other hand, consider a complete absorber of radiation for which  $R = 0$ : this is not a conductor, but rather an idealized perfectly "black" object. Then, at normal incidence,

$$F_{black} = \frac{A \langle S_i \rangle}{c} = \frac{1}{2} F_{max} \quad (I.5)$$

For an isotropic scattering surface, the pressure due to the isotropically reflected radiation is only the one-third of that due to one directional regular reflection.

"Isotropically" means the surface scatters the incident energy density  $S$  into all the reflected directions with equal likelihood and the probability that each component of the light wave will be in an element of solid angle  $d\Omega$  is proportional to  $d\Omega$ . So the total pressure is the integration of the values of all the components over the entire solid angle  $4\pi$ .

Similar to the equations I.4 and I.5, the pressure due to each component in the scattered the light can be expressed, if we let  $R = 1$ , as

$$dF' = A \cos^2 \theta_j \vec{S}_j \cdot \hat{n} \frac{d\Omega_j}{c} \quad (I.6)$$

$$F' = \frac{2\pi}{3c} A \langle S_j \rangle$$

where  $\langle S_j \rangle$  is a constant for isotropic scattering, and solid element  $d\Omega = 2\pi \sin \theta_j d\theta_j$ . Also from the conservation of the energy, the total incident energy  $A \langle S_j \rangle \cos \theta_j$  should be equal to the total scattered energy  $A 2\pi \langle S_j \rangle$ . Hence, the equation can be re-written as

$$F' = \frac{A \langle S_j \rangle \cos \theta_j}{3c} \quad (I.7)$$

If we are still to take a cubic grain as a example to investigate the differential torque imposed on it due to the solar radiation force. For the simplicity, once of the surfaces is divided into equal parallelograms (Radzievskii (1954), of which one parallelogram has perfect mirror-reflecting surface (albedo is supposed to be 1) and the other one is an isotropically diffusing surface. If we assume that the rotational axis is approximately parallel to the dividing line of the non-uniform face (uneven albedo), then the force exerted on the mirror half of the surface can be obtained from equation I.5 as

$$F_m = \frac{2AE}{r^2 c} \cos^2 \theta_i \quad (I.8)$$

Where  $c$  is the light speed and  $E(r)$  is the solar constant at the distance of  $r$  from the Sun.  $a$  is one side dimension of the cube. Also

$$E(r) = \frac{E_0}{r^2} \quad E_0 = \text{solar constant} \quad (I.9)$$

From the equations I.5 and I.8, we can obtain the radiation net force imposed on the isotropically diffused or re-emitting half of the surface:

$$F_d = F_m + F' = \frac{A \cos \theta_i}{c} \left[ \frac{\langle S_i \rangle}{3} + \frac{2E_0}{r^2} \cos \theta_i \right] \quad (I.10)$$

Therefore, the differential torque created on the cube is given by

$$\bar{M} = \frac{1}{\pi} \int_{-\pi/2}^{\pi/2} M_{\theta_i} d\theta_i = \frac{E_0 a^3}{4r^2 c} \left( \frac{1}{2} - \frac{2}{3\pi} \right) \quad (I.11)$$

We know  $\bar{M} = I \, d\omega/dt = \frac{a^5 \rho \, d\omega}{6 \, dt}$ , then

$$\omega = \bar{M} \times \frac{6 \, t}{a^5 \rho} \quad (I.12)$$

According to Timoshenko (1942), the stress  $\sigma$  developed in a rotating solid disk of radius  $b$  is given by

$$\sigma = \frac{3+\mu}{32} a^2 \rho \omega^2, \quad (I.13)$$

where  $\rho$  is the density and  $\mu$  is the Poisson ratio.

From the equations I.12 and I.13, we have

$$t = \frac{2a^4}{3\bar{M}} \sqrt{\frac{2\sigma\rho}{3+\mu}} \quad (I.14)$$

$$\text{where } \bar{M} = \frac{E_0 a^3}{4cr^2} \left( \frac{1}{2} - \frac{2}{3\pi} \right),$$

### K- Particle Spin Due to Solar Wind Ions

In Chapter II we discussed rotational bursting of dust particles and its possible effect on the brightness. In this chapter we will attempt to calculate the spin rate and see if rotational bursting does take place. To calculate the spin rate caused by solar wind ion impacts, we first assume a unidirectional ion flux emitting radially from the sun. The spin vector of the dust particle performs a random walk in the y-z plane, with the x axis pointing towards the sun. The successive jumps of the spin vector can only be along the y or the z axis. Since this process is random, and we assume that the ions have no random velocity of their own, the root mean square value of the angular momentum transferred to the dust particle by each collision is given by:

$$\delta L = \left[ \frac{1}{2} \int_0^s (\bar{M}_i v r)^2 dr \right]^{1/2} \sim \frac{M_i v s}{\sqrt{3}} \quad (K.1)$$

where  $s$  is the dust particle's radius, and  $M_i$  and  $v$  are the ion's mass and velocity, respectively (Harwit, 1973). This angular momentum transfer, after  $N$  collisions, can be calculated using a random walk calculation using the sum of different numbers of steps  $n$  and jumps of the spin vector of length  $l$ . If  $N = n$  is the sum of different numbers of steps, then the root mean square value of the lengths of the jumps becomes:

$$l_{RMS} = \left[ \frac{\sum n_i l_i^2}{N} \right]^{1/2} \quad (K.2)$$

The "root mean square deviation" is defined as:

$$\Delta = \left[ \frac{\text{sum of (distances)}^2}{\text{sum of all possible paths}} \right]^{1/2} \quad (K.3)$$

The sum of the "mean square deviation":

$$\sum \Delta_i^2 = \sum n_i l_i^2 = N l_{RMS}^2 \quad (K.4)$$

or:

$$\Delta = \left[ N l_{RMS}^2 \right]^{1/2} = N^{1/2} l_{RMS} \quad (K.5)$$

Therefore:

$$\langle L^2 \rangle^{1/2} = N^{1/2} \delta L \quad (K.6)$$

where  $\langle L^2 \rangle$  is the final root mean square angular momentum transferred to the dust particle. The number of impacts on the dust particles per unit time from the solar wind ions is:

$$N = \pi s^2 F t \quad (\text{K.7})$$

where  $N$  is the number of impacts,  $s$  is the dust particle's radius in cm,  $F$  is the flux of solar ions in  $\text{cm}^{-2} \text{sec}^{-1}$ , and  $t$  is the time in sec. Substituting in equation K.6 we get:

$$\begin{aligned} \langle L^2 \rangle^{1/2} &= (\pi s^2 F t)^{1/2} \frac{\bar{M}_i v s}{\sqrt{3}} \\ &\sim \sqrt{F t} \bar{M}_i v s^2 \end{aligned} \quad (\text{K.8})$$

The resulting spin of the dust particle due to this angular momentum transfer is:

$$\omega = \frac{L_R}{I} \quad (\text{K.9})$$

where  $\omega$  is the rotation of the dust particle in radians/sec,  $L_R$  is the rotational angular momentum, and  $I$  is the moment of inertia  $= \frac{2}{5} m s^2$  for spherical particles. Substituting K.9 into K.8 we get  $\omega$  in rotations/sec:

$$\omega = \frac{10^{-21} \sqrt{F t} v}{\rho s^3} \quad (\text{K.10})$$

where  $\rho$  is the dust particle's specific density in  $\text{gm/cm}^3$ , and  $t$  is in years. To find the maximum spin rate that the particle can withstand without bursting, we equate the centripetal force/unit area to the tensile strength of the spherical particle:

$$\frac{F_c}{\text{area}} = \frac{m s \omega^2}{2 \pi s^2} \approx T \quad (\text{K.11})$$

and:

$$\omega_b = \frac{1}{2 \pi s} \sqrt{\frac{T}{\rho}} \quad (\text{K.12})$$

where  $\rho$  is the bursting angular speed in rotation/sec,  $T$  is in  $\text{dyne/cm}^2$ ,  $\rho$  is in  $\text{gm/cm}^3$ , and  $s$  is in cm.

Now we have a formula by which we can calculate the spin rate without introducing any damping mechanism. Let us now ask the following questions:

- (a) Do the dust particles reach the bursting angular speed  $\omega_b$ ?
- (b) If they do, at what heliocentric distance do they burst? (It is assumed that the particles are spiraling in towards the sun from the asteroid belt under the P-R effect).

In order to answer these questions and others, a computer program was written to calculate both  $\omega$  and  $\omega_b$  under conditions expected to be encountered by the dust.

Since equations K.10 and K.12 are both dependent on the radius of the particles, sputtering should be taken into account. Sputtering by solar wind protons and particles is most effective at kilovolt energies, and the erosion rate of a dust particle is proportional to the flux of ions in the solar wind. The erosion rate can be obtained in terms of  $ds/dt$ , from the shrinkage of the mass of the particle:

$$\frac{dm}{dt} = -4\pi s^2 \frac{ds}{dt} \quad (\text{K.13})$$

Table 3

Sputtering Rate values used in the Spin Calculations.

<u>Zone</u>	<u>t in yr.</u>	<u>Heliocentric Distance in A.U.</u>	<u>Sputtering Rate in Å/yr.</u>
1	10	2.0 - 1.0	0.05
2	10	1.0 - 0.50	0.1
3	1	0.50 - 0.30	0.3
4	0.2	0.30 - 0.25	0.56
5	0.1	0.25 - 0.2	1.3
6	0.1	0.20 - 0.15	2.2
7	0.1	0.15 - 0.1	5

To include this effect in our calculations, values for  $ds/dt$  in units of Å/yr were taken from Bandermann (1967) for different heliocentric distances. Table 3

shows the values used for each zone of heliocentric distance and their increased importance as these distances get smaller.

In order to calculate  $\omega$  over a long period of time, such as the P-R life time, one must include the effect of shock waves passing through the interplanetary medium and interacting with the dust. Therefore we calculated the cumulative spin rate  $\omega_q$  under quiet conditions or steady flow of the solar wind and the spin rate accumulated under disturbed conditions. For  $\omega_q$  we used a constant value of  $v = 400$  km/sec and  $N_i = N_0/r^2$  in the flux term, where  $N_0$  was taken to be  $5/\text{cm}^3$  at 1 A.U. This calculation was performed by starting with a sample of dust particles of various sizes located at 2 A.U. from the sun and letting these particles

Table 4

Input Parameters for Spin Calculations.

<u>Size (in u)</u>	<u><math>\rho</math> (gm/cm<sup>3</sup>)</u>	<u>T (dyne/cm<sup>2</sup>)</u>	<u><math>N_{\text{flare}}</math> (per yr.)</u>
0.1	7.86	$2.0 \times 10$	20 and 50
0.5	"	"	"
0.1	2.40	$6.9 \times 10$	"
0.5	"	"	"
0.1	8.90	$1.0 \times 10$	50
1.0	"	"	"
0.1	3.50	"	"
1.0	"	"	"
10.0	7.86	$2.0 \times 10$	"
100.0	"	"	"
10.0	2.40	$6.9 \times 10$	"
100.0	"	"	"

spiral in towards the sun by the P-R effect (neglecting ion drag). During this time we calculate the heliocentric distance from equation H.9 at timed steps appropriate for each zone (Table 3). In the meantime,  $\omega_b$  is calculated from equation K.12 for every time that there is a change in the size of the particle due to the afore-mentioned sputtering effect.

In order to calculate  $\omega_d$  we have made the following assumptions: (a) an average of 20 or 50 shock waves occur per year during the P-R life time of the particle, (b) the average interaction time between the dust and each shock front is one hour, (c) the velocity of each shock front has a deceleration with heliocentric distance which goes as  $1/r^2$ , (d) the velocity of the shock at 1 A.U. = 750 km/sec (Chao and Lepping, 1972), and (e) the number density of ions in the shock front is also considered to have a  $1/r^2$  dependence on heliocentric distance (Dryer, 1975). Table 4 shows the size, density, and tensile strength of the dust particles used in these calculations.

Figures 7a to 7e show the results of these calculations: plots of spin rate and bursting angular speed in rotations/sec versus the heliocentric distance of the particle. The spin rates climb gradually as the particles approach the sun, and the particles reach bursting speeds in few cases at distances very close to the sun. For example, in Figure 7b, iron particles and tektites of size  $0.1\mu$  acquire rotational speeds above  $10^9$  /sec at heliocentric distances of  $\sim 0.15$  A.U. However, for fewer shocks/year these particles attain a lower rotational speed. Also these figures show the effect of particle size upon rotational velocity (small size particles spin faster than larger ones). Finally the effect of  $\rho$  can be seen by comparing the cases of iron ( $\rho = 7.86 \text{ gm/cm}^3$ ) and tektites ( $\rho = 2.4 \text{ gm/cm}^3$ ). The higher rotational speed for iron would not be expected from inspection of equation K.10. However, since iron particles have longer P-R lifetimes than tektite particles (as can be seen from equation H.9), they are subjected to a longer collision time and, therefore, acquire a higher spin rate.

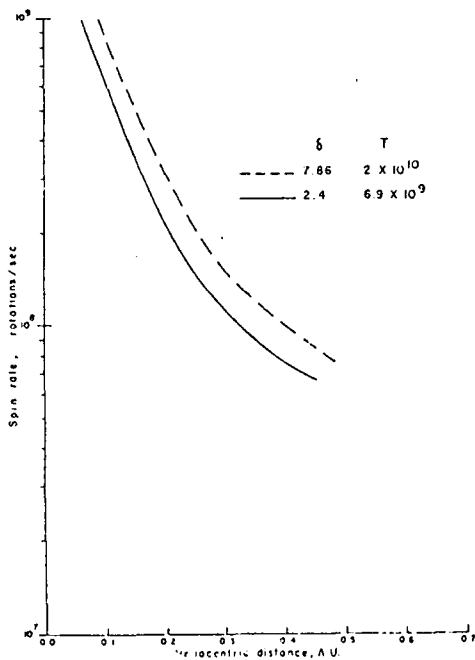


Fig. 7a. The spin rate of  $0.1\mu$  dust particles as a function of heliocentric distance (based on 20 flares/yr).  $\omega_b = 0.80 \times 10^7$  rot./sec for iron, and  $\omega_b = 0.95 \times 10^7$  rot./sec for tektites.

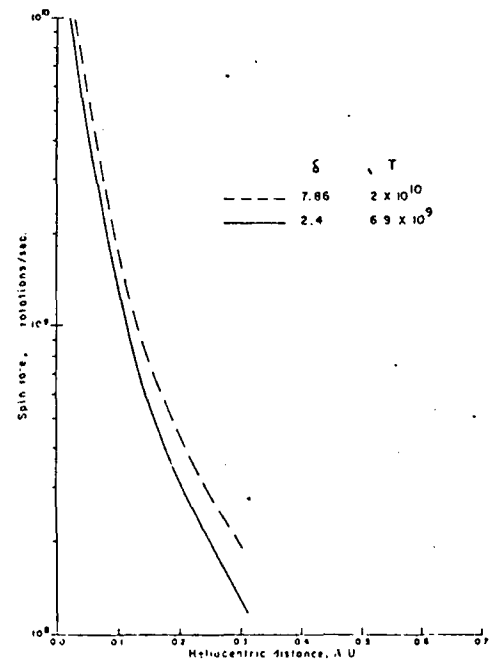


Fig. 7b. The spin rate for  $0.1\mu$  particles as a function of heliocentric distance (based on 50 flares/yr).  $\omega_b = 0.80 \times 10^7$  rot./sec for iron, and  $\omega_b = 0.95 \times 10^7$  rot./sec for tektites.

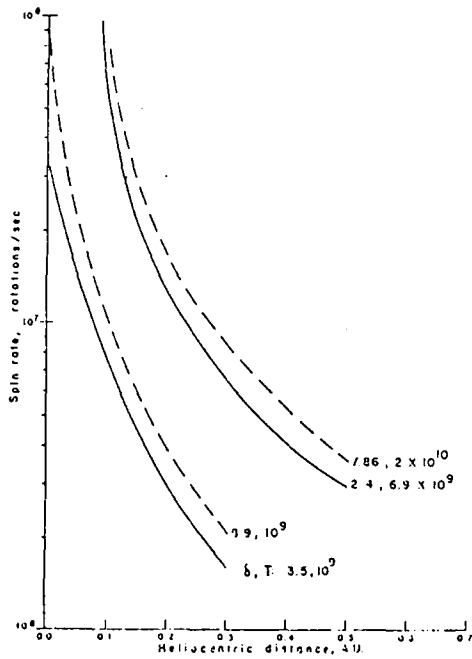


Fig. 7c. The spin rate for  $0.5\mu$  particles (upper curves), and  $1\mu$  particles (lower curves) versus heliocentric distance (based on 50 flares/yr).  $\omega_0 = 0.16 \times 10^9$  rot./sec for iron, and  $\omega_0 = 0.17 \times 10^9$  rot./sec for tektites (upper curves).  $\omega_0 = 0.17 \times 10^9$  rot./sec for nickel, and  $\omega_0 = 0.27 \times 10^8$  rot./sec for silicate (lower curves).

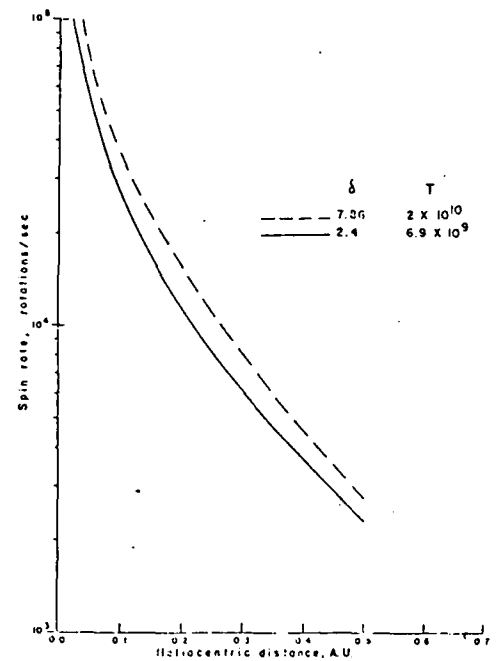


Fig. 7d. The spin rate for  $10\mu$  particles versus heliocentric distance (based on 50 flares/yr).  $\omega_0 = 0.80 \times 10^7$  rot./sec for iron, and  $\omega_0 = 0.85 \times 10^7$  rot./sec for tektites.

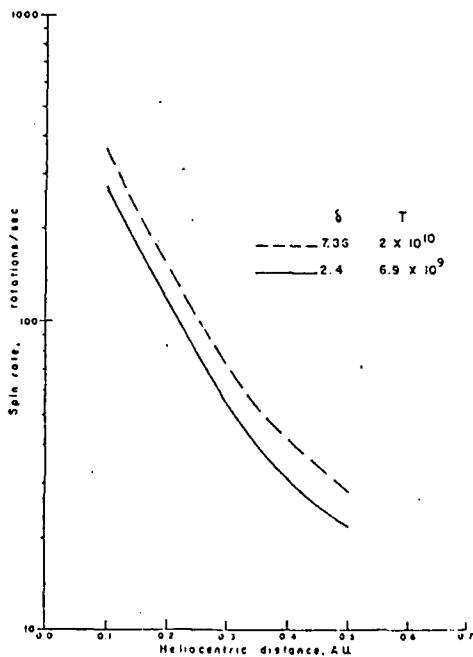


Fig. 7e. The spin rate for  $100\mu$  particles versus heliocentric distance (based on 50 flares/yr).  $\omega_0 = 0.80 \times 10^6$  rot./sec for iron, and  $\omega_0 = 0.85 \times 10^6$  rot./sec for tektites.

We have ignored in this calculation any damping mechanisms such as magnetic damping, electrical damping, and damping caused by the sense of collision of the ions with respect to the rotational direction of the dust particle (Harwit, 1970). Correction for these damping mechanisms would have been necessary if the calculations showed a definite rotational bursting. Therefore, we consider these results, shown in Figures 7a-e, as an upper limit for this mechanism.

## L- PARTICLES ELECTRIC CHARGE

Another possible way to disrupt the dust particles is by giving them a very high charge that would create a stress large enough to overcome the tensile strength of the particle. This mechanism is similar to rotational bursting in the sense that it can lead to brightness fluctuations, if it takes place on a large scale. Before discussing this possibility we list the two most important processes that play a role in the electrical charge of the particle (Belton, 1966): (a) photoelectric ejection of electrons from the grain by high energy photons from the sun, and (b) electron and ion accretion process. Standeford (1968) evaluated these two processes in detail. Employing the assumption that the grain has an initial net positive charge, he found an equilibrium charge of +14 volts (the electric potential was used instead of the charge, since for spherical particles the potential is independent of particle radius). From a more detailed analysis, Belton (1966) found that dust particles have potentials of +5 to +10 volts. He also estimated that they may be as high as +30 volts provided that allowance has been made for the x-ray and extreme ultraviolet radiation of the sun. Belton (1967) also found that the equilibrium potential decreases as a function of heliocentric distance. He attributed this decrease to both the increase in temperature of the interplanetary gas and the rapid increase in electron density in the outer part of the corona.

During the passage of a shock wave, the velocity and number density of the plasma increase considerably. Therefore, it is expected that an increase in the flux of protons will result in a higher positive potential for the particle. Belton (1966) discussed this problem and concluded that more data are needed on the various factors contributing to the charge before these calculations can be definitive. Regarding the possibility of particle disruption due to a high electric charge, the question arises as to the magnitude of the charge necessary to cause such a disruption. This question was discussed by Opik (1956), who pointed out that a surface stress results from this electric potential due to electrostatic repulsive force. This force acting on a sphere of radius  $s$  and charge  $Q$  is:

$$F = \epsilon_0 \frac{Q^2}{s^2} \quad \text{L.1}$$

where  $\epsilon_0$  is the permittivity. Rewriting equation L.1 using the electric potential instead of the charge, we have:

$$F = 8.85 \times 10^{-7} \frac{V^2}{s^2} \left( \frac{\text{dyne}}{\text{cm}^2} \right) \quad \text{L.2}$$

where  $V$  is in volts and  $s$  is in cm. The necessary condition for disrupting a particle is to have the surface stress greater than the particle's tensile strength; i.e.,:

$$\frac{8.85 \times 10^{-7} V^2}{s^2} > T \quad \text{L.3}$$

or:

$$s < 9.4 \times 10^{-4} V T^{-1/2}$$

L.4

where  $s$  is the minimum radius in cm. required to disrupt the particle for a given charge and tensile strength.

Now, from equation L.4, one can estimate the range in particle sizes where disruption may take place if the charge on the dust particle reaches as high as 100 volts. For iron particles we find that only particles of  $s < 0.0066\mu$  would be disrupted; for tektites, only particles of  $s < 0.011\mu$  would be disrupted by this effect. Since this effect can only disrupt very small particles, it cannot lead to any observable change in the brightness.

### M- PARTICLE INTERACTION WITH THE INTERPLANETARY MAGNETIC FIELD

The magnetic forces affecting the dust particles are associated with the three components of the interplanetary magnetic field:  $B_r$ ,  $B_\phi$ ,  $B_\theta$ . Figure 8 shows the heliocentric coordinate system of the interplanetary magnetic field as suggested by Parker (1958). The points P and P' are projections onto the celestial sphere of the north and south poles of rotation, respectively. The fundamental great circle is the projected solar equator,  $\theta$  is the polar angle measured from P toward P',  $\phi$  is the azimuthal angle measured from some fixed origin O, and  $r$  is the heliocentric distance.

The effects of perturbing forces upon the dust particle's orbit can be calculated following methods described by Moulton (1914) and Smart (1953). The interplanetary magnetic field exerts two forces: Lorentz force and convective force. Bandermann (1967) and Standeford (1968) developed mathematically the end result of such forces on the orbit of a particle. This development was based on Parker's (1958) spiral model of the interplanetary magnetic field, which considered  $B_\theta$  to be zero. In other words, there are no forces that depend on heliographic latitude, and the streamlines of the solar wind flow and the lines of magnetic force are strictly radial. However, recent satellite data show the existence of a  $B_\theta$  component, which we will discuss later in detail. Figure 9 (Coleman and Rosenberg, 1971) shows a sketch indicating qualitatively the curvature of the interplanetary field in the  $r\phi$  plane for an active and quiet sun.

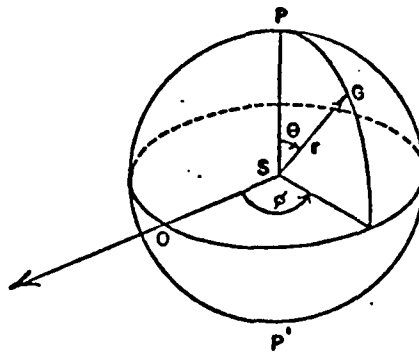


Figure 8. Heliocentric coordinate system for the interplanetary magnetic field (Standeford, 1968).

Bandermann (1967) and Belton (1967) concluded that a non-zero average  $B_\theta$  component, if it exists, can apply a convective force large enough to drastically change the orbit of a dust particle and ultimately lead to a very short lifetime compared to the P-R lifetime. In this section we will mainly be concerned with this magnetic force and its strong potential for causing a dynamical change in the zodiacal dust cloud. Parker (1963) showed that the passage of a shock wave

through the interplanetary medium would disturb the spiral shape of the interplanetary magnetic field lines and create kinks. If such kinks exist in the  $B_\theta$  component, then the resulting forces may change the spatial and size distribution of the dust, which may lead to an observable brightness change. To investigate this possibility we would like to find the effect of a non-zero average  $B_\theta$  component on the semi-major axis of the dust particle's orbit.

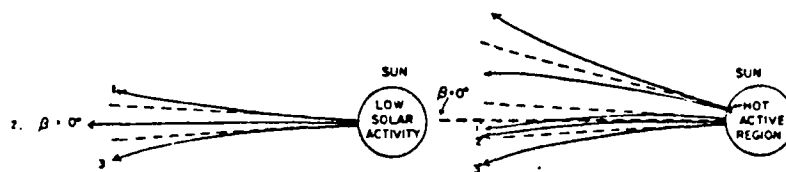


Figure 9. Sketch showing qualitatively the curvature of the interplanetary magnetic field lines, which results in a  $B_\theta$  component. On the right is the distortion that might be expected from a hot spot in the northern hemisphere (Coleman and Rosenberg, 1971).

The total force on the dust particle can be separated into Lorentz force and convective force which are given by:

$$\vec{F}_L = V_0 \frac{s}{c} \vec{v} \times \vec{B} \quad \text{M.1a}$$

$$\vec{F}_c = V_0 \frac{s}{c} \vec{w} \times \vec{B} \quad \text{M.1b}$$

where  $V_0$  is in volts,  $s$  is the radius of the particle,  $\vec{v}$  and  $\vec{w}$  are the velocities of the dust particle and the solar wind, respectively. The convective force is due to an electric field generated by the moving plasma, which creates a time dependent magnetic field. However, of an existing non-zero average  $B_\theta$  component, which is given by:

$$B_\theta = B_0 \left( \frac{R_0}{r} \right) \sin \theta \quad \text{M.2}$$

where  $B_0$  is the magnitude of  $B$  at 1 A.U., and  $R_0$  is the sun-earth distance. The  $r$  dependence is taken from Burlaga and Ness (1967), as opposed to Shapiro, et al. (1966), who took  $B_\theta = B_0 (R_0/r)^2$ . Describing the interplanetary magnetic field in a polar coordinate system with the polar axis coincident with the sun's axis of rotation directed northward gives  $B = \hat{r}B_r + \hat{\theta}B_\theta + \hat{\phi}B_\phi$ , where  $\hat{r}$ ,  $\hat{\theta}$  and  $\hat{\phi}$  are unit vectors in the coordinate directions.

To find the effect of the convective force due to a non-zero average  $B_\theta$  component, we have from equation M.1b

$$\vec{F}_c = \frac{V_0 s}{c} [\vec{w} \times (B_r \hat{r} + B_\theta \hat{\theta} + B_\phi \hat{\phi})] \quad \text{M.3}$$

Setting  $\vec{w} = w\hat{r}$ ,

$$\vec{F}_c = \frac{V_0 s w}{c} (B_r \hat{r} \times \hat{r} + B_\theta \hat{r} \times \hat{\theta} + B_\phi \hat{r} \times \hat{\phi}) \quad \text{M.4}$$

Therefore,

$$\vec{F}_c = \frac{V_0 s w}{c} [-B_\theta \hat{\phi} + B_\phi \hat{\theta}] \quad \text{M.5}$$

We separate the force into the components R, S, and W (Figure 10), where R is directed radially outward from the sun, S is perpendicular to R and lies in the orbital plane, and it is taken to be positive in the direction of increasing true anomaly  $f$ . W is the force perpendicular to the orbital plane and is taken to be positive in the direction of the orbital pole P. The dust particle is located at G, and the great circle OQ is the projection of the orbit onto the celestial sphere, where the points P and P' are the poles of the orbit. The arc OQ is the longitude of the ascending node, and QL is the argument of perihelion.

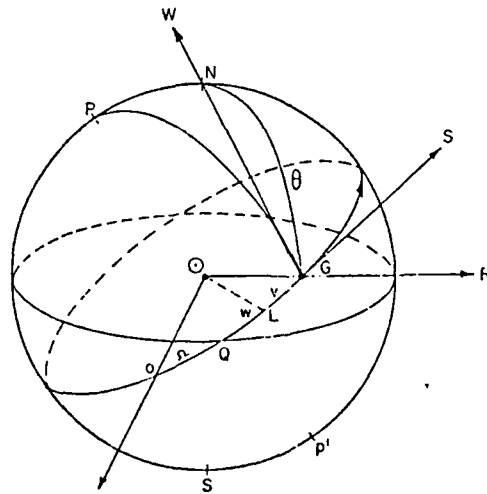


Figure 10. The component R, S, and W of the perturbing force acting on a dust particle orbiting the sun.

The force components can be found from:

$$R = \vec{F}_c \cdot \hat{R} = 0 \quad \text{M.6a}$$

$$S = \vec{F}_c \cdot \hat{S} = -\frac{V_0 s w}{c} B_\theta (\hat{\phi} \cdot \hat{S}) + \frac{V_0 s w}{c} B_\phi (\hat{\theta} \cdot \hat{S}) \quad \text{M.6b}$$

$$W = \vec{F}_c \cdot \hat{W} = -\frac{V_0 s w}{c} B_\theta (\hat{\phi} \cdot \hat{W}) + \frac{V_0 s w}{c} B_\phi (\hat{\theta} \cdot \hat{W}) \quad \text{M.6c}$$

The instantaneous time rate of change in the semi-major axis of the dust particle due to a perturbing force can be found from the sources mentioned earlier:

$$\frac{da}{dt} = \frac{2a^{3/2} e \sin f}{\sqrt{\mu} (1-e^2)^{1/2}} R + \frac{2a^{5/2} (1-e^2)^{1/2}}{\sqrt{\mu} r} S \quad \text{M.7}$$

where:

$$\mu = GM_0 - \frac{\pi s^2 Q_{pr} E_0}{mc}$$

G is the gravitational constant,  $Q_{pr}$  is the radiation pressure efficiency,  $E_0$  is the solar constant, and  $M_0$  is the mass of the sun. Therefore, since  $R = 0$ , and since only the  $B_\theta$  component is of interest,

$$S = -\frac{V_0 s w}{mc} B_\theta (\hat{\phi} \cdot \hat{S}), \text{ per unit mass.} \quad \text{M.8}$$

To evaluate the term  $(\hat{\phi} \cdot \hat{S})$ , we see from Figure 11 that  $\hat{\phi} \cdot \hat{S} = \cos X$ ,  $\widehat{PG} = 90^\circ$  and  $\widehat{PN} = i$ . Thus, in the spherical triangle QNG

$$\cos X = \frac{\cos i}{\sin \theta}$$

and

$$S = -\frac{V_0 s w}{mc} B_0 \frac{R_0}{r} \cos i \quad \text{M.9}$$

We can now rewrite equation M.7 as:

$$\frac{da}{dt} = \frac{2a^{5/2} (1-e^2)^{1/2} V_0 s w B_0 R_0 \cos i}{\sqrt{\mu} r^2 mc} \quad \text{M.10}$$

Since our main interest here is the instantaneous change in the semimajor axis,  $a$ , due to a sudden appearance of a strong  $B_\theta$  component, equation M.10 need not be averaged over the whole orbit. Therefore, by integrating equation M.10 and rearranging, we find

$$\frac{1}{a_2^{3/2}} = \frac{1}{a_1^{3/2}} + \frac{2.74 \times 10^6 V_0 w B_0 (1-e^2)^{1/2} \cos i}{\sqrt{\mu} r^2 \rho s^2 c} \Delta t \quad \text{M.11}$$

where  $a_1$  and  $a_2$  are the initial and final semimajor axes in A.U., respectively.  $\Delta t$  is the time that  $B_0$  is acting on the particle. If  $B_0$  points to the south ecliptic pole, then dust particles in direct orbits would spiral toward the sun due to this effect, whereas particles in retrograde orbits will be ejected from the solar system. The opposite will be true if  $B_0$  points to the north ecliptic pole.

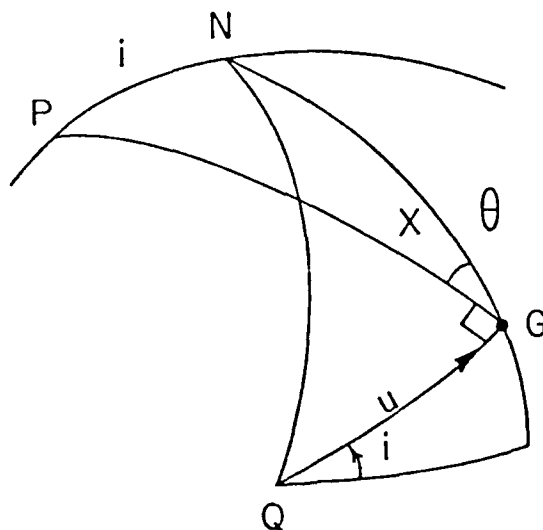


Figure 11. A sketch of the spherical triangles GNP and GNQ.

Using equation M.11, we can find the effect of a sudden  $B_0$  component on the semi-major axes of the dust particles. In surveying the interplanetary magnetic field data from earth orbiting satellites measured over the period 1963-1974 (King, 1975), we chose an unusually high  $B_0$  component on October 27 and 28, 1967. On these two days an hourly average of 11.4 gammas was registered by the AIMP 1 (EXPLR 33) satellite.

In Table 5 we show the result of using equation M.11 to estimate the effect on the semi-major axes of the dust particles using this high level of  $B_0$ . In this calculation we assumed circular orbits and values of  $V_0 = 10$  volts,  $B = 11.4 \times 10^{-5}$  gauss,  $i = 0$ ,  $t = 3600$  sec, and  $w = 7 \times 10^7$  cm/sec. Two types of particles (iron and silicates) with two sizes (1 and  $10\mu$ ) were used, and were placed at 0.5 and 1 A.U. from the sun. We see that this effect is important for particles of size  $< 10\mu$ , and may lead to a sudden change in the size distribution for these particles. However, the magnitude ( $a_1 - a_2$ ) does not increase toward small heliocentric distances by an appreciable amount. Therefore, it does not lead to sudden concentrations of particles  $< 10\mu$  at smaller heliocentric distances, as one might expect, and we do not anticipate an observable change in brightness due to this effect.

Table 5

Calculated Effects on the Semi-Major Axes of the Dust Particles

<u>S (<math>\mu</math>)</u>	<u><math>\rho</math> (gm/cm<sup>3</sup>)</u>	<u>a<sub>1</sub> (A.U.)</u>	<u>a<sub>2</sub> (A.U.)</u>
1	2.5	1	0.953
10	"	"	0.999
1	7.86	"	9.984
1	2.5	0.5	0.467
10	"	"	0.499
1	7.86	"	0.489
1	2.5	0.1	0.0867
10	"	"	0.0997
1	7.86	"	0.0952

# N- PARTICLE- PARTICLE COLLISION

The dynamics of collision between small particles that are orbiting the sun have been developed by Dohnanyi (1978), and later also discussed by Zook et al. (1979). The former study (Dohnanyi) was designed to investigate whether there are enough collisions between the Asteroids to account for supporting the zodiacal cloud, the latter (ZOOK) was an attempt to explain the observed  $\beta$  meteoroids (see Conclusions, and Figure 12) leaving the solar system due to their reduction in size by collisions with each other for the solar radiation to blow them out of the solar system.

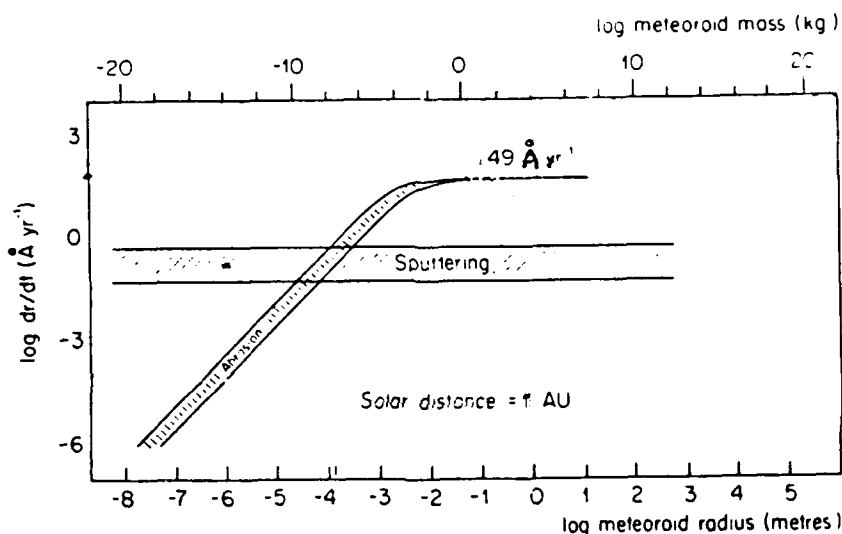


**Figure 13** Meteoroid impact erosion rates (abrasion) of particles compared with solar wind sputtering rate at 1 AU from the Sun, as a function of the particles' radii,  $R$

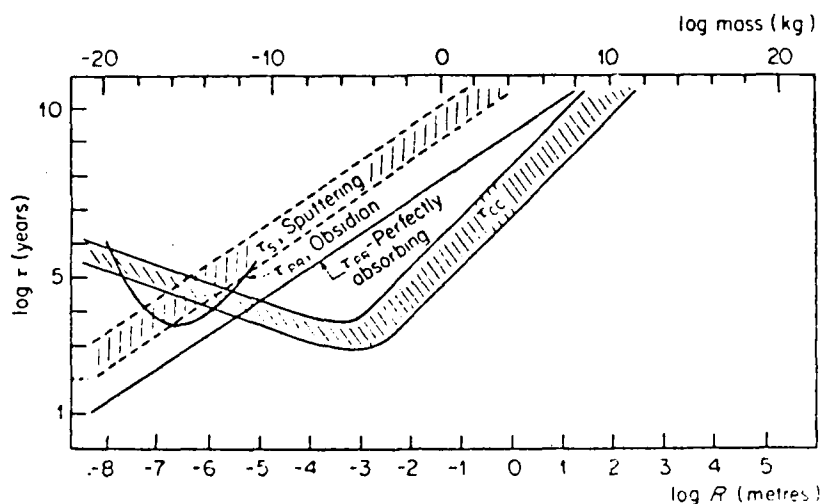
Here, we will be only concerned with the survival times of the particles under collisional events. Also we like to include the effect of erosion of the particles due to gradual mass loss from the surface of the particles resulting from erosive collision. Figure 13, shows a comparison between erosive collision and sputtering (erosion caused by solar wind particles hitting the particle), as a function of log of the radius of the particles, and at a distance of 1 AU from the sun. It is clear from Figure 13, that collisional erosion is higher than sputtering for sizes between  $10^{-4}$  to  $10^{-2}$  meters.

Figure 14, shows the particle survival times (in log years) at 1 AU from the sun, as a function of their effective radii in log meters and log mass, due to catastrophic collisions and sputtering. The survival time for particles larger than  $10^{-12}$  kg

or larger than a few micrometers is dominated by catastrophic collisions, at 1 AU from the sun. However, micrometer-sized and smaller particles are strongly

affected by the P-R effect and by sputtering. Sputtering completely dominates the P-R effect for particles smaller than  $0.1 \mu\text{m}$ .

Particle-Particle collision is heavily effected by the number density of the particles at the desired location in space. For example, for interplanetary particles collisions it is only enhanced near the sun due to the enhanced number density. It is obvious that unless the number density of particles orbiting the Earth is highly enhanced, there is no reason to consider this effect.



**Figure 4** Particle survival times at 1 AU from the Sun, as a function of their effective radii  $R$ , in metres

### O-THE INTERACTION OF SPACE BASED LASER BEAMS WITH SMALL PARTICLES

This section deals with the complex problem of what happens when a cloud of particles are deployed in space and are subjected to laser beams. Obviously, the particles will be subjected to radiation pressure in the forward direction of the beam and will receive linear momentum in that direction. If the beam is much wider than the cross section of the particles then the shape of the beam (i.e. Gaussian vs. doughnut), and the shape of the particle plays an important role here. If the particle is highly irregular in shape then it will begin to leave the beam in either modes. Figure 15 shows an extreme case where a wedge will leave the beam. On the other hand, if the particles are spherical then an interesting situation arises. If the beam is Gaussian and the spherical particles are transparent they will stay in the beam and move to its maximum intensity region as shown in Figure 16a. This results in suppressing the laser beam. If the particles are reflective then they leave the beam. In both cases the laser beam will drive a hole through the cloud of particles. If however, the laser beam has a doughnut mode and the particles are transparent, then they will leave the beam, whereas reflective particles will move to the center of the beam (Figure 16b). We hope that this area of research will gain more importance and funds will be allocated to continue this investigation theoretically and by observations.

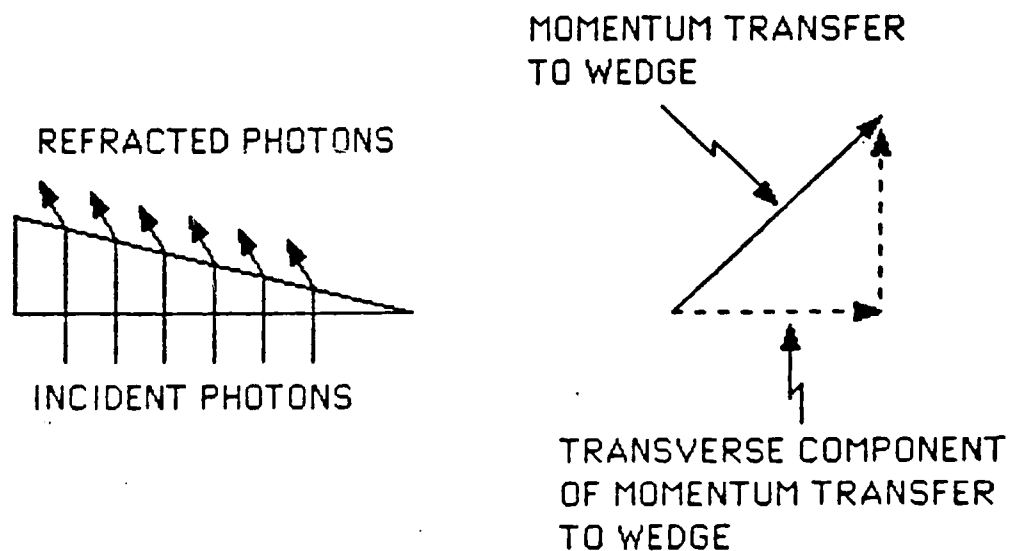


FIGURE 15

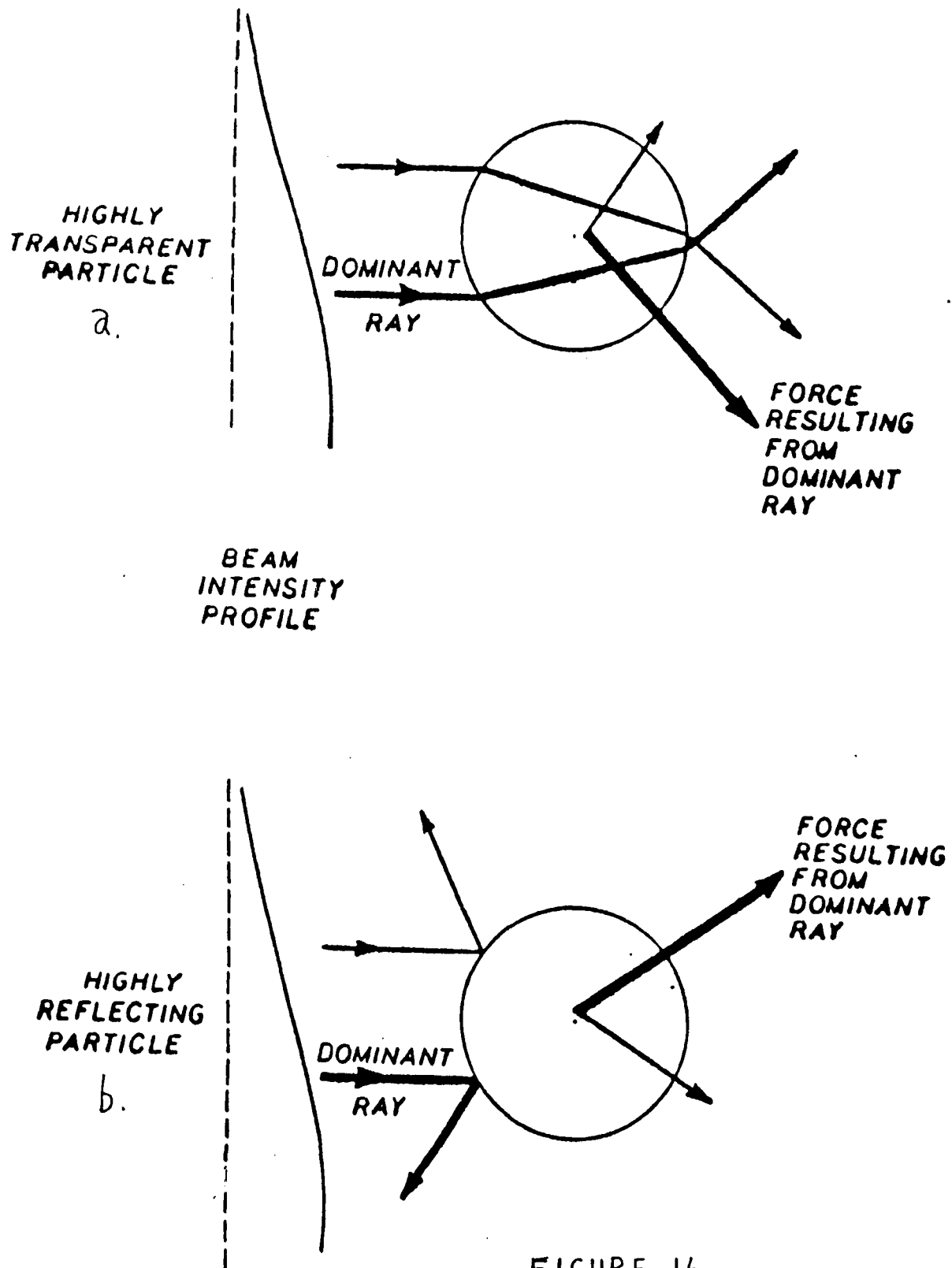


FIGURE 16

## CONCLUSIONS

This project was designed to study the dynamical forces acting on solid particles in space. This included the forces acting on the particles in an Earth's orbit and in interplanetary space. From a glance at the table of contents one can scope the forces involved in this study. Basically these forces were related to solar radiation, solar wind, the interplanetary magnetic field, and the environment in an Earth's orbit.

The forces acting on solid particles in an Earth's orbit are mainly from: solar radiation pressure, atmospheric drag, and the Earth's magnetic field. Radiation pressure will create a diffuse symmetric concentration of particles near the ecliptic plane. This symmetry of concentration about the ecliptic plane is almost undisturbed by the gravitational perturbations beyond a geocentric distance of 7.7 Earth radii. The oblateness of the Earth destroys the ecliptic symmetry of orbiting dust particles larger than an approximately determined critical size that varies from 1 to 100 for ratios of  $a/R_E$  (where  $a$  is the semi-major axis of the particle's orbit and  $R_E$  is the radius of the Earth) from 2 to 8 respectively. This decrease in the critical size as a function of geocentric distance is such that within 1 to 2 Earth radii from the Earth's surface essentially all ecliptic symmetry is destroyed. Radiation pressure also causes large-amplitude oscillations in the eccentricity of the particle's orbit. This make this perturbation the dominant factor in determining the lifetimes of the particle's in orbit. Furthermore, when the area to mass ratio exceeds about  $1500 \text{ cm}^2/\text{gm}$  the lifetime of an orbiting particle is less than 1 year. The effects of coulomb drag and P-R drag are negligible by comparison.

The effect of atmospheric drag on the particle's Earth orbit included two types of effects; one is to investigate the rate of momentum transfer due to the collisions of the solid particles with the air at 500 km (for Example) above the surface of the Earth and including the recoil of atmospheric particles from the orbiting solid particles. Equations describing these forces are listed and their incorporation into the Gaussian perturbation equations is suggested. The other effect is the charging of the orbiting particles by their interaction with the atmospheric plasma is discussed. Two competing mechanisms effecting the charging of the particles, 1) the electrons are approximately 60 times faster than positive ions will negatively charge the particles. 2) the photoionization during the daytime by the absorption of solar UV photons and the ejection of electrons may not keep the particles negatively charged. The magnitude of these competing effects are dependent on the geocentric distances of the orbiting particles.

The effect of the Earth's magnetic field on the particle's orbital elements are found to be negligibly small compared to radiation pressure. Only for very small particles, much less than 1  $\mu\text{m}$  across, would the Lorentz force be dominant. The Earth's magnetic field does serve to trap mostly electrons into radiation belts, which can charge dust particles to high negative potentials in the shadow of the Earth. This allows Coulomb drag to affect the particles, which can create either a positive or negative drag on the dust, depending on its semimajor axis.

Dynamical forces that exists in the interplanetary medium which effect the orbital elements of the particles were investigated. Among these the Poynting-

Robertson drag is the dominant. This is true everywhere except in the vicinity of planets or very close to the sun (the F-Corona region) where ion drag from the ejected solar plasma dominates over the P-R drag. A formalism for calculating the ratio of ion drag to the P-R drag is derived, where the value of this ratio is constant (i.e. independent of heliocentric distance; 0.26). However, this ratio will break down inside the F-Corona region. We have also evaluated this ratio under the conditions of solar flare emanating shock waves that propagate in the interplanetary medium.

Coulomb drag from solar wind ions is less important, but, it can be significant in the vicinity of planets where electrons may be in much higher concentration than the quiet solar wind. It can be significant also in the F-Corona region where the dust particles encounter electron densities of the order of  $10^8/\text{cm}^3$ .

The rotation of solid particles in the space environment is investigated. Three spin mechanisms are investigated: the windmill effect which rotates particles by the interaction of solar photons with surface irregularities of the particles; the albedo/radzievskii effect which spin the particles due to the differential absorption and reflection of solar light resulting from the chemical inhomogeneity of the particles; and a statistical spin mechanism resulting from solar wind ion impacts on the particles. The interest in the various spin mechanisms here is the eventual breakup or bursting of the particles due to the stress from spin overcoming the tensile strength of the particles. This is a way to eliminate particles by sending them into hyperbolic orbit which will take them out of the solar system. This only happens when the fragments of the particles reach a critical size that allows solar radiation pressure to overcome the gravitational attraction of the sun. Such particles i.e. leaving the solar system have been observed by satellites and spaceprobes and were given the name  $\beta$  meteoroids, where  $\beta$  is the ratio of solar radiation pressure over the solar gravitational attraction. The particles leave the solar system when the value of  $\beta$  is close to 1.

Out of the three spin mechanisms, the windmill effect and the albedo effect are the most promising in breaking the particles in a shorter time than the solar wind statistical mechanism. This is so, since these two mechanisms are non-statistical and depend on a physical parameter, the effective moment arm of the particle. However, the lifetime of the particles are in thousands of years. They can also be made shorter by shining an intense beam on them such as laser light, and, especially, if the laser light is circularly polarized. This can be thought of as a way of eliminating space debris in the future if other measures fail.

Particles can also burst if they are highly electrically charged. This possibility is gaining a lot of interest among researchers in the field of meteoroids and micro-meteoroids entering the Earth's atmosphere, since there is suspicion of breakup due to high electrical charge. We found that a particle will burst if the surface stress is greater than the particle's tensile strength, namely:

$$s < 9.4 \times 10^{-4} V T^{-1/2}$$

where  $s$  is the minimum radius in cm required to disrupt for a given charge  $V$  (here charge is expressed in volts for spherical particles) and tensile strength  $T$ . High potential is needed to burst big particles. For example, for highly pure silicate particles and a potential as high as 100 volts, particles of only  $0.011 \mu\text{m}$  will burst. If the particles are porous and highly irregular in shape, then perhaps bigger particles will burst at 100 volt charge. This is a very interesting problem, since we know roughly that the positively charged interplanetary particles are between 10-14 volts, but it is difficult to know the charge of man made particles in space. Further investigation is needed for this problem.

# REFERENCES

- Armstrong, T.P., Krimigis S.M. and Behannon, K.W., (1970), J. Phys. Res., Vol. 75, 5980.
- Bandermann, L.W., (1968), Ph.D. Dissertation, University of Maryland.
- Belton, M.J.S., (1964), Ph.D. Dissertation, Univ. of California, Berkley.
- Belton, M.J.S., (1966), Science, Vol. 151, 35-44.
- Belton, M.J.S., (1967), In Proceedings, Symp. "On the Zodiacal Light and the Interplanetary Medium, NASA Sp. 150 (J.L. Weinberg Ed.), 301-306.
- Burlaga, L.F. and Ness, N.F., (1967), Tenth International Conference on Cosmic Rays, Calgary, Alberta.
- Burns, J.A., Lamy, P.L., and Soter, S. (1979), Icarus, 40, 1-48.
- Chow, C.Y., (1967), AIAA J., 5, 2281.
- Coleman, JR., P.J. and Rosenberg, R.L., (1971), J. Geophys. Res., Vol. 76, 2917-2926.
- Deforest, S.E. (1972) J. Geophys. Res., 77, 651.
- Dohnanyi, J. S., (1978), In Cosmic Dust, pp. 527-605, John Wiley and Sons,
- Dryer, M., (1975), Space Science Reviews, Vol. 17, 277-325.
- Gosling, J.T., Asbridge, S.J., Bame, A.J., Hundhausen, I.B., and Strong I.B., (1968), J. Geophys. Res., 73, 43.
- Hameen-Anttila, K., (1962), Ann. Acad. Scient. Fenn., Av1, 112.
- Harwit, M., (1963), J. Geophys. Res., 68, 2171.
- Harwit, M., (1970), Nature, 226, 61.
- Harwit, M. and Vanysek, V. (1971), Bulletin of the Astronomical Institutes of Czechoslovakie, Vol. 22, No.1, 18-21.
- Harwit, M., (1973), Astrophysical Concepts, John Wiley and Sons Inc.
- Jastrow, R. and Pearse, C.A., (1957), Journal Geophys. Res., Vol. 62, No.3, 413-423.
- King, J., (1975), Interplanetary Magnetic Field Data Book, NSSDC-75-04, NASA.
- Lamy, P.L., (1976), In Notes of Physics: Interplanetary Dust and Zodiacal Light, (Eds. H. Elsasser and H. Fechtig, H.), pp. 437-442, Springer-Verlag, Berlin.

- Lyttleton, R.A. (1976), Astrophys. Space. Sci., 44, 119-140.
- Moulton, F.R., (1914), An Introduction to Celestial Mechanics, New York: MacMillan Co.
- Mukai, T., Yamamoto, T., Hasegawa, H., Fujiwara, A., and Koike, C. (1974), Publ. Astron. Soc. Japan, 26, 445-458.
- Nakagawa, Y., Wu, S.T. and Han, S.M., (1973), Solar Phys., Vol. 30, 111.
- Opik, E.J., (1956), Irish Astron. J., Vol. 4, 84.
- Paddack, S.J., (1973), Ph.D. Dissertation, Catholic University of America, Washington D.C.
- Paddack, S.J. and Rhee, J.W., (1975), Geophys. Res. Letters, 2, No. 9, 365-367.
- Paddack, S.J., (1969), J. Geophys. Res., 74, 4379-4381.
- Parker, E.N., (1958), Astro. Phys. J., 128, 664.
- Parker, E.N., (1963), Interplanetary Dynamical Processes, Vol. VIII, Monographs and Texts in Physics and Astronomy, New York: Interscience Publ.
- Peale, S.J., (1966), J. Geophys. Res., 71, 911-933.
- Poynting, H.J. (1903), Phil. Trans. Roy. Soc. A., 202, 525.
- Radzievskii, V.V., (1954), Dokl. Akad. Nauk. SSSR, Vol. 97, No. 1, 49-52.
- Robertson, H.P. (1937) Monthly Notices Roy. Astron. Soc., 97, 423.
- Shapiro, I.I. (1963), In The Dynamics of Satellites by (M. Roy, Ed.), pp. 257-312, Academic Press, New York.
- Shapiro, I.I., Lautman, D.A., and Colombo, G. (1966), J. Geophys. Res., 71, 5694-5704.
- Shapiro, I.I. and Jones H.M. (1961) , J. Geophys. Res., 66, No. 12, 4123-4127.
- Smart, W.M., (1965), Spherical Astronomy, Cambridge University Press.
- Sparrow, J.G., (1975), Geophys. Res. Letters, 2, 255-257.
- Standeford, L., (1968), Ph. D. Dissertation, Univ. of Illinois.
- Timoshenko, S., (1942), Strength of Materials, D. Van Nostrand, Princeton, New Jersey.
- Van de Hulst, H.C. (1957), Light Scattering by Small Particles. Wiley, New York.
- Wu, S.T., and Fu, T.S., (1970), J. Appl. Phys., 41, 791.
- Wyatt, S.P. Jr., and Whipple, F.L. (1950), Ap. J., 111, 134-141.

Zook, H.A., and Berg, O.E., (1975), Space Sci., 23, 183-203.

I: PRELIMINARY RESULTS ON LIGHT SCATTERING BY  
LASER LEVITATED PARTICLES

Nebil Y. Misconi<sup>1</sup>, Keith F. Ratcliff<sup>2</sup>, Edwin T. Rusk<sup>1</sup>,  
John P. Oliver<sup>3</sup>, and Wan-Xian Wang<sup>1</sup>

1. University of Florida, Space Astronomy Laboratory
2. State University of New York at Albany, Department of Physics
3. University of Florida, Department of Astronomy

ABSTRACT

A new light scattering facility utilizes a laser-particle levitation technique to measure the angular distribution of light scattered by solid particles of size range 10 to 100 microns. The performance of the facility is illustrated by an excellent match between the observed scattering from a 33  $\mu\text{m}$ -diameter sphere and the Mie theory prediction.

INTRODUCTION

This paper and the paper that follows (II: An Apparatus for Photometry of Light Scattered by Laser Levitated Particles) are the first two in a series of papers, III: Scattering by spheres; IV: Scattering by Spheroids; V: Scattering by Clusters and Irregular Particles; describing light scattering by solid particles in the size range of 10 to 100 microns. Knowledge acquired on light scattering by particles in this size range and others is very important for studies in low light Astronomy and Astrophysics that involve scattering of starlight from clouds of particles. For example, in the study of the zodiacal light - which is sunlight scattered by interplanetary dust - an understanding of light scattering is required in order to deduce information on the physical parameters of the dust and the cloud.

In studies of the zodiacal light (before 1976), it was believed that the zodiacal dust that contributes mostly to the observed brightness was in the sub-micron and little over 1 micron size range. However, Giese<sup>1</sup>, found that particles in the 10 to 100 micron size range contribute most of the zodiacal light, with a typical particle being 30 microns in size. The main source of information on the light scattering nature of the zodiacal dust is the formulation of an empirical light scattering function deduced from the data by inverting the zodiacal light brightness integral (see for example Lienert)<sup>2</sup>. This empirical scattering function is made under the unrealistic assumption that the scattering nature of the particles is the same throughout the cloud. Methods involving modeling the zodiacal light have been limited to using Mie Theory calculations for spheres. Such results are unrealistic.

Making direct measurements of the scattered light in the size range of 10-100 microns has been difficult. This difficulty is due to finding suitable methods of suspending these particles. One approach has been the use of electrostatic suspension and confinement of the particles<sup>3,4</sup>. Another approach is to measure the light scattered by particles dropped in a laser beam passing through the field of view of a nephelometer<sup>5</sup>. A third approach (to date applied only as an analog to scattering of visible light by sub-micron size particles) has been to measure microwave radiation scattered off large-sized (decimeters) model particles using microwave radiation<sup>6</sup>. This method is useful since the light scattering distribution depends on the  $x$  parameter namely,

$$x = \frac{2\pi a}{\lambda}$$

where  $\lambda$  is the wavelength of the electromagnetic radiation and, for a spherical particle,  $a$  is the radius of the sphere.

It is noteworthy to say that the method of laser-particle levitation has distinct advantages that the other methods, previously mentioned do not have. It gives the particle

the freedom to move i.e. rotation, which allows scattering measurements covering all surfaces of the particle, and not just in one particular orientation. Furthermore, unlike the analog method described above the particles measured are not models, they are particles of the actual size and index of refraction being studied, although a limitation of the laser levitation technique is the necessity of using non-absorbing particles, because even a small amount of absorption would result in the particles being vaporized.

### METHOD

In our apparatus, the levitated particle is supported by a three dimensional optical trap formed above the focus of a lens by the laser beam. The radiation incident upon the particle serves the dual purpose of both levitating the particle and providing the radiation whose scattering is being measured. Here, momentum is transferred to a particle in the process of scattering radiation. This momentum transfer balances the weight of the particle (levitation), and also provides confinement of the particle in the transverse direction<sup>7</sup>. The transverse confinement is illustrated in Figure 1. The fact that the particle is a transparent sphere and that the profile of the laser beam is Gaussian (TEM<sub>00</sub> mode) creates this transverse confinement. The higher intensity near the maximum of the beam creates a stronger restoring force that pushes the particle always toward the maximum of the beam. Ashkin<sup>5</sup> measured this transverse confining force and found it to be one half the force needed to balance the weight of the particle (1/2 g). Ratcliff, Misconi and Paddack<sup>8</sup>, found a similar strength for the transverse force in an earlier laser-particle levitation experiment at Goddard Space Flight Center, where they also developed for the first time a three beam optical confinement bottle to trap irregular particles by splitting the argon beam into two antiparallel beams plus a vertical beam.

Ashkin<sup>9</sup> published photographs showing the kinds of scattering patterns in the forward direction produced by levitated clusters of spheres in the laser beam (geometrically irregular particles), with levitation of particles confined to sizes of approximately between

20 and 40 microns. With our current apparatus we have achieved levitation of particles up to 95 microns in size ( $x=600$ ). This required an initial laser energy of approximately 15 watts to lift the particle off the glass plate. While photography of light scattering patterns can show the qualitative nature of the scattering, photometric measurements and comparison with theory is the best way to study scattering. Our plans call for levitating particles of much bigger size (hundreds of microns) using a 600 W Nd:Yag laser at 1.06 microns.

Our scattering facility (see paper II for details) has been designed to make photometric measurements of the angular distributions of light scattered from 10 to 100 micron sized particles. We have also developed a method by which we can retrieve the levitated particle from the beam (see paper II for details) after we have made the scattering measurements, to inspect and photograph the particle using optical microscopes. This enables us to characterize the scattering pattern resulting from existing irregularities on the particle. We believe that our studies in the size range of 10 to 100 microns are very well suited to give information needed for understanding the nature of the zodiacal light.

Photometric measurements of the scattered radiation is made by a goniometer-mounted photodiode (paper II) in steps of  $0.5^\circ$  through a range of scattering angles from  $16^\circ$  to  $167^\circ$ , the limit on the range of scattering angles being determined by the size of the light baffle. This range of angles allows adequate discrimination of the effect of particle shape on angular distribution.

## RESULTS

Because Mie scattering theory is exact, measurements of the angular distribution of radiation scattered from spheres was used to provide diagnostics for the experiment. In Figure 2, we show the measured (discrete points) and theoretical (continuous curve) angular distributions for a perfect sphere 33.0 microns in diameter ( $x = 202$ ). The particle used to obtain data plotted in Figure 2 is composed of suprasil glass ( $n = 1.459$ ) which is

highly pure (absorption coefficient =  $5 \times 10^{-4} \text{ cm}^{-1}$ ). The polarization of the incident radiation was aligned  $37^\circ$  to the normal to the scattering plane, which is the case when the half-wave plate is removed from the beam path (see paper II).

The  $2^\circ$  opening angle of our photodiode averages over a few oscillations of the detailed scattering pattern. In presenting the theoretical curve, we have therefore similarly averaged over a  $2^\circ$  interval. There are two regions in Figure 2 of particular note. The steep rise which occurs around  $150^\circ$  is due to refracted laser light emerging at the rainbow angle. Its location is sensitive to the index of refraction but insensitive to size of the sphere. Our measured data reproduced the monochromatic rainbow structure quite accurately both in position and amplitude. By contrast the structure seen in the range of scattering angles between  $80^\circ$  and  $110^\circ$  is very sensitive to both the index of refraction and the exact size of the sphere. The structure found for scattering angles in the  $80^\circ$  to  $110^\circ$  range fit both the positions and relative sizes of the maxima. There was a slight divergence from the theoretical curve at the smallest scattering angles. This effect appeared more strongly in the scattering curves for spheres which had numerous small irregularities on the surface. We suspect that although this particular sphere appeared "clean", surface irregularities were responsible here also.

Since the original test measurements that were shown in figure 2, the apparatus was modified to give a larger range in scattering angle ( $16^\circ$ - $167^\circ$ ), to read in smaller increments of scattering angle, and to allow for a variation in polarization of the incident beam. Figure 3 shows the complete scattering curve of a suprasil sphere of diameter  $34.09 \mu\text{m}$  superimposed on the theoretical curve. The size of the particle in this case was not measured experimentally but deduced from the agreement between the Mie curve and the measured data. The top curve was taken when the electric vector of the incident beam was perpendicular to the scattering plane and the bottom curve (shifted down by a factor of 10) refers to scattering with the polarization vector in the scattering plane.

Many details will follow in Paper III (presently in the data-analysis stage) of this series which will present an in-depth analysis of our measurements of scattering by spherical particles, and of the scattering by perfect vis-a-vis imperfect spheres.

In the forthcoming papers in this series, we will also compare the scattering curves that we obtain experimentally from spheroids and irregular particles with the empirical scattering function of the zodiacal light. This will be the first attempt to compare two differently obtained scattering functions and to look for possible agreements.

### THEORY

Comparison with theory can be difficult, because of the sensitive dependence of the scattering curves on the diameters of the spheres. The accuracy in measuring particle sizes optically is limited to the wavelength of light. Changes in the light scattering pattern can become significant in size differences as small as 2% of the wavelength of the incident beam. Figure 4 shows this variation in three theoretical Mie scattering curves where the particle diameters vary from 34.08 - 34.10  $\mu\text{m}$ . Here each successive curve has been lowered by .75 for clarity. A comparison of scattering curves to theory can be used to measure particle sizes to much greater accuracy, and the huge volume of theoretical data required is possible using today's high speed computers. We have used this method in determining the size of several particles, including those shown in figures 2 and 3. More accurate sizing (to  $\pm 0.1 \mu\text{m}$ ) is available using electron microscopy, which has been already used very successfully by Brownlee and his associates by making SEM photographs of individual cosmic dust particles collected from the upper atmosphere (see for example, issues of Cosmic Dust Catalog, Planetary Materials Branch, NASA, LBJ Space Center, Houston, Texas). We will use our aforementioned technique for recapturing the levitated particle, and obtaining SEM photographs for future analyses.

The structure of the scattering curves are equally sensitive to the index of refraction of the spheres. Because our test spheres have an absorption of  $10^{-4}/\text{cm}$ ., we need consider

only the real part ( $n$ ) of the refractive index. In the size range of our test particles, a difference of 0.001 in  $n$  becomes significant. At present, the values given for the scattering angles are accurate to  $\pm 1.5^\circ$ , (they are internally consistent to  $\pm 0.01^\circ$ ). This allows a direct measurement of  $n$  to  $\pm 0.015$  by measuring the rainbow angle. We will calibrate the system so that absolute angular measurements can be made to within  $.1^\circ$  in a future refinement of our experiment.

There is a question of this method, concerning the structure of the laser beam, that we would like to address. The beam diverges from a plane wave because of two different aspects. First, there is a natural Gaussian brightness distribution across the beam. This problem, and how it effects our experiment, will be discussed in paper III. Secondly, to generate a stable vertical position, the beam must be focused. This question can be addressed theoretically, by substituting a spherical wavefront for the plane wave in standard Mie calculations. The amplitude functions for the scattering of a plane wave by a sphere are:

$$S_1(\theta) = \sum_{n=1}^{\infty} \frac{2n+1}{n(n+1)} \{a_n \pi_n(\cos\theta) + b_n \tau_n(\cos\theta)\},$$

$$S_2(\theta) = \sum_{n=1}^{\infty} \frac{2n+1}{n(n+1)} \{b_n \pi_n(\cos\theta) + a_n \tau_n(\cos\theta)\},$$

$$\text{where } \pi_n(\cos\theta) = \frac{P_n^1(\cos\theta)}{\sin\theta},$$

$$\tau_n(\cos\theta) = \frac{d}{d\theta} P_n^1(\cos\theta).$$

and  $a_n$  and  $b_n$  are the scattering coefficients.

If the incident wave is a diverging spherical wave (figure 5), then, after applying boundary conditions and using mathematical simplification, the corresponding expressions are:

$$S_1(\theta) = \sum_{n=1}^{\infty} \frac{2n+1}{n(n+1)} \left\{ a_n \pi_n(\cos\theta) + b_n \left[ \tau_n(\cos\theta) + \left( \frac{a}{l} \right) p_n(\cos\theta) \frac{\sin^2\theta}{f(\cos\theta)} \right] \right\},$$

$$S_2(\theta) = \sum_{n=1}^{\infty} \frac{2n+1}{n(n+1)} \left\{ b_n \pi_n(\cos\theta) + a_n \left[ \tau_n(\cos\theta) + \left( \frac{a}{l} \right) p_n(\cos\theta) \frac{\sin^2\theta}{f(\cos\theta)} \right] \right\},$$

where  $f(\cos\theta) = 1 + 2(a/l)\cos\theta + (a/l)^2$ . Here  $a$  is the radius of the sphere, and  $l$  is the distance from the focus to the particle. The maximum deviation between the two cases only approaches 1% if  $a/l$  is 0.01. In the case of our 5 cm focal length lens, a particle radius of 25  $\mu\text{m}$  and focal distance of 2 mm gives  $a/l = .005$ .

We have found a good match with the theory in spite of using a divergent Gaussian beam.

## CONCLUSION

We have established a laser-particle levitation facility capable of making light scattering measurements for various sizes and shapes of highly transparent silica particles in the size range of 10-100  $\mu\text{m}$ . This paper introduces a series of papers by describing the method of levitation used for making angular distribution measurements of the light scattered by these particles. Two examples are given (Figures 2, 3) of the measured angular distribution of light scattered by high purity silica perfect spheres, for angles between 16 to 167°. These measurements were compared to Mie theory directly, and demonstrate the accuracy, angular resolution and angular coverage of measurements made using this approach.

### ACKNOWLEDGEMENTS

We would like to express our appreciation to Dr. A. Ashkin for earlier very helpful discussions and Dr. Ru T. Wang for his shared insight into scattering phenomena. This research was totally supported by The Air Force Office of Scientific Research, AFOSR Contract F49620-85-C-0117.

### References

1. R. Giese and E. Grun, "The Compatibility of Recent Micrometeoroid Flux Curves with Observations and Models of the Zodiacal Light", in "Interplanetary Dust and Zodiacal Light" (H. Elsasser and H. Fechtig, eds.), "Lecture Notes in Physics", 48, 135, Springer Verlag, Berlin-Heidelberg-New York, (1976).
2. C. Leinert, H. Link, E. Pitz, and R. Giese, "Interpretation of a Rocket Photometry of the Inner Zodiacal Light", *Astron. and Astrophys.*, **47**, 221, (1976).
3. R.H. Zerull, R.H. Giese and K. Weiss, "Scattering Functions of Nonspherical Dielectric and Absorbing Particles vs Mie Theory," *Appl. Optics*, **15**, 777, (1977).
4. K. Weiss-Wrana, R.H. Giese, and R.H. Zerull, "Microwave and Laser Facilities to Determine Scattering and Colour Signatures Related to the Physical Properties of Dust Particles," *Properties and Interactions of Interplanetary Dust* (R.H. Giese and P. Lamy, eds.), D. Reidel, Dordrecht, 219, (1985).

5. P. Blik, Ph.L. Lamy and G. Courtes, "Preliminary Results of a Dust Scattering Experiment," **Properties and Interactions of Interplanetary Dust** (R.H. Giese and P. Lamy, eds.), D. Reidel, Dordrecht, 231, (1985).
6. A.C. Lind, R.T. Wang and J.M. Greenberg, "Microwave Scattering by Nonspherical Particles," **Appl. Opt.**, **4**, 1555, (1965).
7. A. Ashkin and J.M. Dziedzic, "Optical Levitation by Radiation Pressure", **Applied Physics Letters**, vol. **19**, No. 8, 283, (1971).
8. K.F. Ratcliff, N.Y. Misconi and S.J. Paddack, "Radiation Induced Rotation of Interplanetary Dust Particles; a Feasibility Study for a Space Experiment," **Solid Particles in the Solar System** (I. Halliday and B.A. McIntosh, eds.), D. Reidel, Dordrecht, 391, (1980).
9. A. Ashkin and J.M. Dziedzic, "Observation of Light Scattering from Nonspherical Particles Using Optical Levitation", **Applied Optics**, Vol. **19**, No. 5, 660, (1980).

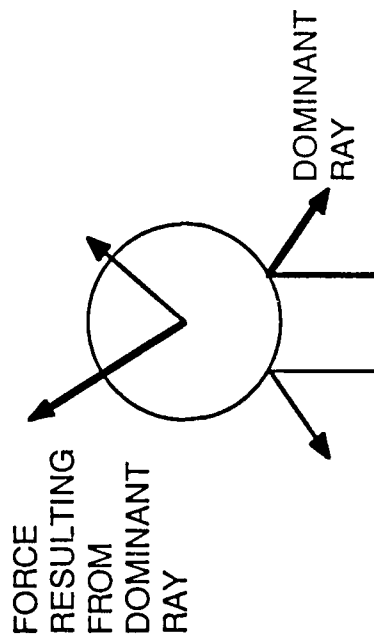
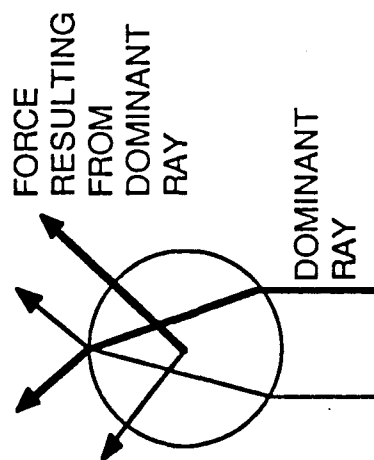
## FIGURE CAPTIONS

Figure 1. Optical forces resulting from variations in the intensity profile of the incident radiation for a highly transparent particle and a highly reflective particle.

Figure 2. Scattering of laser light ( $\lambda = 514.5 \text{ nm}$ ) off of a highly pure (absorption coefficient =  $5 \times 10^{-4} \text{ cm}^{-1}$ )  $33.0 \text{ }\mu\text{m}$  perfect sphere of suprasil glass ( $n=1.459$ ). The experimental measurements (dots) are compared to Mie theory (solid curve).

Figure 3. Scattering of laser light ( $\lambda = 514.5 \text{ nm}$ ) off of a  $34.09 \text{ }\mu\text{m}$  sphere of suprasil glass similar to the one in figure 2. The experimental measurements (dots) are compared to Mie theory (curve); the size of the sphere is determined from this agreement. The top curve was taken when the electric vector of the incident beam was perpendicular to the scattering plane and the bottom curve (shifted down by a factor of 10) with the polarization vector in the scattering plane.

Figure 4. The variation in three theoretical Mie scattering curves where the particle diameters vary from  $34.08 - 34.10 \text{ }\mu\text{m}$ . Here each successive curve has been lowered by a displacement of .75 in  $\log I$  for clarity.



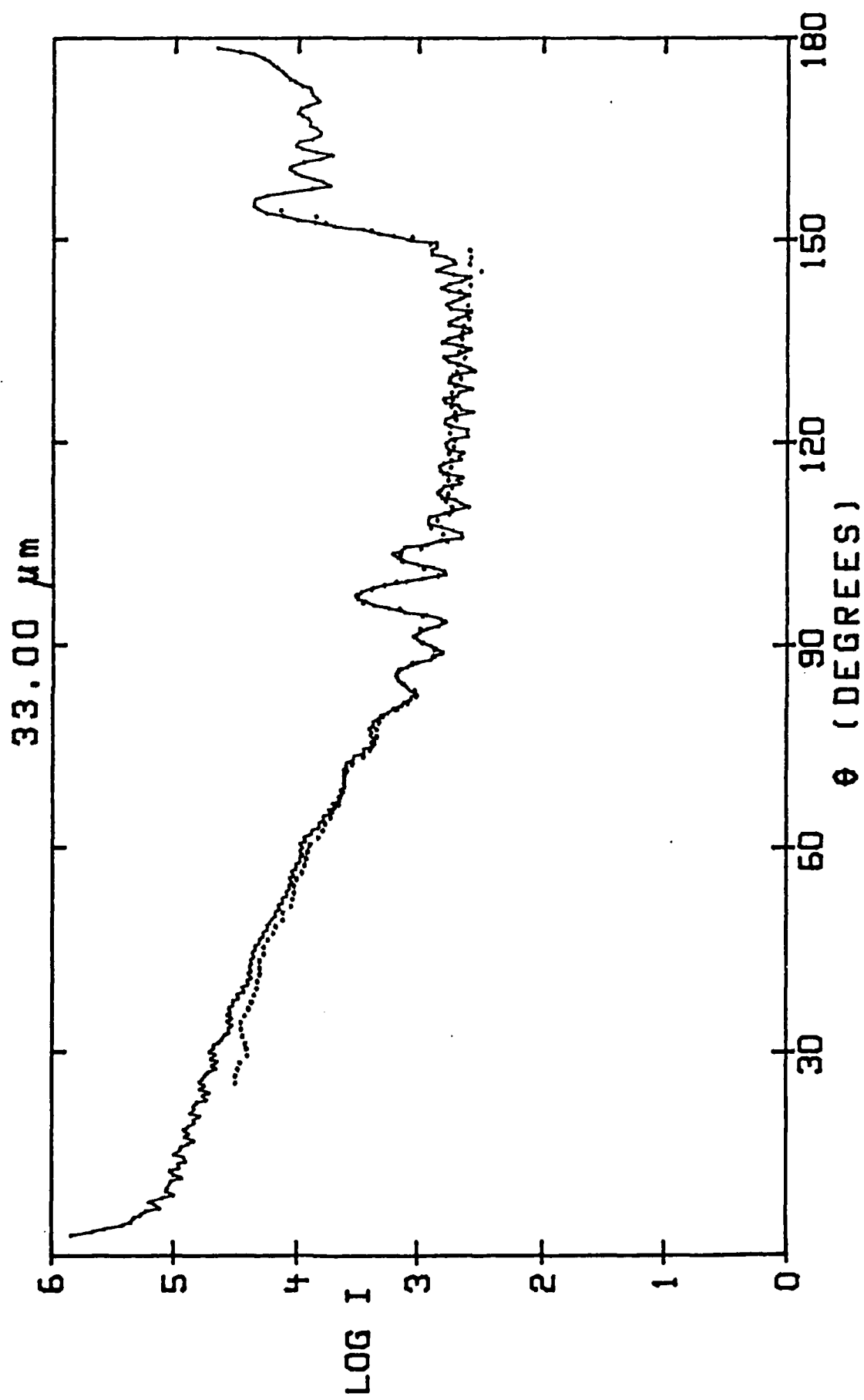
BEAM  
INTENSITY  
PROFILE

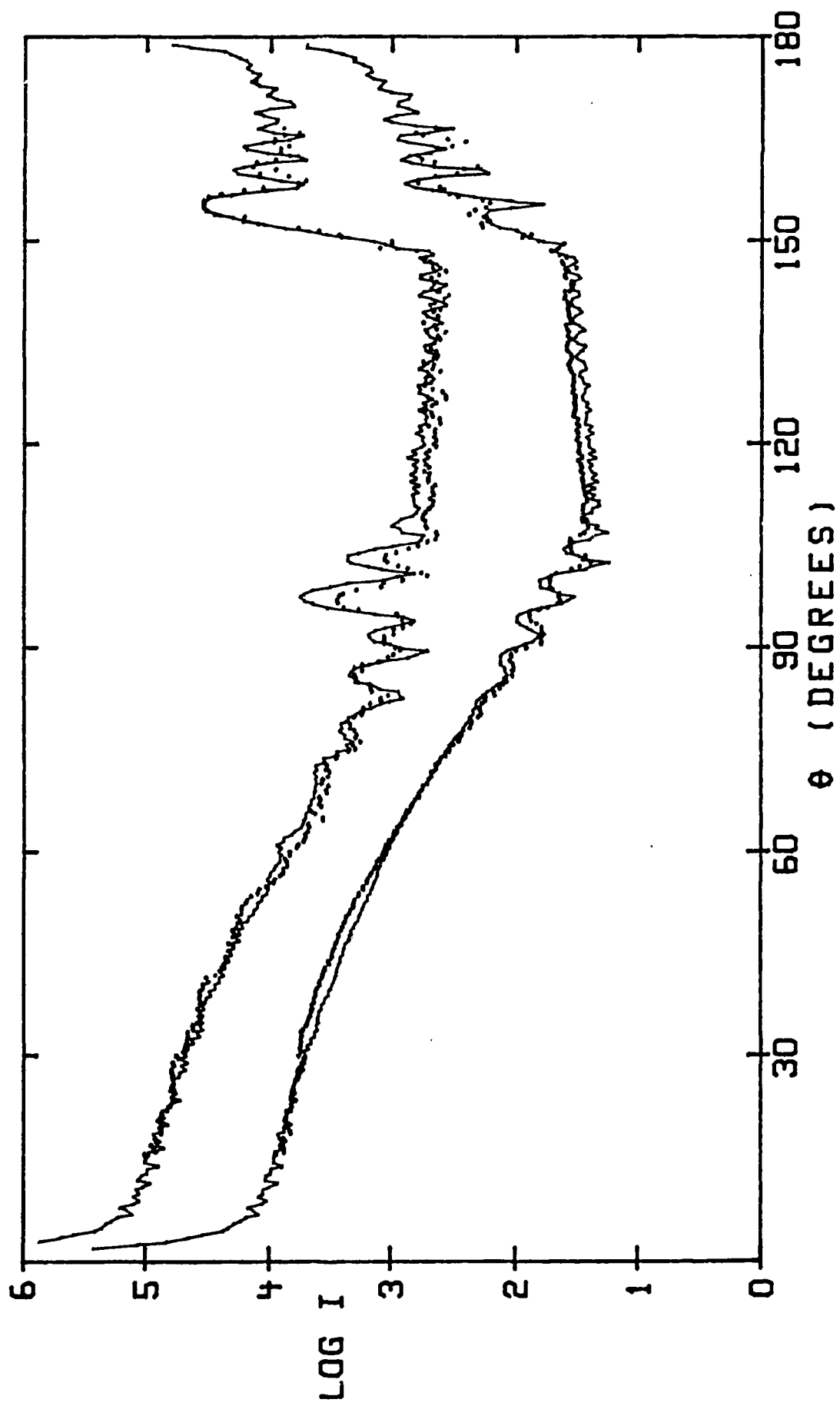


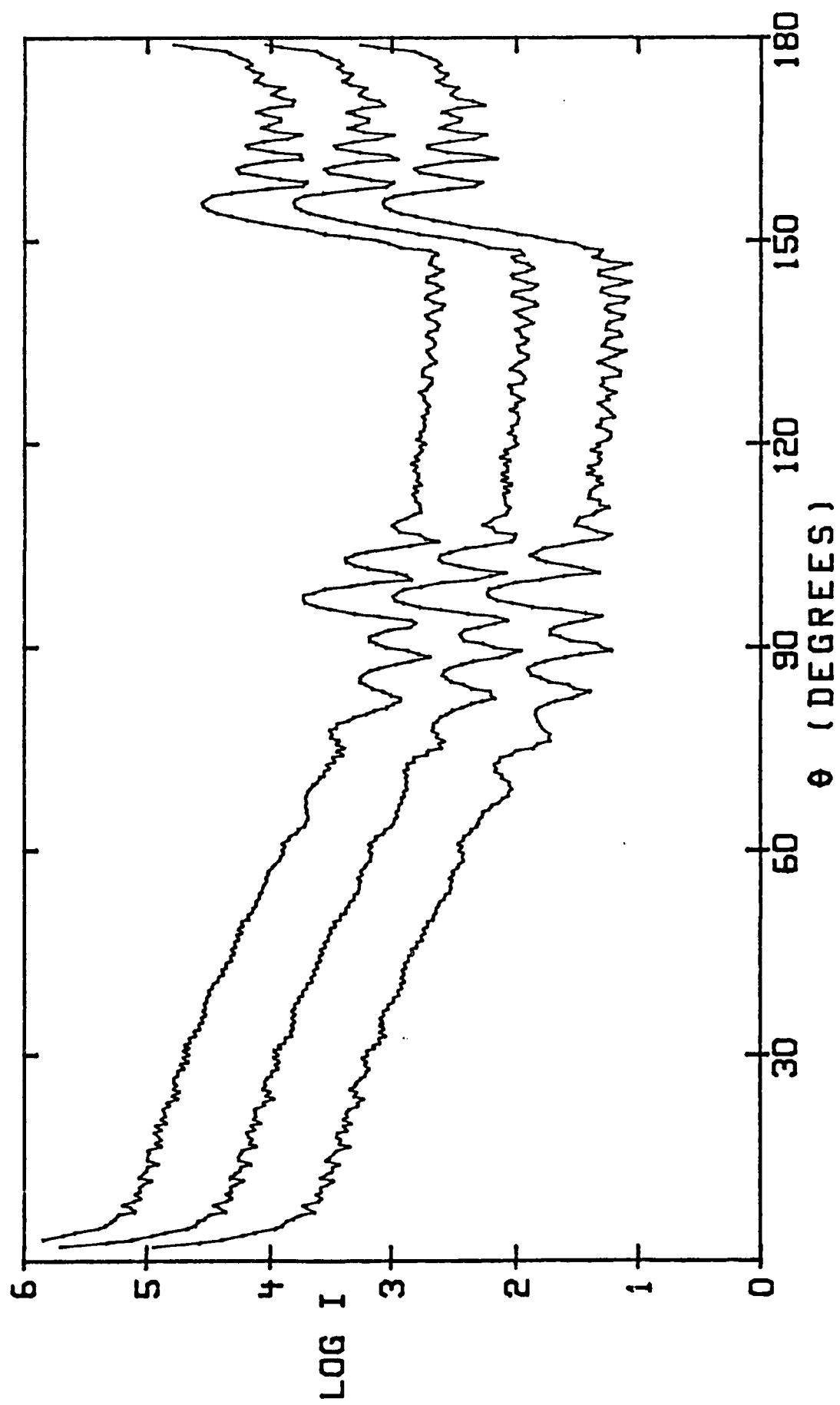
HIGHLY  
TRANSPARENT  
PARTICLE



HIGHLY  
REFLECTING  
PARTICLE







## II: An Apparatus for Photometry of Light Scattered by Laser Levitated Particles

John P. Oliver<sup>1</sup>, Nebil Y. Misconi<sup>2</sup>, Edwin T. Rusk<sup>2</sup>, and Keith F. Ratcliff<sup>3</sup>

<sup>1</sup>University of Florida, Astronomy Department

<sup>2</sup>University of Florida, Space Astronomy Laboratory

<sup>3</sup>State University of New York, Albany, Physics Department

### ABSTRACT

An apparatus is described which allows the levitation of small (10 micron to 90 micron diameter) dielectric spheres in a vertical laser beam. A goniometer mounted photodiode allows the measurement of laser energy scattered from the particle over a range in scattering angles from 15 degrees (forward scattering) through 170 degrees (back scattering). The polarization plane may be selected at will. Imaging systems provide a close-up view of the particle at 0 and 90 degrees from the beam direction, and the far field scattering pattern can be examined over a wide range of angles. A computer provides for control and data acquisition.

### INTRODUCTION

The scattering of electromagnetic radiation by small dielectric particles is a process of interest in the study of many fields ranging from meteorology and atmospheric physics to the study of the interplanetary and interstellar media. This paper describes an experimental apparatus for the measurement of scattering from dielectric particles suspended in a vertical laser beam. It is the second in a series of five papers. An introduction to scattering and laser levitation has been presented in Misconi et al. (Paper I)<sup>1</sup>. The results of our research are presented in Paper III, Paper IV, and Paper V to be submitted at a later date.

## APPARATUS

The system is assembled on an optical table for vibration isolation. The optical components are assembled on a three-dimensional optical bench. The overall layout of the apparatus is shown in Figure 1. The individual components and systems are described below.

## LASER

The laser is a Spectra Physics Model 171-09 Argon laser with a nominal power of 18 watts in multi-line mode and 7.5 watts when the single 5145 angstrom line is selected. The beam is a vertically polarized TEM-00 mode directed horizontally on the optical table. A high quality prism on a precision 3-axis adjustable prism table directs the beam up the primary vertical optical bench member.

The laser is controlled by a Spectra-Physics model 270 power supply. The laser power can be stabilized automatically by the power supply through the use of a photodiode mounted near the laser exit aperture. This detector and a second power detector mounted after the 0 degree viewing right-angle prism are interfaced to the computer system.

## LEVITATION OPTICS

The levitation lens consists of one of a set of anti-reflection coated lenses of 5.0, 7.5, and 10.0 cm. focal length mounted in parfocal lens holders. The choice of lens to use for levitation depends upon the desired beam waist diameter for the particular particles to be levitated. The selected levitation lens holder is mounted in an x-y translation lens mount to allow precise collimation of the optical system. This mount is in turn located on a precision vertical slide with a 5.0 cm travel. The upper travel limit is set by a micrometer. A constant tension spring balances the weight of the moving parts and keeps the slide against this stop during focus adjustment. The micrometer allows precise positioning of the beam waist relative to

the particle on the launching plate for levitation and then allows the raising of the particle approximately 1 cm. to the center of the goniometer for scattering measurement. For wide field viewing of particles on the launching plate the levitation lens can be lowered approximately 2 cm. below the focused position and latched. This spreads the beam at the launching plate enough to allow imaging a larger area on the plate for particle selection.

### LAUNCHING PLATE

The particles to be levitated are spread on a microscope cover glass centered on the laser beam. Typically the Van der Waals forces binding the particles to the plate are several orders of magnitude greater than the force exerted by laser beam although occasionally particles will "self-levitate" when the beam waist is brought beneath them. Ashkin and Dziedzic<sup>2</sup> (1971) have described a means of freeing particles from a plate. A piezo-electric crystal bonded to the glass launching plate is excited by a signal from a sweep oscillator, vibrating the plate and causing the particles to "jump" free of the launching plate. It is necessary to control the amplitude of the vibration to avoid imparting excessive velocity to the particles so that they may be captured by the beam. Provision is made for continuously repeated bursts with a variable repetition rate, as well as for single bursts. The launching plate assembly is mounted on a vertical slide which allows it to be lowered well below launch height after a particle is levitated to allow clearance for the goniometer during scattering measurements. The entire assembly is mounted on an x-y translation mount to allow the launching plate to be moved relative to the laser beam for particle selection.

### SCATTERING CHAMBER

When levitated, the particle is extremely sensitive to disturbances caused by air currents. Therefore a cylindrical chamber encloses the goniometer and launching plate assembly. The levitation lens and the forward scattering viewing lens assemblies extend into the chamber through openings which have sliding seals

to reduce air flow. A flat window is provided for the 90 degree image. A hinged door allows access to the launching plate for introduction of particles.

#### PARTICLE VIEWING OPTICS

In order to examine the orientation and motion of the levitated particle, lens systems above the particle (at the 0 degree scattering angle) and to the side of the particle (at the 90 degree scattering angle) project near field images of the particle on a screen. The forward scattering image shows the particle silhouetted against the focused laser beam at the equilibrium height. This beam is reflected off the front surface of a prism to bring it into proximity with the 90 degree image and to reduce its intensity to a value more comparable with that of the 90 degree image. The majority of the laser beam is refracted in the prism and passes on to a Laser Precision Model RT-20-C Power Meter.

Both the forward scattering and the 90 degree viewing systems consist of an objective lens of 7.5 cm focal length and a projection lens of 5.0 cm focal length. The objective lens of the 0 degree viewing system is mounted in an x-y translation lens mount which is in turn mounted on a micrometer-driven slide to allow precise focusing on the launching plate as well as on the particle after levitation. The forward and 90 degree lens systems each provide a magnification of approximately 500 diameters at the screen. Thus a typical 40 micron diameter particle has an image diameter of 2 cm. This scale has proven convenient for direct viewing and measurement with a dial caliper as well as recording with a camera system.

#### FAR FIELD VIEWING

It has proven instructive to view directly as much as possible of the far field scattering pattern of levitated particles. Therefore one half the circumference of the scattering chamber has been constructed of clear plastic. This window has been covered with colored plastic to reduce the intensity of the scattering pattern viewed upon it. The far field scattering from the particle can be viewed on this surface from 45 degrees to 120 degrees scattering angle over a range of almost 180 degrees

in azimuth. In addition the top of the chamber has a clear plastic lid. The forward scattering viewing optics obscure the particle at angles closer than 18 degrees to the forward scattering direction and the top support ring of the chamber obscures the view beyond 36 degrees scattering angle. The relatively bright back-scattering typical of spherical particles beyond (approximately) 150 degrees can be viewed projected on the launching plate support up to about 175 degrees scattering angle.

### GONIOMETER

A goniometer mounted photodiode photometer moves in a vertical plane centered on the particle when the particle is levitated at analysis height in the laser beam (detail drawing in Figure 1). The diode has a 1.0 mm. diameter active surface and is located 22 mm. from the particle. A tapered baffle restricts the photometer to a two degree field of view.

When the goniometer is looking at backscattered radiation (90 to 170 degree scattering angle) it is important to avoid background scattered light. When looking at a scattering angle of 135 degrees, the background is illuminated by light scattered at 45 degrees from the particle. Since the scattering at 45 degrees can be several orders of magnitude greater than the scattering at 135 degrees a "light trap" is mounted on the opposite side of the particle from the photometer. This counterposed trap is a small machined "cone-in-cone" designed to ensure that rays scattered back towards the photometer will typically undergo more than 10 reflections (see the detail drawing in Figure 1). The surface of the light trap is black anodized aluminum. Measurements indicate that the light trap scatters less than 0.01 percent of the light incident on it back into the photometer.

The goniometer can rotate from about 16 degrees scattering angle through about 170 degrees scattering angle. Beyond these limits, the diode housing and/or the light trap encroach on the laser beam. The goniometer is driven by a DC motor through a worm and worm wheel. The goniometer and worm wheel are mounted directly on the shaft of a precision potentiometer which provides position feedback

to the control system. A servo motor controller allows manual or computer operation of the goniometer.

The entire goniometer assembly is mounted so that it can be rotated in azimuth around the vertical beam axis to select the scattering measurement plane.

#### POLARIZATION ROTATION

The laser beam is linearly polarized in the vertical plane. A quartz half-wave plate mounted in a 360 degree rotation mount is located just below the levitation lens. The half-wave plate has been mounted so that at position 0 degrees the E vector of the laser beam is in the vertical plane defined by the goniometer motion. A rotation of half-wave plate through 45 degrees places the E vector perpendicular to the goniometer measurement plane. Thus the levitated particle can be illuminated by linearly polarized light at any desired angle to the measurement plane.

#### PARTICLE CAPTURE

It is difficult to pre-select a particle which will be successfully levitated. Some particles are bound too tightly to the launching plate to be released by the PZT driver. Other particles may prove too unstable (once levitated) for the sustained levitation necessary for scattering measurements. In order to allow examination and photographic recording of particles for which scattering data have been obtained, we have designed a particle capture plate mechanism. A clean microscope cover glass is moved quickly into the beam well below the levitated particle. Generally this can be accomplished without interrupting the beam long enough to cause the particle to drop. After the capture plate has been moved into place, the particle may be lowered into contact with the plate by lowering the levitation lens. The capture plate can then be placed under a microscope so that the particle can be studied and photographed.

### DATA ACQUISITION AND CONTROL SYSTEM

A PC/AT compatible computer system is used for data acquisition and instrument control (Figure 2). A Data Translation model DT2801A interface board provides eight 12-bit analog-to-digital input channels with adjustable gain at a sampling rate up to 20 KHz. Two 12-bit digital-to-analog output channels provide control signals for the goniometer position and the laser power. Data and software are stored on a 40 MByte hard disk. A magnetic tape drive provides for archival storage of data and software. High resolution graphics display the photometry and scattering signals in real time. All program functions can be controlled by a "mouse" pointing device. This method of user input has proven much superior to the use of keyboard commands or function keys for most purposes. A digital CCD camera control and image processing board provides 8 MBytes of image storage. These data can be moved to hard disk or display memory as desired under program control.

The system software is written in FORTH which has proven to be a useful language for this system. The goniometer photometer signal is sampled at 1000 samples-per-second. The raw signal can be displayed in real time at up to 62.5 points-per-second for examination of vibrating or rotating particles. For scattering measurements the goniometer is moved in 0.5 or 1.0 degree steps through a pre-determined range (typically 16 to 143 degrees or 40 to 167 degrees). After the goniometer has settled at each position, the photometer output is sampled for a period between 0.5 and 4.0 seconds. These data are averaged and stored at a rate of 64 samples-per-second. The time of the start of each sample is determined to an accuracy of 1 millisecond for correlation between measurements at different goniometer positions as well as correlation with the digital CCD camera images.

### CAMERA SYSTEMS

Three camera systems are used to record the near and far field images of levitated particles for documentation, review, and analysis. The vertically adjacent forward scattering and 90 degree close-up images are recorded by a conventional

CCD television camera whose output is displayed and recorded by a video recorder. In addition a computer controlled CCD camera views these images. This camera can be configured to record up to 256 images in immediate succession interval of 1/240th of a second. These images can be played back at a slower rate to the display as well as stored to disk for later analysis. A third hand-held CCD "camcorder" television camera allows recording the far field images and other aspects of the levitation and measurement process. The high speed shutter of this camera has proven useful in "freezing" the images of rapidly rotating and/or vibrating particles.

### CONCLUSIONS

The apparatus describe herein has proven to be a reliable and effective system for the levitation of small dielectric particles, and for the measurement of scattering from those particles. Scattering can be measured in a selected plane of polarization over the range of scattering angles from 15 degrees to 170 degrees with a resolution of 2 degrees. In addition to scattering data, camera systems allow the recording of near and far field images of the levitated particles for determination of particle orientation and rotation.

### ACKNOWLEDGEMENTS

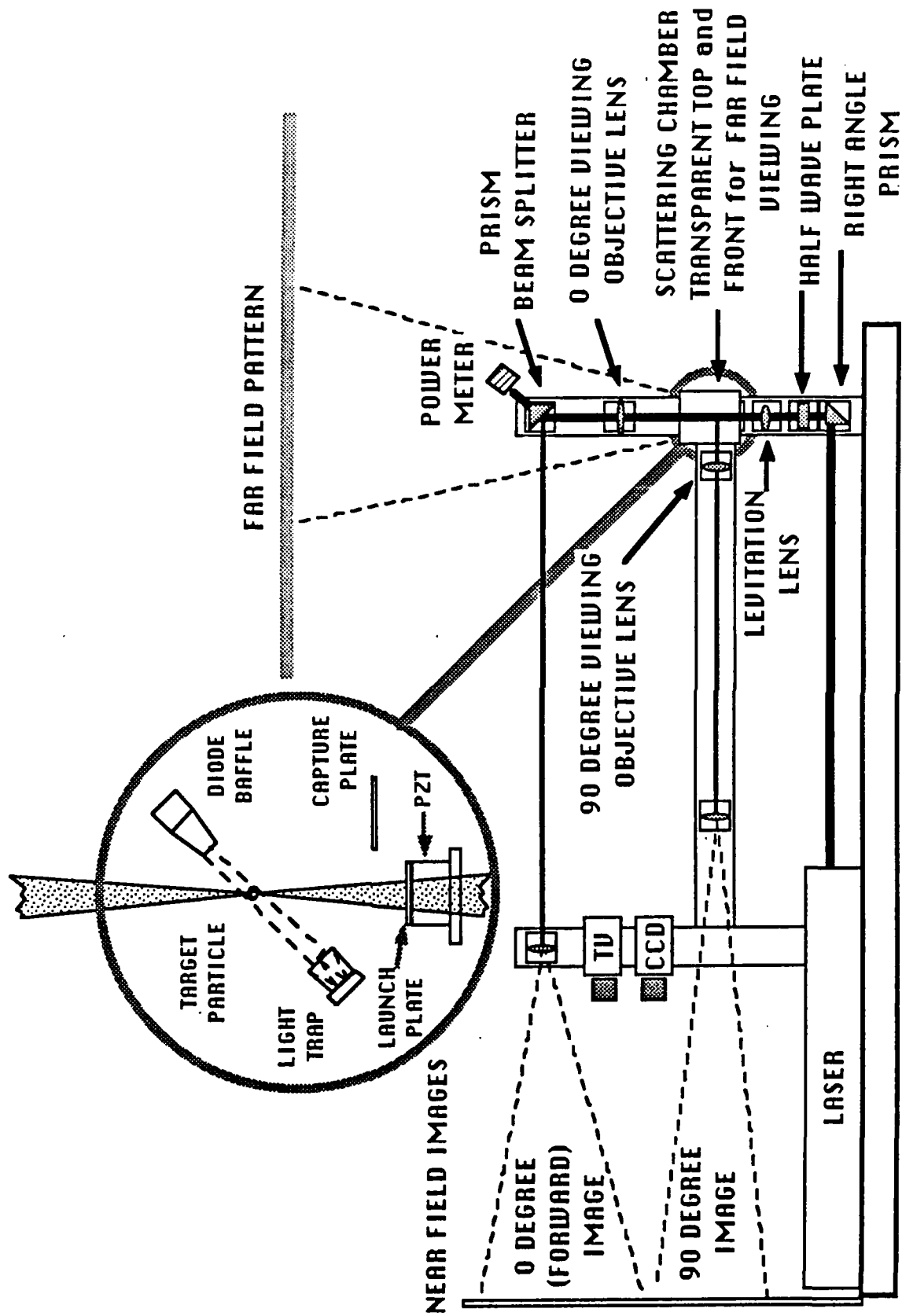
We wish to thank Jack McKisson, Don Ely, and Charles Crum for help with the design and assembly of the apparatus. G.Eichhorn also provided helpful discussion. We wish to dedicate this paper to the memory of H. Mack Mann for his many contributions to the design of this experiment.

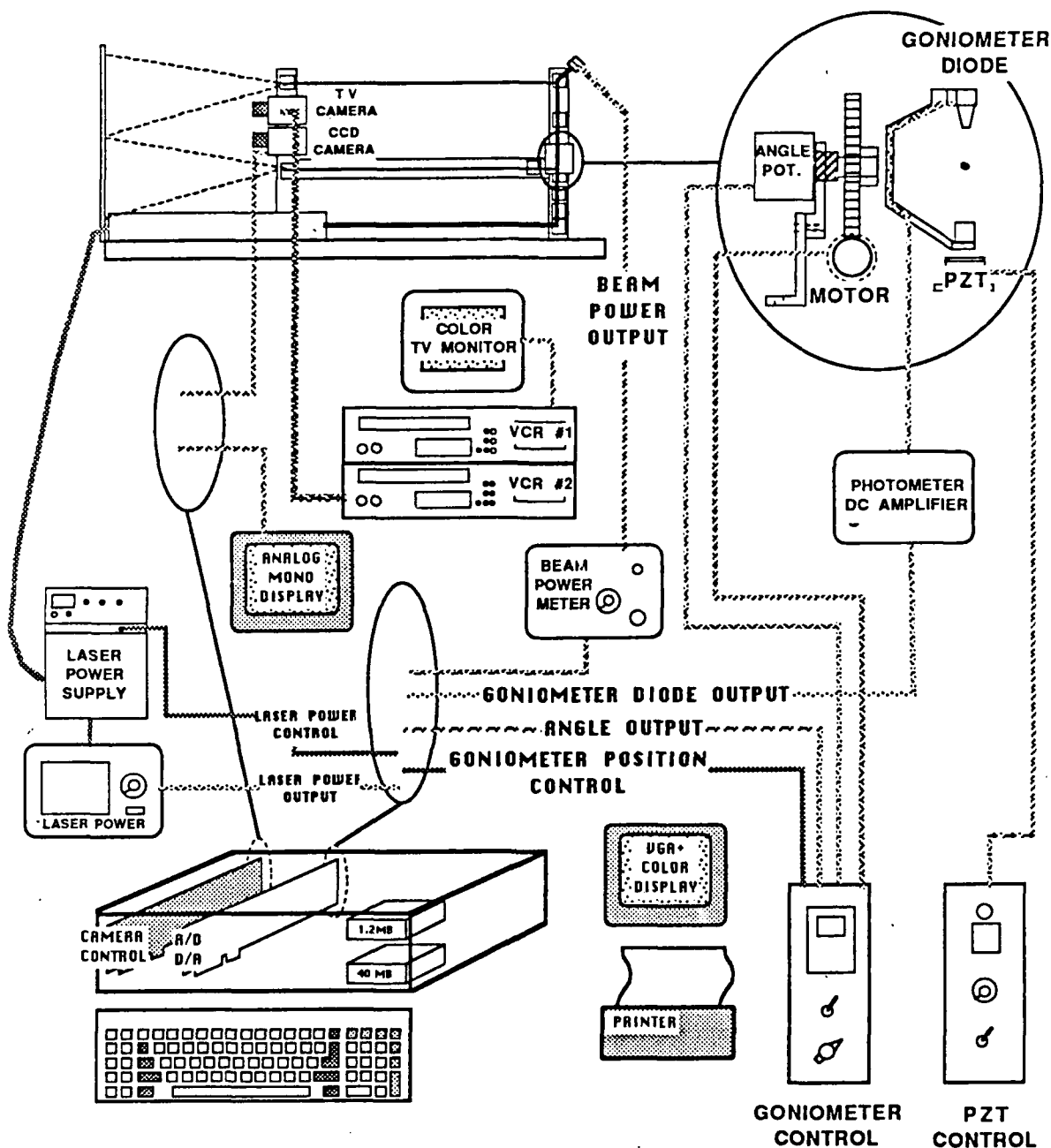
### REFERENCES

1. N.Y. Misconi, K. F. Ratcliff, E. T. Rusk, J. P. Oliver and W. Wang, "I: Preliminary Results on Light Scatering by Laser Levitated Particles", Submitted to *Applied Optics*, (1989).
2. A. Ashkin and J. M. Dziedzic, "Optical Levitation by Radiation Pressure", *Applied Physics Letters*, 19, 283, (1971).

## FIGURE CAPTIONS

1. A sketch of the overall layout of the apparatus showing the various components used in this experiment.
2. A sketch of the associated controls, goniometer, camera system, and the micro computer that controls the instrument.





DYNAMICAL EFFECTS OF JUPITER, THE INNER PLANETS, AND POYNTING-ROBERTSON DRAG ON THE LIFETIME OF INTERPLANETARY DUST

EDWIN T. RUSK, NEBIL Y. MISCONI, AND  
BO A. S. GUSTAFSON

SPACE ASTRONOMY LABORATORY, UNIVERSITY OF FLORIDA,  
1°10 NW 6th Street, Gainesville, Florida 32609  
U.S.A.

(Received 16 May 1988)

**Abstract** - Wyatt and Whipple (1950) identified a constant ( $W$ ) in the relation between orbital semimajor axis ( $a$ ) and eccentricity for interplanetary particles under the influence of Poynting-Robertson drag. Perturbations due to the planets were found to cause changes in  $W$ , including a nearly monotonic decrease for particles with semimajor axes less than 2 AU. Based on the calculated orbital evolution (Gustafson et al., 1987a) of some two hundred dust particles released from comet P/Encke and perturbed by the planets Venus, Earth, Mars, and Jupiter as well as radiation pressure and drag and corpuscular drag, values were found for the changes in  $W$  as a function of  $a$ . Most frequently, particles showed a decrease in  $W$ , corresponding to an increase in eccentricity over that predicted from P-R drag. This effect should be accounted for in future dynamical calculations that include Poynting-Robertson drag.

INTRODUCTION

Poynting-Robertson drag (henceforth P-R drag) is an effect of solar photon pressure which acts to oppose the velocity of a small particle in solar orbit, creating a drag under which the particle slowly spirals in to the sun (Poynting, 1903; Robertson, 1937). Wyatt and Whipple (1950) solved the equations of motion of a spherical particle under the influence of P-R drag and found a relationship between semimajor axis ( $a$ ) and eccentricity ( $e$ ),

$$W = a e^{-4/5} (1-e^2) \quad , \quad (1)$$

which remained constant as the particle spiraled inward toward the sun. In their paper, the constant which we have and will continue to denote by " $W$ " was given the symbol " $C$ ". This relationship was used to determine the P-R lifetime, which is the time it takes for a particle to spiral in to the sun from its source, for particles in elliptical as well as circular orbits.

From 1983 to 1985, using numerical simulations, Misconi and Gustafson collaborated to determine whether or not the action of the inner planets on cometary dust was responsible for the present observed spatial distribution of interplanetary dust. The zodiacal light measurements in the inner solar system show that, to within observational accuracy, the symmetry plane (the plane of

semimajor axes less than 2 AU. Outside of 2 AU, there was a general trend toward decreasing  $W$  at an even faster rate of change, although there were regions where the median value of  $W$  sharply increased. These rapid variations in  $W$  between 2.0 and 2.9 AU resulted from the high initial eccentricities of the particles ( $e=0.884$  at release from comet P/Encke), due to which their orbital paths brought them close to Jupiter's orbit. Most particles had several encounters with Jupiter before settling down into less variable orbits.

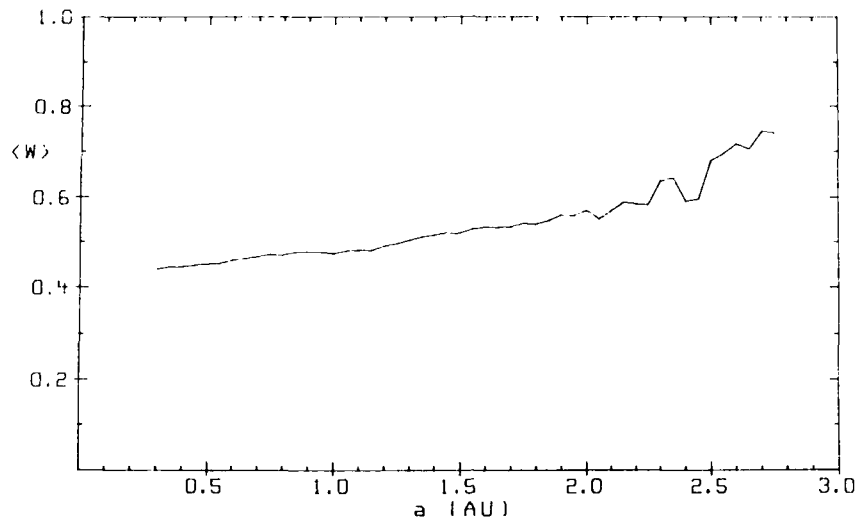


Figure 1. Median value of the Wyatt-Whipple constant vs. semimajor axis, for cometary dust perturbed by the inner planets and Jupiter.

As a side note, an additional fifty-two particles were perturbed into orbits with semimajor axes greater than 4 AU by close encounters with Jupiter, and had to be rejected in this analysis of dust orbits in the inner solar system. Such a mechanism does not solve the "dust budget" problem, since it merely delays the particle's entry into the inner solar system. In fact, eight of these particles (out of a superset of 255) were perturbed into hyperbolic orbits.

The large anomalies just inside 2.5 AU are apparently due to a 3/1 resonance (for an in-depth study of particles crossing resonances, see Gonczi et al., 1982, 1983a, 1983b) with Jupiter at 2.47 AU (based on the longer orbital period of a 30  $\mu$ m particle due to radiation pressure). In this region, a rapid decrease in semimajor axis was found (see paper 2). The 18.5% increase in mean time the particles spent crossing the 4/1 resonance region (between 2.1 and 2.0 AU) described in paper 2, does not appear in figure (1). The reason for this is that only a few particles contributed to affect the mean value.

In figure (2), the median values of  $dW/da$  (note that this is  $\langle dW/da \rangle$ , not  $d\langle W \rangle/da$ ) are plotted, again vs. semimajor axis. We have limited the plot to the region inside of 2 AU where the curve in figure (1) appeared relatively smooth. The median value of  $dW/da$  is not constant as would be expected from figure 1, but rather it starts out at a high value and approaches zero as semimajor axis approaches zero. Strong deviations from a smooth curve are seen at semimajor axes just below 1.8 AU and 1.6 AU. These correspond to the 5/1 and 6/1 Jovian resonances. A small dip between 1.4 and 1.35 AU may be related to the 7/1 resonance at 1.403 AU.

It is apparent that Jupiter has a strong effect on  $W$ . What about the other planets? The variations from smoothness between 0.6 and 0.45 AU do not

means to measure the effects of planetary perturbations on particles undergoing Poynting-Robertson drag. It is suggested that this method could prove useful in the study of the effects of other forces, such as the Lorentz force of the interplanetary magnetic field, acting on dust under the influence of P-R drag (paper in preparation).

There is a marked lack of visible effect on the Wyatt-Whipple constant during the particles' crossing of resonances with the inner planets. We conclude that, at least for particles in highly eccentric orbits such as those of cometary origin, the inner planets do not significantly reduce the infall rate of dust due to P-R drag and, in fact, cannot overcome the shortening of the P-R lifetime of the dust due to the effect of Jupiter.

We believe that the alignment of the symmetry plane of the zodiacal dust with the orbital planes of Venus and Mars was unlikely to have been caused by those planets. We suggest that those planets and the dust may have been co-aligned by Jovian perturbations in conjunction with other forces such as radiation pressure, the solar magnetic field, and/or other planets not included in this study. The possibility that the Jovian perturbations were enhanced through an interaction with perturbations by the inner planets has not been ruled out.

#### ACKNOWLEDGMENTS

This research was supported by NSF Grant AST-8206152. Partial support was provided by AFOSR Contract F49620-85-C-0117.

#### REFERENCES

- Brouwer, D. and A.J.J. Van Woerkom (1950), The secular variations of the orbital elements of the principal planets, A. P., 13, Part II, 81-107.
- Gonczi, R., Ch. Froeschle and Cl. Froeschle, (1983), Poynting-Robertson drag and orbital resonance, Icarus, 51, 633-654.
- Gonczi, R., Ch. Froeschle and Cl. Froeschle, (1983), Trapping time of resonant orbits in presence of Poynting-Robertson drag, Dynamical Trapping and Evolution in the Solar System (V.V. Markellos and Y. Kozai, eds.), D. Reidel, Dordrecht, Netherlands, 397-410.
- Gonczi, R., Ch. Froeschle and Cl. Froeschle, (1983), Evolution of three dimensional resonant orbits in presence of Poynting-Robertson drag, Asteroids Comets Meteors (C.I. Lagerkvist and H. Rickman, eds.), Uppsala University Press, Uppsala, Sweden, 137-143.
- Gustafson, B.A.S. (1985), Planetary Perturbations: Effects on the shape of a cloud of dust in circular heliocentric orbits, Properties and Interactions of Interplanetary Dust (R.H. Giese and P. Lamy, eds.), D. Reidel, Dordrecht, Netherlands, 385.
- Gustafson, B.A.S. and N.Y. Misconi (1983), Can cometary dust perturbed by the inner planets be an explanation for the observed distribution of interplanetary dust?, Cometary Exploration, 2, (T.Gombosi, Ed.), Hungarian Academy of Sciences, 121.
- Gustafson, B.A.S. and N.Y. Misconi (1986), Interplanetary dust dynamics I. Long-term gravitational effects of the inner planets on zodiacal dust, Icarus, 66, 280-287.
- Gustafson, B.A.S., N.Y. Misconi and E.T. Rusk (1987a), Interplanetary dust dynamics II. Poynting-Robertson drag and planetary perturbations, Icarus, 72, 568-581.
- Gustafson, B.A.S., N.Y. Misconi and E.T. Rusk (1987b), Interplanetary dust dynamics III. Shape and orientation of remnants of P/Encke's dust cloud, Icarus, 72, 582-592.